THE DEVELOPMENT OF AN EFFECTIVE JAM CODE AGAINST THE CONICAL-SCAN SEEKER

by

Tsholofelo M. Malatji

Submitted in partial fulfillment of the requirements for the degree
Master of Engineering (Electronic Engineering)

in the

Department of Electrical, Electronic and Computer Engineering
Faculty of Engineering, Built Environment and Information Technology

UNIVERSITY OF PRETORIA

January 2020

SUMMARY

THE DEVELOPMENT OF AN EFFECTIVE JAM CODE AGAINST THE CONICAL-SCAN SEEKER

by

Tsholofelo M. Malatji

Supervisor(s):	Prof. W. P. du Plessis
Department:	Electrical, Electronic and Computer Engineering
University:	University of Pretoria
Degree:	Master of Engineering (Electronic Engineering)
Keywords:	Jamming waveform, jam code, jam signal, conical-scan, reticle, counter-measures

There remains a wide proliferation of second-generation frequency-modulated conical-scan seekers in the hands of irregular forces, while the understanding of what makes a jam signal effective remains unclear. It is generally known that the jam-to-signal (J/S) ratio, the jam signal frequency, and the duty cycle are the parameters that need consideration when developing an effective jam code, but the effect of using different jammer waveforms is not generally known. The general consensus in the literature seems to indicate that the effective jam signal parameters should be close to those of the target signal. It is known that the jam signal that matches the target signal will only beacon the target and not provide protection, therefore the jam signal should not perfectly match the target signal for effective jamming. However it is not clear which parameters should be close to and which should differ with the target signal. The literature also generally uses the low frequency type of jam signal and the effect of other types of waveforms is not known.

Due to the sensitive nature of this topic, a simulation model and a hardware model of the conical scan seeker was not available to the author and as a result a representative simulation model was designed for conducting the experiments. The simulation model was extensively tested and validated to ensure representative behaviour. This study investigated the effect of the critical jam signal parameters

against different jammer waveforms namely: the fixed carrier, low frequency, amplitude modulation (AM), frequency-modulation (FM) and the AM-FM jam codes. The study tested the effect of the critical parameters across the different jam waveforms and a comparison of the tested waveforms was conducted. The parameters used to compare the jam signals were the maximum achieved seeker error, the minimum J/S ratio required to achieve a significant effect, the range of effective frequencies or modulation indices and the lowest effective duty cycle. The AM jam signal achieved the greatest seeker error when compared to the other jam waveforms with a maximum error of 1.1°. The AM jam signal however achieves this error, with a J/S ratio of 50. The AM-FM jam signal achieved an error of 0.97° at a J/S ratio of 20 which is less than half of the required J/S ratio with the AM jam signal. The AM-FM hybrid jam signal was found to be the most robust in a wide range of modulation indices. This jam waveform was found to be the least sensitive against changes in the modulation index. The jam signal was found to be less power intensive when compared with other waveforms since significant jam effect was achieved at low J/S ratios. The best parameter combination for this jam signal was a J/S ratio of 20, a modulation index of 2.5, a modulation frequency of 100 Hz and a duty cycle of 50%. The maximum seeker error induced by this parameter combination is 0.97°. With the stated advantages, the AM-FM hybrid jam signal was found to be the most effective jam signal against the conical-scan seeker.

Contrary to the general guide provided in the literature, the most effective jam signal does not contain parameters that are similar to the target induced parameters. The conclusion of this work was therefore that the most effective jam signal does not necessarily have to be similar to the target signal to be effective against the conical-scan seeker. The unique result found in this study is attributed to the wide range of jam signal waveforms that were tested. The results show that the effects of the critical parameters (J/S ratio, frequency and duty cycle) vary with the change in jam waveform.

LIST OF ABBREVIATIONS

AGC	automatic gain control
AM	amplitude modulation
APT	acquisition, pointing and tracking
BPF	band-pass filter
CSIR	Council for Scientific and Industrial Research
DC	direct current
DIRCM	directed infrared countermeasure
FM	frequency-modulation
FOV	field of view
FPA	focal plane array
HPF	high-pass filter
HPL	high-power laser
IFOV	instantaneous field of view
IR	infrared
J/S	jam-to-signal
LOS	line of sight
LPF	low-pass filter
LWIR	long wave infrared
MANPADS	man-portable air-defence system
MAW	missile-approach warning
MTV	Magnesium/Teflon/Viton
MWIR	medium wave infrared
N/A	not applicable
NIR	near infrared
OBL	optical break lock
OSSIM	Optronic Scene Simulator
POE	point of effect
SWIR	short wave infrared

TABLE OF CONTENTS

CHAPTER 1 INTRODUCTION

1.1 PROBLEM STATEMENT

1.1.1 Problem Context

Since their invention in the 1960s, MANPADSs have remained a cause of concern for the majority of governments worldwide [1]. Statistics show that of all the aircraft lost in combat, 80% were due to MANPADS missiles [2]. The ease of use, low expense and long shelf life of these devices, makes them desirable for irregular or terrorist groups. This makes it critical to develop sufficient countermeasure techniques against such threats. MANPADS have significantly advanced since the 1960s, but the technological advancements made the MANPADS to be excessively more expensive. It can therefore be argued that if a non-regulated group desires to acquire a MANPADS, the older generation MANPADS would be preferred due to the lower cost. The spreading of MANPADS missiles amongst non regulated groups has also been significantly reduced through the years but a large number of the early generation MANPADS still remain unaccounted for [3, 4]. This makes the early generation MANPADS a threat against both military and civilian aircraft. The first generation MANPADS makes use of a spin-scan AM technology and the second generation MANPADS uses the conical-scan (also known as con-scan) FM technology to direct itself to the target. These are the two technologies that are most widely used by irregular or terrorist groups [5].

A large concerted effort has been made to develop effective countermeasures against MANPADS missiles. The main types of countermeasure techniques that are employed against these threats can either be off-board the platform or on-board. Off-board countermeasures include smoke screens and decoys such as flares [6]. On-board countermeasures can be deception or destruction jammer systems. Flares provide an effective countermeasure against the early generation missiles, but they are less effective against modern missiles [7]. Furthermore, their protection capability is limited because only a limited number of flares can be carried on-board the platform [8]. Since flares burn at high

temperatures, they also pose a fire hazard in the case of an emergency [9]. Whereas flares have been shown to be effective against the first generation spin-scan MANPADS, it has been shown that flares are less effective against the second generation conical-scan MANPADS seeker due to the scanning and signal processing used in these seekers [10]. It is therefore necessary to consider effective jamming techniques against the second generation conical-scan MANPADS seeker.

An active jammer has the advantage that it can be repeatedly used in subsequent engagements, flexibly using different jam codes to counter different threat types. But effective missile seeker jamming requires that the jam code be matched to the missile type [11]. Determining and confirming the missile type during an operational mission is no simple task. As an alternative to low-power jamming, high-power lasers (HPLs) have been considered for the purpose of destroying sensitive missile components. The use of a HPLs would eliminate the need to identify and classify the missile seeker before administering a jam code [11]. The disadvantage of using HPLs however, is that the power required for the HPL is so much higher than the power required for a jamming laser. This makes the use of HPLs impractical in many situations, such as on small platforms [11, 12]. Due to the damage caused by HPLs it is also risky to place such devices on civilian aircraft which operate in civilian territory such as airports, since this could have destructive effects if pointed at the wrong object. Jamming lasers on the other hand cause deception of the missile at power levels that are safe for civilians and the civilian environment [11].

1.1.2 Research gap

Due to the security nature of this topic, the types of jam signal waveforms that are effective against the conical-scan seeker are known only to the select few in intelligence circles and with valid reason. This is as a result of each government developing the information for their own use. This makes the field of jam code development to grow at a slower pace due to the isolated efforts of different organizations, of which the resultant information is kept confidential. Arms control legislation prohibits public/academic access to the missile seekers for practical testing. Hence, the development of jam codes for research or academic purposes is restricted to the use of simulation to model the missile behaviour. This limitation has delayed the development of good understanding in terms of jam code development and this includes the understanding of jam signal waveforms that are effective against missiles in the open literature.

While limited research on jam signal development against the conical-scan seekers has been published,

there is no literature on the effect of different types of jam signal waveforms against these seekers. The literature mentions and tests the effect of the J/S ratio, the frequency and the duty cycle of the jam signal, but this generally pertains to a simple form of waveform modulation [13–19]. The literature generally deals with a low frequency jam signal and tests the above mentioned critical parameters against this jam signal [13–19]. The conclusions from these works are therefore restricted to the low frequency jam signal, and the conclusions cannot be generalized to other jam signal waveform, as other waveforms have not been tested. This limitation therefore necessitates the investigation of the effect of using different jam signal waveforms in an attempt to identify the most effective jam signal modulation waveform. This study will give understanding in terms of the effect of these parameters on the different waveforms, but this will also show the type of jam signal waveforms that are possibly more effective against the conical-scan seeker. The research will also aid in future development of jam code signals for more effective DIRCM systems that use jamming [12, 20, 21].

The majority of studies are not clear on the effects that the critical parameters have on different jam waveforms [13–18]. The general consensus in the literature is that the jammer signal should be similar to the target signal for maximum jamming effectiveness. The range of frequencies that are generally tested are 50 Hz to 150 Hz and this leads to the conclusion that the low frequency jam signal waveform is used. Does this therefore mean that the low frequency jam signal is the most effective against the con-scan seeker or could other waveforms be more effective? There is also a clear emphasis that the jam signal should be similar to the target signal for maximum effectiveness. Simple logic suggests that the jam signal should not exactly match the target signal because this would enhance the target signature making it easier to track. Therefore which parameters should be similar and which parameters should be different? The literature is not clear on the type of jam signal waveform that should be considered for successful jamming and whether having AM or FM in the waveform has any effect. It is also not clear if the critical jam signal parameters have the same effect for the different jam waveforms, and which parameters should be similar or different from the target's behaviour. Some sources suggests that the jam signal frequency must be close to the target signal frequency to ensure jammer success [13–16, 18, 19]. Others suggest that the jammer frequency is successful when it is twice the target signal frequency [17]. The literature reports frequently on the effect of the required J/S ratio. The general consensus seems to indicate that the jam signal intensity must be much higher than the target intensity [13–19]. However, how much higher the J/S ratio should be is not clear in the literature. It is also not clear if the effect of J/S would be the same for different waveforms. These conflicting conclusions necessitate further research in the effects of the jam signal parameters on different jam

signal waveforms.

1.2 RESEARCH OBJECTIVE AND QUESTIONS

The research aims to identify the most effective jam signal waveform against the conical-scan seeker. This means a number of jam signal waveforms have to be tested in order to determine the most effective jam signal waveform. Since each waveform would be effective with different parameter combinations, the most considered parameters in the literature will be used in order to test the effectiveness of each jam signal waveform [13–18]. The parameters that will be evaluated for this purpose are the J/S ratio, the jam signal modulation and carrier frequency, and the duty cycle of the carrier and modulation signal. The parameters that will be used to quantify the effectiveness of the jam signal are the magnitude of the greatest error produced, the minimum J/S ratio required, the minimum duty cycle required, and the range of effective frequencies.

The research questions that stem from the research objective are listed below.

- Which jam waveform is the most effective against the conical-scan seeker?
- What is the best parameter combination of the most effective jam signal in terms of J/S ratio, jam frequency and duty cycle?

1.3 HYPOTHESIS AND APPROACH

1.3.1 Hypothesis

It is hypothesized that the most effective jam signal against the conical-scan seeker will consist of a carrier signal and a modulation signal that operate at a constant frequency. Furthermore the carrier signal is hypothesized to operate at a frequency that is close to the target frequency and the modulation signal at the nutation frequency. Both the carrier and modulation signals are hypothesized to be effective at a duty cycle of 50%. This jam signal is hypothesized to reach the greatest error at the maximum J/S ratio of 100. The reasoning behind the hypothesis is given in the following paragraph.

The hypothesis suggests that the jam signal waveform that will produce the greatest effect against the conical-scan seeker should firstly consist of a fixed carrier frequency. It is known that the conical-scan seeker consists of a front end carrier filter which extracts the carrier signal that is generated by the seeker optics [19]. The filter isolates the desired carrier signal so that other noise components can be removed from the signal. This therefore means a signal operating at a frequency other than the seeker generated carrier frequency will be attenuated and would therefore not be effective against the seeker.

It is therefore deemed necessary for the carrier frequency of the effective jam signal to be close to or equal to the target carrier frequency that is generated by the seeker optics.

The hypothesis requires that the modulation frequency of the jam signal match the nutation frequency. This is in order to create a consistent effect in the seeker, by applying the jam signal at the same position each cycle. This ensures that the effect against the seeker accumulates to produce a high seeker error.

The hypothesis also states that the effective jam waveform carrier and modulation signals, operate at 50% duty cycles. This is required in order to add AM to the target signal by switching the jam signal on for 50% of the scan cycle and switching it off in the middle of the cycle. This is bound to make it difficult for the processor to demodulate the target position. If the detector amplitude drastically changes in the middle of a scan, the processor AGC will attempt to adjust the detected amplitude so that the signal can be processed. If this change is done in the middle of the scan, half of the information might be lost because of the abrupt change in the signal amplitude. If the change is done earlier than half of the scan cycle (less than 50% duty cycle) then the AGC circuit might have enough time to adjust the signal amplitude and more than 50% of the target information might be recovered. If the change is done later than 50% of the scan cycle (duty cycle greater than 50%), then the AGC might not have enough time to adjust the signal amplitude and since the frequency information can still be recovered from this signal, the target information can still be recovered. The hypothesized effective jam signal is therefore expected to be effective because of the interruptions it creates in the AGC circuit. The signal operating at 50% duty cycle is expected to cause the most interruptions to the AGC circuit.

It is hypothesized that the jam signal will be most effective at a J/S ratio of 100 since this is the maximum J/S ratio that will be tested in the study. It is generally known that an increase in the J/S ratio, causes an increase in the seeker error [13–19]. It can therefore be expected that the greatest effect should be achieved at the highest tested J/S ratio.

The above mentioned hypothesis addresses the research questions stated in Section 1.2 as follows:

- Which jam waveform is the most effective against the conical-scan seeker?

  - One that consists of a carrier signal and modulation signal which operate at a constant frequency.

- What is the best parameter combination of the most effective jam signal in terms of J/S ratio, jam frequency and duty cycle?

  - The best J/S ratio for this jam signal is hypothesized to be 100.
  - The carrier frequency should be close to the target frequency and the modulation frequency should be equal to the nutation frequency of 100 Hz.
  - Both the carrier and modulation duty cycles are expected to be 50% for the best performance.

1.3.2 Approach

An empirical approach was used here, comprising the development of simulation models to represent the behaviour of the seeker under study and then to study the interaction between the jam signal and the seeker. The execution of hypothesis testing was conducted in two phases. Laboratory hardware testing of the jam signals developed in this study could not be conducted because a physical seeker could not be obtained for testing (due to security reasons).

The first phase entailed the development and testing of the seeker model. Each subsystem of the seeker model was designed and individually tested to confirm correct operation. The output signals generated from each subsystem were compared with other published results for the same seeker and this was used to validate the seeker model. The second phase of the study entailed the development and testing of jam code signals. The jam signal laser was designed to be a point source spatially co-located with the target point source. The jam laser intensity was adjusted relative to the target signal to achieve the required J/S ratio level. A number of jam signal waveforms were selected for testing and the J/S ratio, carrier and modulation frequency and the duty cycles were varied to test the effect of these parameters on the effectiveness of the jam signal waveform against the seeker. The jam signal waveforms that were used to test the hypothesis were the fixed carrier, low frequency, AM, FM and the AM-FM hybrid jam signal waveforms.

The literature does not provide jam signal waveforms and only a low frequency type of jam signal waveform is used in most studies [13–19]. It was therefore decided to compare waveforms that have variable amplitude with those that have variable carrier signals; this comparison formed the basis for

the chosen waveforms used for testing. The critical parameters that were used in testing the effect of each jam signal waveform were (1) the J/S ratio, (2) carrier and modulation frequency, and (3) the carrier and modulation duty cycle. Each parameter was tested with the other parameters at fixed, pre-selected default values. The value at which each parameter produces the greatest effect on average across the different waveforms was selected as the default value for that parameter.

The effectiveness of a jam waveform will be measured by comparing the maximum error each jam waveform can produce. The maximum error is defined as the maximum radial displacement from the center of the reticle that is induced by the presence of the jam signal. The greater the seeker error induced, the better the jam waveform will be considered. The second parameter that will be considered in quantifying jam signal success will be the minimum J/S ratio required to produce a considerable effect. If jam signal A requires a lower J/S ratio to achieve the same error as jam signal B, it will be concluded that jam signal A is the more effective jam signal. Another parameter that will be used to measure effectiveness is the minimum duty cycle required to be effective. The last parameter that will be used to measure effectiveness is the range of frequencies at which the jam waveform is effective. These criteria will be combined to conclude which jam waveform produces the greatest effect against the con-scan seeker. The reasoning behind the selection of the above mentioned parameters for jam success quantification, is given below.

1. The magnitude of the seeker error is chosen because the greater the seeker error is, the greater the miss distance will be between the missile and the target. When the miss distance is large, then the protected platform or target is safe. It is therefore fitting to consider the magnitude of the error produced in the seeker by the jam code signal as a measure of the jam signal waveform effectiveness.
2. The J/S ratio has a direct impact on power consumption by the jammer system, it was therefore found fitting to score the jam signal waveform that requires a lower J/S ratio, a higher score than one that requires a higher J/S ratio to achieve the same result.
3. The duty cycle at which a jam signal is effective is an important parameter since it affects the power consumed by the jammer system. The lower the duty cycle the better.
4. The range of effective frequencies is important for flexibility purposes. Since the frequency of the attacking missile is generally unknown in a combat scenario, it is possible to have a frequency mismatch between the designed jam signal frequency and the missile seeker operating frequency. The frequency of the attacking missile might also differ from the design frequency

due to design tolerances and also due to the wear of the mechanical parts of the missile. This necessitates that a successful jam signal be effective in a wide range of carrier frequencies since the threat missile is unknown.

1.4 RESEARCH GOALS

The goal of this research is to identify the most effective jam signal waveform against the conical scan seeker. Different jam signal waveforms will therefore be tested against the seeker and the effectiveness of each one quantified. The effect of a jam signal will be quantified based on the magnitude of the seeker error produced, the minimum J/S ratio required, the minimum duty cycle required, and the range of effective frequencies. Since the effect of the jam signal is dependent on the signal parameters used, the effect of the J/S ratio, the jam signal frequency and the duty cycle were tested for the different jam signal waveforms. As a result the secondary output of the research is the understanding of the effect of these parameters in each jam signal waveform.

1.5 RESEARCH CONTRIBUTION

A number of studies have been conducted on the effect of a jam code signal against the conical-scan seeker, but of the conducted studies, none tests the effect of different jam code signal waveforms. This study tested the effect of the critical jam signal parameters, which are the J/S ratio, the jam signal carrier and modulation frequency and the duty cycle for the fixed carrier, low frequency, AM, FM and AM-FM jam signal waveforms. The literature only shows the effect of the jam parameters in the low frequency jam signal waveform. This study has shown that the effect of the jam signal parameters cannot be generalized since the effect varies for different jam signal waveforms. This research will provide guidance in terms of the most effective jam signal waveform and the understanding of the suitable parameters that produce the largest error.

The results obtained from jam signal testing are only as accurate as the seeker model used to obtain such results. It was imperative that the seeker model be designed in such a way that it produces the expected behaviour of the seeker under study. As such, the model design was thoroughly tested and the results of this design process are published in the international conference article *Jammer signal effectiveness against the con-scan seeker* [22]. A thorough study was conducted on the effect of the critical jam signal parameters which are the J/S ratio, the carrier and modulation frequencies and the duty cycle and this study resulted in an international journal paper titled *Analysis of the jam signal effect against the conical-scan seeker* [23]. The performance of the seeker was validated using a tool developed by the research institute Council for Scientific and Industrial Research (CSIR) of South

Africa together with Denel Dynamics called Optronic Scene Simulator (OSSIM) [24]. The effect of applying jam codes against the OSSIM simulator are published in an international conference paper titled *Propagation of a jam code signal in the conical-scan seeker processor* [25].

The study compared different jam signals and their effects against the conical-scan seeker. The main finding from the study was that the AM-FM hybrid jam signal is the most effective jam signal against the conical-scan seeker when compared with the other tested waveforms. The AM-FM hybrid jam signal was found to be the most robust in a wide range of modulation indices. This jam waveform was found to be the least sensitive against changes in the modulation index. The jam signal was found to be less power intensive when compared with other waveforms since significant jam effect was achieved at low J/S ratios. The best parameter combination for this jam signal was a J/S ratio of 20, a modulation index of 2.5, a modulation frequency of 100 and a duty cycle of 50%. The maximum seeker error induced by this jam signal is 1°. The conclusion of this work was therefore that the most effective jam signal does not necessarily have to be similar to the target signal to be effective against the conical-scan seeker.

1.6 OVERVIEW OF STUDY

The structure of this document and the contents of each chapter are summarised here.

1.6.1 Chapter 2: MANPADS concepts and evolution

This chapter describes the basic concepts that are applicable to the operation of the infrared MANPADS. A basic introduction to infrared radiation is provided and the history behind the development of MANPADS is given. The development of countermeasures as a result of improvements in the MANPADS missile is described. Then the issue of proliferation is explained and its implications to both military and civilian aircraft. A basic outline of the operation of the conical-scan seeker is also provided in this chapter. The FM principles as used in the conical-scan seeker are explained and finally the chapter is concluded.

1.6.2 Chapter 3: Modelling and simulation

The details of the conical-scan seeker simulation model that was developed are presented in this chapter. The seeker optics, seeker processing and the seeker tracking are described in detail. The process that was undertaken to validate the seeker model is given in detail for each subsystem in order to create confidence in the model. The subsystems are tested in both the time and frequency domains, to test for expected behaviour. The static gain curve of the model is presented and compared with other found gain curves. The tracking performance of the designed seeker is then presented and compared.

1.6.3 Chapter 4: Jam signal effectiveness

This chapter describes the tests that were conducted to evaluate jam signal effectiveness against the conical-scan seeker. The chapter begins with a definition of how effectiveness will be quantified and the parameters that will be used for this purpose. The setup that was used for jam signal testing is then described for the different parameters that were tested. The description of the tested jam waveforms and their characteristics is then presented. The results obtained for the fixed carrier, low frequency, AM, FM and the AM-FM hybrid jam signals are then given in detail. Each jam signal is tested in the effect of the J/S ratio, carrier and envelope frequency, carrier and modulation duty cycle, and the time taken to achieve the greatest error as applicable for each waveform.

1.6.4 Chapter 5: Comparison of jam signal waveforms

A summary of the findings for all the jam signal waveforms is presented and the results are compared in this chapter. The results are compared in the category of the J/S ratio, carrier frequency, modulation frequency, duty cycle and the time taken to achieve the greatest error. A discussion on the best performing jam signal is then given.

1.6.5 Chapter 6: Conclusion and future work

The conclusion of the findings of this study are presented and the most effective jam signal waveform discussed. The limitations of the study are presented and the prospects of future work are then discussed. The exploration of more critical parameters that should be considered in the future are also discussed in this chapter.

CHAPTER 2 MANPADS CONCEPTS AND EVOLUTION

2.1 CHAPTER OBJECTIVES

This chapter serves as an introduction to the history and development of the MANPADS missile and to give the basis of operation of this system. The chapter begins with an introduction to the IR spectrum and the relevant terminology as related to IR missiles. The chapter then gives a historical treatment of the use of IR devices for defence of one's forces and attack of enemy forces and how this use has changed over time. The development of countermeasures in response to these threats and the proliferation of the threat is then explained. The operation of the second generation missile is then explained in the different subsystems that make up the system. The second generation missile consists of the conical-scan seeker which will be considered in this study.

2.2 INTRODUCTION TO INFRARED RADIATION

2.2.1 Infrared spectrum

The electromagnetic spectrum is the distribution of wavelengths and frequencies in which radiation occurs as illustrated in Figure 2.1 [26]. The convention is to use frequency to describe radio waves and wavelength to describe the higher frequency waves. The infrared spectrum is in the range 0.74 μm to 14 μm [27].

The atmospheric aerosol scatters radiation and molecules absorb radiation at specific wavelength regions. The extent of the absorption is a function of the humidity (amount of water vapour), the altitude at which the atmosphere is observed, the distance of the source to the detector, the aerosol concentration of the observed area (dust, smoke, etc.), and the whether conditions in which the atmosphere is observed (rain, haze, cloudy sky, etc.) [28, Chapter 4]. The transmission of infrared radiation through the atmosphere is shown in Figure 2.2. As seen in the figure, some of the regions

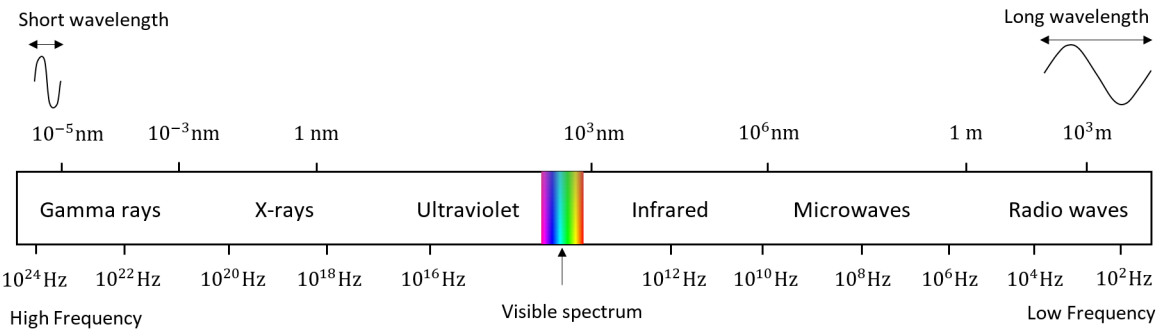

Figure 2.1. The electromagnetic spectrum. By courtesy of Encyclopædia Britannica, Inc., © 2019; used with permission [26].

in the spectrum have almost zero transmission which means that no radiation will pass through the atmosphere in those spectral bands. The main useful bands of interest, with high transmittance, can be broadly categorised as follows [28, Chapter 3] and [29] (definitions are not exact and authors differ):

- Near infrared (NIR) covering the wavelength band λ = 0.75 - 1.4 µm,
- Short wave infrared (SWIR) covering the wavelength band λ = 1.4 - 2.5 µm,
- Medium wave infrared (MWIR) covering the wavelength band λ = 3 - 5 µm,
- Long wave infrared (LWIR) covering the wavelength band λ = 8 - 12 µm.
- Extreme infrared operating in wavelengths greater than 15 µm.

2.2.2 Blackbody radiation

A blackbody is an ideal radiator which absorbs all radiation falling on it with no transmission or reflection [28, Chapter 2], [31]. A blackbody is used as a standard to compare and understand radiating bodies but a true blackbody does not exist in reality. The radiation of a blackbody across different wavelengths is described by Planck's law as shown in Figure 2.3. Planck's law shows that the radiation energy increases with an increase in the radiator temperature. The measure used for radiation power is the emittance denoted as M with units $\mathrm{W\,m^{-2}}$. When the emittance is denoted with the λ subscript as M_λ, then the emittance is a function of the wavelength and not measured across all wavelengths and has the units $\mathrm{W\,m^{-2}\,\mu m^{-1}}$. It can be observed that the locus of the maxima tends towards the lower wavelengths as the temperature increases. Note that at higher temperatures the radiation peaks towards the shorter spectral bands while at lower temperatures the radiation peaks towards the longer spectral bands. At higher temperatures, even though the peak moves towards shorter wavelengths, the

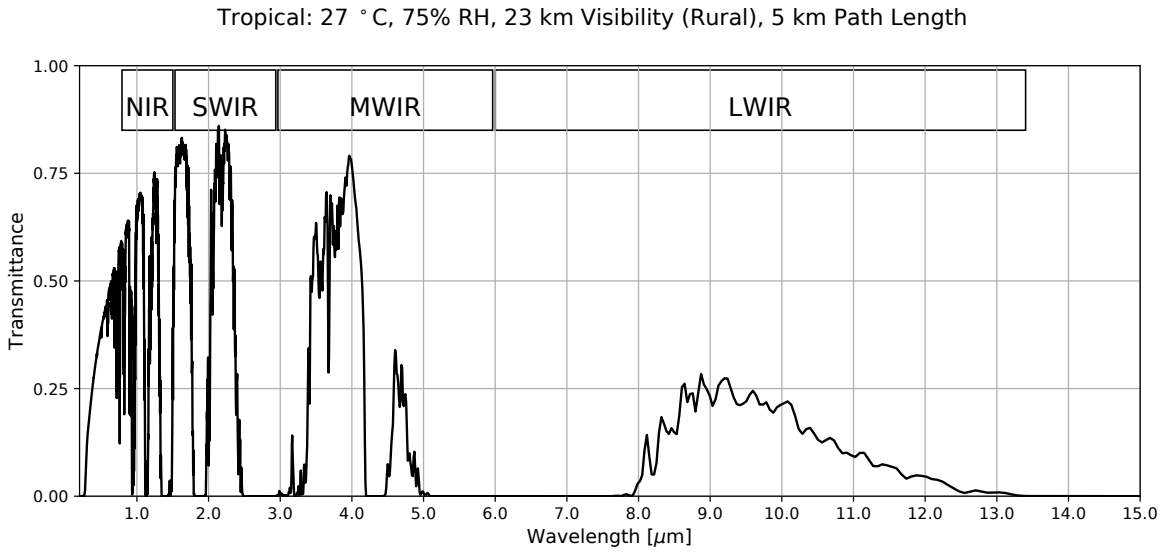

Figure 2.2. Transmission through the atmosphere. Taken from [30], with permission.

blackbody still radiates than at lower temperatures. The first generation MANPADS has a detector operating in the spectral band 1 - 2.5 µm, mainly detecting the hot temperatures of the actual aircraft exhaust, hence the missile was limited to tail on engagements [7]. With the shift in the spectral band of operation from the SWIR to the more commonly used MWIR, the missile was able to engage from different aspect angles due to the MWIR band being more sensitive to other temperatures other than the exhaust. The Stefan-Boltzmann law defines the total blackbody emittance over all wavelengths as

$$M = \sigma T^4 \tag{2.1}$$

where M is the emittance, $\sigma = 5.67 \times 10^{-8}\ \mathrm{W\,m^{-2}\,K^{-4}}$ is the Stefan-Boltzmann constant and T is the object surface temperature in K. This law shows the strong dependence of the emittance on temperature. A doubling of the source temperature will result in the total emittance increasing sixteenfold! This explains why the reduction of the temperature of the engine and other aircraft hot parts can be effective in reducing the signature of the aircraft. Note that over limited spectral bands such as the MWIR or LWIR the increases are less spectacular.

2.2.3 Sources of IR radiation

The main sources of aircraft signature infrared radiation for the IR missile are the hot engine exhaust, the engine plume and the parts of the body that are subject to high aerodynamic heating (Figure 2.4). Aircraft avionics equipment can also result in hot spots on the aircraft fuselage. The hot engine exhaust speaks of the engine metal parts that are exposed and are visible to the missile while the plume speaks

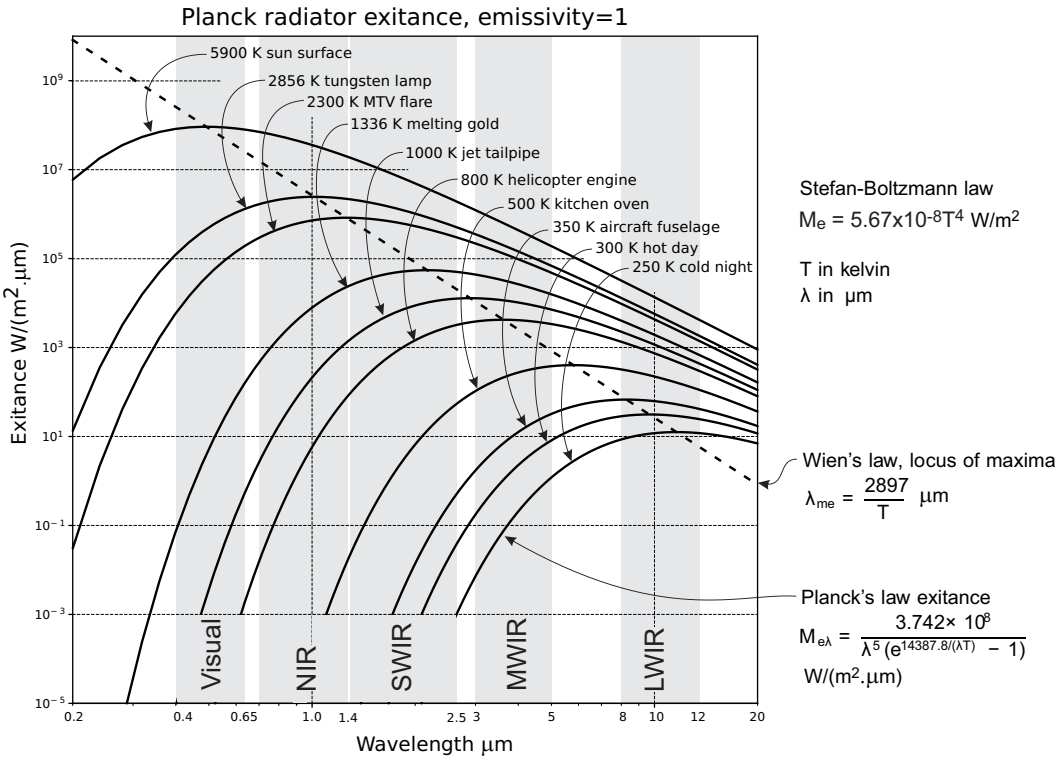

Figure 2.3. Radiation of a blackbody according to Planck's law (temperature in K). Taken from [30], with permission.

of the hot gas that is released as a result of combustion. These are different sources of infrared energy. These parts produce the highest radiation in the infrared spectrum and therefore these are the areas of interest to the MANPADS missile. The radiation produced by the aircraft engine is typically due to the hot metal engine blades and the exhaust walls. The radiation from the engine is therefore proportional to the exposed area of the engine and exhaust walls that are visible to the missile. The design of the engine therefore plays a role in the quantity of the radiation that will be produced.

The aircraft plume is produced by the exhaust combustion gasses. The plume generally consists of CO_2 and water vapour. The majority of the plume signature is due to the CO_2 gas and is significant in the MWIR band [32]. A reduction in the amount of CO_2 produced by the engine is therefore key in reducing the radiation from the plume.

Aerodynamic heating is the heating of a solid body by its passage through air due to friction and compression processes [33]. The amount of heat produced is a function of the speed, altitude and the surface area of the body. In the case of an aircraft, the head or nose, the wing leading parts, the

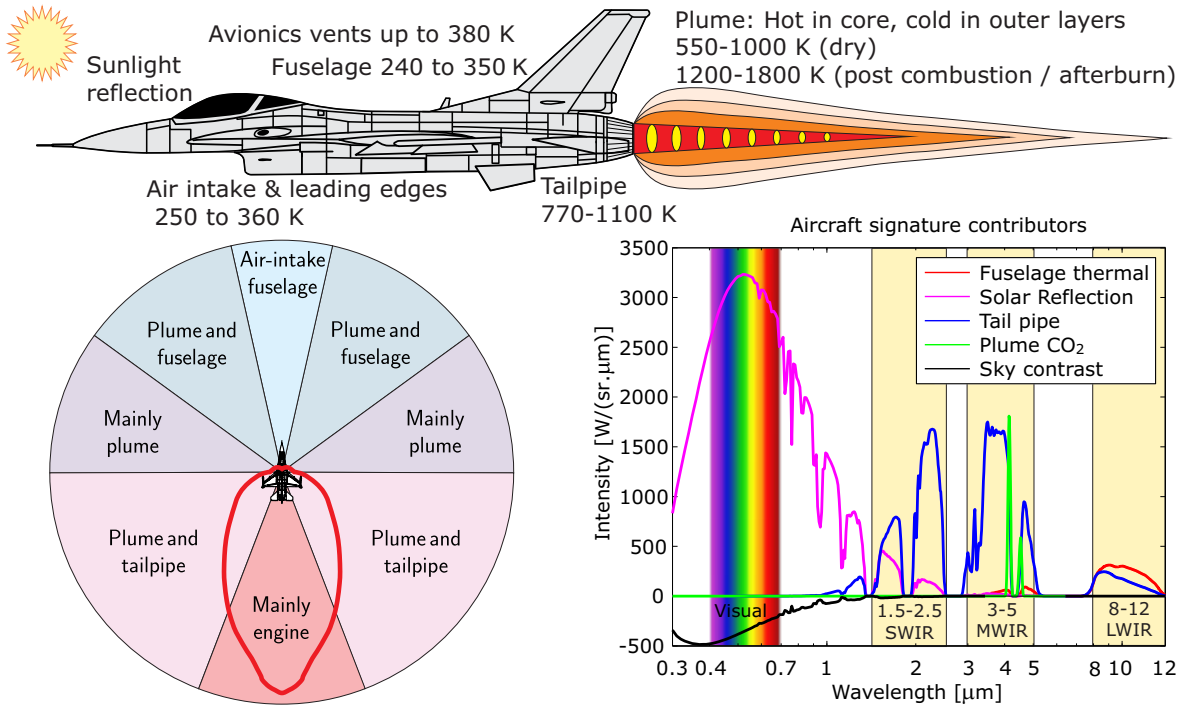

Figure 2.4. Aircraft signature components. Taken from [30], with permission.

vertical and horizontal stabilizers and the aircraft fuselage are the main contributors to the signature from aerodynamic heating [34, 35]. The radiation that will be observed by the missile is a function of the body area that is visible to the missile seeker. The signature produced by aerodynamic heating is therefore a function of the angle at which the missile views the aircraft body since this determines the amount of area that will be visible to the missile. Other sources of infrared radiation which contribute to the target signature are the reflected sunlight and the reflection of the earth-shine on the aircraft body [35, 36].

The radiation that the missile seeker detects is a function of the area that the seeker is exposed to. When the aircraft is at a long range, the radiation as seen by the missile can be approximated as a point source which has spherical radiation which is equally distributed. Given that the cold parts fuselage of the aircraft is mainly radiating in the LWIR, the missile operating in the MWIR at the launch range will mainly detect the aircraft engine and plume [37]. The hottest part of the plume is the part closest to the engine exhaust and can therefore be seen as co-located with the engine exhaust at long range. This supports the choice to represent the target as a point source at long ranges. It is also desirable to find a jam signal that will be effective from a long range and it is therefore adequate to test the effect of the jam signals from long ranges in which the target can be modelled as a point source.

2.3 HISTORY OF MANPADS

The use of optical systems in warfare can be traced back to 212 BC in the Syracuse battle [7]. It is believed that an array of mirrors were used to focus the rays of the sun towards the enemy ship sails in order to burn holes in the sails. This method demonstrated that optical energy can be harnessed and used against the enemy. The use of IR energy for warfare was first studied in the 1930s and during the second world war particularly for surveillance [38]. This led to the study of the use of IR in the detection and tracking of targets of interest. The result was the development of the heat seeking missile which began service in the 1960s [39].

The first generation MANPADS consists of a spin-scan seeker which typically has a spinning rising sun reticle which contains a phasing sector. The spin-scan seeker uses AM to encode the target position. The further the target image is from the center of the reticle, the greater the signal amplitude becomes and this is used to track the target position [40]. The bottom half of the reticle contains a 50% transmission material which is called the phasing sector. The spin-scan seeker produces a null signal when the target is in the center of the seeker field of view (FOV) and therefore the seeker cannot track a target at the center of the FOV. This occurs because the reticle produces no chopping when the target is in the center of the FOV and no modulation can be produced in the center. This causes instability in the AGC and results in the seeker producing a spiral type of steering because it cannot keep the target at the center of the FOV [18, 41]. The spin-scan seeker operates in the 2 - 2.7 µm spectral band and this restricts the seeker to hot targets in a tail-on engagement [41].

The second generation MANPADS is the conical-scan (also known as con-scan) seeker which was developed to correct the flaws found in the spin-scan seeker in the 1970s. The con-scan seeker uses FM to encode the target position. It consists of a stationary reticle and nutating optics which cause the target to move in a circular fashion on the reticle. This type of scanning produces a pulse train signal when the target is in the center of the seeker FOV and an FM signal when the target is off center. This type of modulation allows the seeker to successfully track the target when it is in the center of the FOV, reducing the noise in its tracking signal. The majority of con-scan seekers operate in the 3 - 5 µm which allows them to track a wider range of angles as opposed to the spin-scan seeker which operates in the tail region of the aircraft [31].

The third generation MANPADS consists of the rosette scan seeker which was developed in the 1990s. The rosette scan seeker scans a small instantaneous field of view (IFOV) in a rosette pattern and

consists of a single detector. The IFOV is moved about in a rosette pattern with the pattern of the petals overlapping so that the total FOV is scanned. The advantage of this type of scanning is that the dwell time on the target is very small in each scan and therefore there is little opportunity to jam and deceive the seeker or to decoy the missile with a flare. The rosette scan also has the advantage that is can resolve two targets in its FOV because of the small IFOV [42].

The fourth generation MANPADS is the focal plane array (FPA) imaging seeker which was developed in 2005. The FPA seeker consists of a number of detectors which scan the FOV in a row progression from left to right or in a column progression from top to bottom. The FPA seeker creates an image of the scene and is able to detect the shape of the aircraft. This type of seeker is the most robust against flares and jammers and countermeasures are still being developed to defeat this type of missile [43]. The fourth generation MANPADS is currently not used in warfare but will be used in the near future. The fifth generation MANPADS consists of a full imaging seeker which does not use scanning like the FPA but has constant full view of the scene or FOV.

2.4 PROLIFERATION OF MANPADS

The effect of a MANPADS attack on a civilian plane is enough to draw international attention to the perpetrator, and to cause significant economic impact on the affected state. One hit not only risks the lives of people (both on and off-board the aircraft), but causes trauma and subsequent fear of flying, destruction and loss of property and the possible loss of jobs for those in the travel industry [44]. This type of disturbance is the kind that is desirable to a rebel group who wish to attain significant attention for their cause. With this in mind, a number of agreements have been established to reduce the possibility of MANPADS landing in the wrong hands. The Wassenaar arrangement is one such agreement that 42 states have entered into to bind themselves to certain standards in the use, storage, security and export of MANPADS [45]. The Wassennar agreement was established in the year 1996 and while there are only 42 signatories who abide by the agreement, it has received great approval from the international society and a large number of other states claim to abide by it. The weakness in this agreement though, is that unlike a treaty, the agreement is not legally binding. This therefore means the states that joined the agreement are not legally bound to adhere to the conditions set out in the agreement. The agreement also stipulates that it is at the discretion of the supplying state to satisfy itself that the recieving state complies with the terms of the agreement when exporting arms [46]. Since the agreement is not legally binding, the requirements set out in the agreement are not enforced by any particular body.

While the Wassenaar and other agreements do help to reduce the exchange of dangerous arms to certain states, it should also be noted that dangerous arms such as the MANPADS are generally obtained by rebel groups through theft, corruption and ambush [46]. Theft of government stockpiles generally takes place when a state is weakened as was witnessed in Lybia in the events that took place in 2011 [47]. The Libyan uprising took place when forces that were loyal to Colonel Muammar al-Qaddafi opposed a large number of anti-government protesters who sought to dissolve his government. The civil war persisted for a period of 9 months resulting in almost 20 000 casualties. Under such conditions, the secured stockpiles were at some point left with no security due to the intensity of the war, resulting in easy access of military weapons including MANPADS. The ruling government also hired a large number of Sahel mercenaries in the conflict who took weapons with them once the war was concluded. This also resulted in a large number of MANPADS that were in the government stockpiles to be lost. The Libyan conflict demonstrates that while a Wassennaar agreement might be in place, it is of no use during a war, albeit civil or multi-national. It is estimated that 10 to 20 000 MANPADS were stolen during this war and that they were primarily first and second generation MANPADS [46]. A similar phenomenon took place in the Syrian civil war where a number of foreign and domestic forces are in opposition to the ruling government [48]. The war began in 2011 and currently continues. Four MANPADS attacks took place in 2012 against military aircraft and these took place after alleged raiding of military stockpiles. These two cases illustrate the effect of government destabilization on the proliferation of MANPADS.

Another weak spot in the control of MANPADS proliferation is the weakness of certain borders which make the transport of illegal arms easy. Two first generation MANPADS were launched at a civilian plane in Mombasa, Kenya in the year 2002 [49]. The MANPADS used in the attack were traced back to missiles that were shipped from the Ukraine to Yemen which were allegedly diverted to Mogadishu, Somalia [46]. From Somalia, the MANPADS were illegally smuggled into Kenya where the attack took place.

2.5 OPERATION OF THE SECOND GENERATION CONICAL-SCAN MANPADS

This section describes the general structure of the con-scan seeker. The operation of the seeker is described in four specific stages; the optics, spatial filtering, signal processing and the guidance of the missile. A basic description of the operation of the missile is given here. The infrared radiation from the scene is collected through the optics in the seeker. The radiation is chopped or modulated using a spatial filter called a reticle. The signal is detected using an infrared detector which operates in

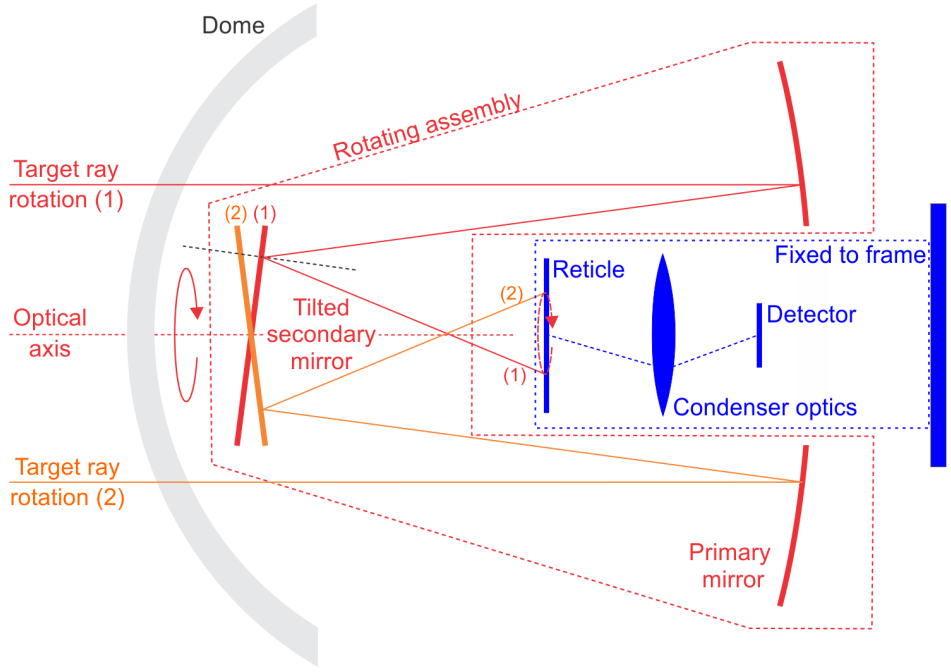

Figure 2.5. Conical scan optics concept. Taken from [30], with permission.

some infrared band. The detected signal is then converted to an electrical signal which can then be processed. The signal is processed and a guidance/steering signal is calculated. The steering signal is used to provide guidance commands to the missile body which causes the missile to turn a certain direction.

2.5.1 Optics

The conical-scan seeker typically consists of a spinning optical assembly comprising the primary mirror, a tilted secondary mirror, and a stationary reticle as shown in Figure 2.5. The rotating assembly provides gyroscopic sight line stabilisation, thereby removing the need for stabilisation hardware.

The primary mirror axis is aligned with the sightline and axis of rotation, i.e., optically stationary with respect to the object-space optical axis. The secondary mirror axis is tilted with respect to the axis of rotation, which is *not optically stationary* with respect to the object-space optical axis. The tilt of the secondary mirror creates an angular offset of the target image on the reticle, bending the optical axis. As the secondary mirror rotates, the image-space optical axis offset (centre of the image) moves in a circle in the focal plane. This effect is called the nutation of the optical axis and effectively shifts the image on the reticle around the reticle centre. The trace of the object-space optical axis on the reticle is called the nutation circle. Note that the image remains upright as the image nutates as shown in

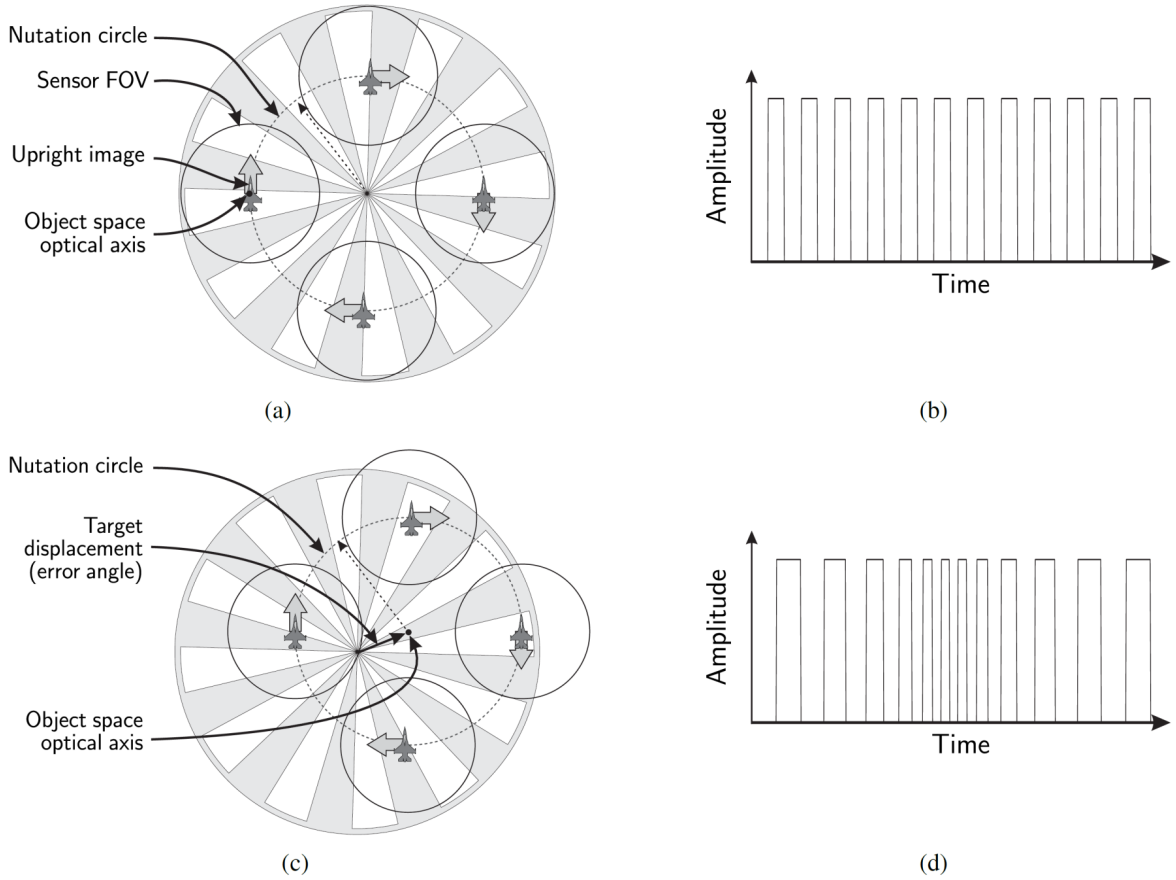

Figure 2.6. Typical wagon wheel reticle (a) with no error, and (b) the associated detector signal, (c) the wagon wheel reticle with a nutation error and (d) the associated detector signal [23]. Used with permission.

Figs 2.6 (a) and 2.6 (c); the image moves, it does not rotate.

2.5.2 Spatial filtering

The reticle has a carefully designed pattern with transparent and opaque regions; often a variation of a simple wagon wheel shape, like that shown in Figure 2.6 [14, 15, 50–54].

The object-space scene is imaged onto the reticle. As the scene image moves across the reticle, the optical flux signal from a small object in object space (the target) is chopped or modulated across the regions of different transparency in the reticle. The signal is detected as a sequence of pulses as the signal is chopped. The target IR signature is long-term constant, hence the modulation of the detector signal being solely a result of the reticle modulation. As a result, the signal from a target can be considered a fixed-carrier FM signal. Large objects (e.g. clouds) cover a large area on the

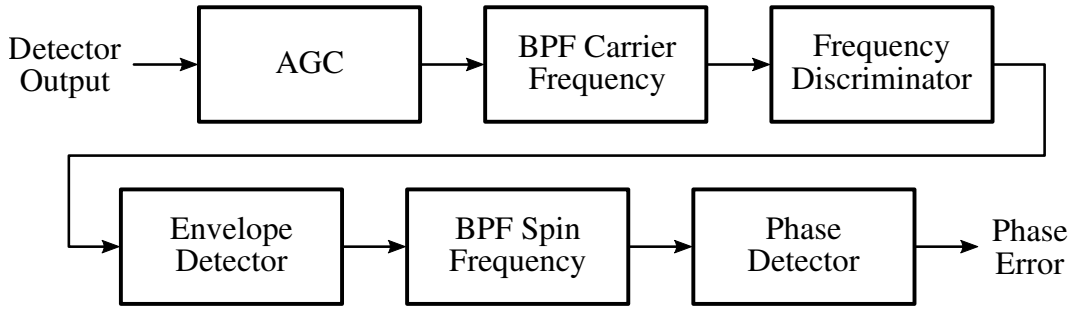

Figure 2.7. Signal processing block diagram [23]. Used with permission.

reticle, several times the reticle spoke width, resulting in an averaging effect, called spatial filtering. The reticle's spatial filtering suppresses large objects in the image, but has less effect on point source targets. The detector is placed behind the reticle, converting the chopped IR signal to an electronic signal. The detector signal is processed to extract the target movement, which is then used to create a steering signal for the seeker.

The nutating movement of a small target spot in the image creates a frequency-modulated signal, with the modulation index depending on the target displacement error relative to the optical axis [13–19]. For an on-axis small target, the nutation circle is centred on the reticle centre (see Figure 2.6 (a)) and the FM modulation depth is zero (see Figure 2.6 (b)). For an off-axis small target, the nutation circle shifts its centre away from the reticle centre (see Figure 2.6 (c)), and the small target chopped signal has a non-zero modulation depth (see Figure 2.6 (d)). The frequency-modulation depth can be used to determine the radial target displacement error angle, and the phase of the modulation signal envelope gives the angular rotation of the target. The target radial displacement error angle and rotational displacement angle can therefore be extracted from the signal by FM demodulation techniques. When a target image moves near the reticle centre, the modulation frequency can become very high. Furthermore, it is not possible to practically realise the very small spoke widths near the centre of the reticle, with the result that the centre of the reticle loses reticle pattern resolution. For these reasons, the centre of the simple wagon wheel reticle is normally modified in practice to overcome these difficulties [55].

2.5.3 Signal processing

A typical block diagram of the signal processing used in the conical-scan seeker is shown in Figure 2.7. This processing block has been used in a number of studies for the conical-scan seeker and is therefore considered representative of the actual processing circuitry [13–17, 19, 55, 56]. The detector signal first

passed through a DC-decoupling stage by using a capacitor (not shown in the diagram). The signal is then passed through the AGC circuit to ensure that the signal is at a constant peak level for processing. The signal amplitude is expected to increase as the missile flies closer and closer to the target and the AGC is required to adjust the signal peak amplitude to remain constant for correct demodulation. Likewise, the AGC will boost weak signals resulting from atmospheric attenuation or very distant targets. Maintaining a constant peak value is important for subsequent processing. The output of the AGC is passed through a band-pass filter (BPF) that is centred at the carrier frequency in order to filter out the background noise from other sources.

The output of the BPF is passed through a frequency discriminator which can be implemented using a low-pass filter (LPF) or high-pass filter (HPF). The frequency discriminator converts the FM information contained in the signal into an AM signal, by running up and down the slope of the discrimination filter. The carrier frequency of the seeker is centred on the center of the slope detector so that frequencies that are below the carrier frequency will be attenuated and the frequencies above the carrier are amplified.

The AM signal is then processed by the envelope detector which will filter out the carrier signal and detect the envelope signal. The envelope signal will be at the nutation frequency of the seeker and this signal will contain the required information to determine the radial and angular position of the target.

The signal is then further filtered using the BPF that is centred at the nutation frequency to remove any high frequency components remaining in the signal. The output of the BPF can then be used to determine the radial position of the target. The phase detector is a comparator circuit which compares the phase of the signal with a reference signal in order to determine the phase difference. This information can be used to determine the angular position of the target in the reticle space.

2.6 CON-SCAN SCANNING PROCESS

In order to understand how the detector signal behaves with changes in the target error, the scanning geometry will be considered. The geometry of the scan parameters with reference to the nutation circle and reticle can be described as shown in Figure 2.8. The radius of the nutation circle is r, the distance between the centre of the nutation circle and the centre of the reticle is given by R_0. The distance between the centre of the reticle and the target image is given by D, and the angle of the nutation vector

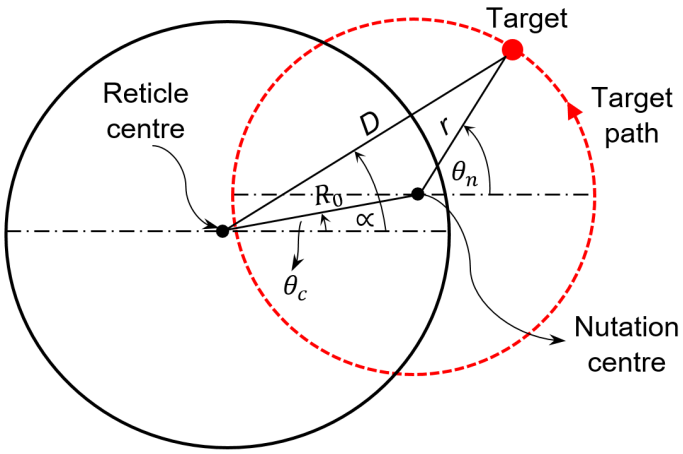

Figure 2.8. Geometry of the scan process in the conical-scan seeker. Adapted from [22], © 2017 IEEE.

is given by θ_n. The angle of the line extended between the reticle centre and the nutation centre is given by θ_c and the angle of the line extended between the reticle centre and the target instantaneous position is given by α. With the reticle centre as reference, the centre of the nutation circle can be expressed in rectangular coordinates as

$$x_n = R_0 \cos(\theta_c) \tag{2.2}$$

$$y_n = R_0 \sin(\theta_c) \tag{2.3}$$

The position of the target can then be expressed as

$$x_t = x_n + r\cos(\theta_n) \tag{2.4}$$

$$= R_0 \cos(\theta_c) + r\cos(\theta_n) \tag{2.5}$$

$$y_t = y_n + r\sin(\theta_n) \tag{2.6}$$

$$= R_0 \sin(\theta_c) + r\sin(\theta_n). \tag{2.7}$$

The angle from the reticle centre to the target is therefore given by

$$\alpha = \arctan\left(\frac{y_t}{x_t}\right) \tag{2.8}$$

$$= \arctan\left(\frac{R_0 \sin(\theta_c) + r\sin(\theta_n)}{R_0 \cos(\theta_c) + r\cos(\theta_n)}\right) \tag{2.9}$$

The instantaneous frequency of an FM signal is given by [57]

$$f_i = \frac{1}{2\pi}\frac{d\phi}{dt}. \tag{2.10}$$

where ϕ is the phase of the signal. If the phase of the signal is given as $\phi = (\alpha + \psi)$, then the instantaneous frequency can be computed as

$$f_i = \frac{1}{2\pi}\frac{d}{dt}\left[\arctan\left(\frac{R_0\sin(\theta_c)+r\sin(\theta_n)}{R_0\cos(\theta_c)+r\cos(\theta_n)}\right)\right]. \tag{2.11}$$

Deriving Equation 2.11 and using trigonometric identities, it can be shown (see Appendix A) that the instantaneous frequency is

$$f_i = \frac{f_n\left[1+\frac{R_0}{r}\cos(\theta_c-\theta_n)\right]}{1+\left(\frac{R_0}{r}\right)^2+2\left(\frac{R_0}{r}\right)\cos(\theta_c-\theta_n)} \tag{2.12}$$

where f_n is the nutation frequency of the seeker. Substituting $\rho = \frac{R_0}{r}$,

$$f_i = f_n\frac{1+\rho\cos(\theta_c-\theta_n)}{1+\rho^2+2\rho\cos(\theta_c-\theta_n)}. \tag{2.13}$$

For zero target error (i.e. nutation circle centred on reticle centre) then $\rho = 0$. As the target error increases, ρ increases and when the nutation circle fully exits the reticle or the FOV then $\rho = 2$. This is because the distance from the centre of the reticle to the nutation centre must equal the nutation circle diameter for the circle to be completely off the reticle. When $\rho = 1$, the nutation circle is halfway off the reticle with 50% of the scan cycle occurring on the reticle and 50% off the reticle. It can be seen from Equation 2.13 that when $\rho \ll 1$, the denominator is approximately 1 and the instantaneous frequency is then

$$f_i \approx f_n\left(1+\rho\cos(\theta_c-\theta_n)\right). \tag{2.14}$$

This produces an instantaneous frequency that varies sinusoidally with time since θ_n is a function of time. The produced signal is a pure FM signal. Due to the denominator in Equation 2.13 having multiple components of ρ; an increase in ρ, causes the denominator amplitude to increase faster than the amplitude of the numerator. This implies that the maximum value of the denominator will be greater than the numerator value and the minimum value will be less. As the minimum values approach zero, the division will cause infinitely high output values. This translates to high frequency components when the nutation circle center moves further away from the center of the reticle. This is because the wagon wheel reticle produces extremely high frequency components when the target image nutates close to the center of the reticle where the spoke width is very small. This phenomenon produces an infinitely large bandwidth which makes demodulation of the signal difficult. Due to this difficulty, the con-scan seeker is designed to operate within a small range of errors, and maximizes on those.

2.7 STATIC GAIN CURVE

The static gain of a system describes the ratio of the output to the input under steady state conditions [58]. The static gain curve is used to evaluate the performance of a system and to determine the best operation region of the system. The conical-scan seeker has the typical static gain curve shown in Figure 2.9. As

seen in the figure, the conical-scan seeker has a linear region where the measured output is proportional to the geometric error. Driggers [58] approximates this region to be only 10% of the total FOV. Beyond this linear region, the measured output no longer corresponds to changes to the input. This is because the frequency components that are present in the detector signal at large errors exceed the bandwidth of the demodulator thus causing the demodulated signal to be distorted. The static gain curve shows that the seeker will produce minimal steering when the target is far off center thus causing the target to be lost. This is why the conical-scan seeker is said to be optimal for tracking but not good for target acquisition [59].

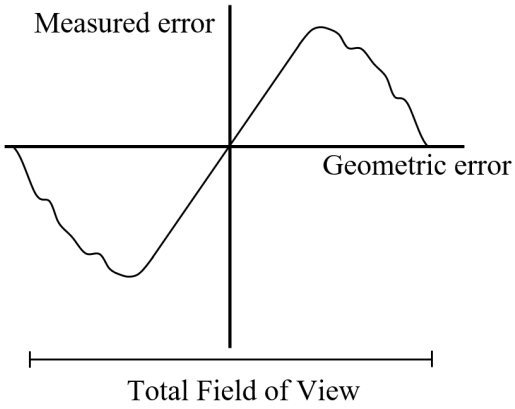

Figure 2.9. Typical static gain curve. Adapted from [19]. Used with permission.

2.8 IR COUNTERMEASURES

2.8.1 History of IR countermeasures

One of the many instances where optical dazzling was used in battle, was in the year 1415 when the sun was used to dazzle the French soldiers in the Battle of Agincourt [7]. The English archers of King Henry would wait for the sun to dazzle the soldiers eyes before they would shoot at the soldiers. Other tactics that were used over the centuries include the use of smoke screens to deny the enemy to see the attacker, the use of paint patterns to disguise equipment and machinery, the technique of “flying out of the sun” to conceal an attacking aircraft. The exploitation of infrared energy occurred during the second world war particularly for surveillance. During the second world war, a number of radar based countermeasures were developed and these were later applied to the optical space. The first demonstration (in Europe) of the use of a laser for damage was illustrated in 1964 to damage a target 100 m away [39].

The heat seeking missile started service in the 1960s and this immediately created a need for countermeasure development against the missile. One of the first countermeasures developed in response to the heat seeking missile is the Magnesium/Teflon/Viton (MTV) flare [9, 60]. The dispensing of the flare created a high enough infrared signature that could decoy the heat seeking missile. This was a short lived victory with the introduction of the second generation MANPADS in the 1970s which was more resistant to the MTV flare [41].

The missile technology was further advanced by introducing the two color missile which could reject the MTV flare by using two spectral bands to track the target [61]. The signature of the target is measured in both the SWIR and the MWIR infrared bands, and the ratio of the two bands is used to determine if a flare is present in the FOV. The MTV flare has a strong signature in the MWIR and a weak signature in the SWIR and can therefore be identified by the two colour missile [61]. The spectral flare was then developed in the 1980s to defeat the spectral missile and was found to be effective against the second generation MANPADS [62].

The development of jammers began in the late 1960s making use of a hot, radiating, element and a mechanical chopper on-board the aircraft [7]. These jammers are called thermal jammers and they typically have a wide beamwidth. The thermal jammer radiates in all angles and makes use of the mechanical chopper to create pulses in the radiated signal. The disadvantage with the thermal jammer is that it fails to produce high enough J/S ratios to produce break-lock especially in the conical-scan seeker based missiles. This limitation is due to the wide beamwidth in the thermal jammer which causes less energy to fall on the seeker FOV. Due to the jammer radiating in all angles, a large amount of radiation that could have been focussed on the threat, is wasted. These limitations led to the development of lasers for use in infrared countermeasures.

Laser jammers were first tested against infrared missiles in the mid 1970s and were shown to be effective [39]. The challenge that was encountered then and still remains a challenge in the present age is that the known laser materials do not have natural resonance at the frequencies of the infrared threats [11]. This requires that frequency multiplication be used to generate a laser signal in the frequency band of interest and this results in a loss of laser power [11]. Another challenge with a laser jammer is the need for accurate directing of the beam to the seeker head, considering how narrow the laser beam is. This requires accurate tracking of the missile throughout the jamming process, this complicates the jamming engagement. This type of jamming is encompassed in the DIRCM system

which has been shown to be effective against conical-scan and other seekers and has been successfully deployed in some developed countries [63].

2.8.2 DIRCM system

The DIRCM system is used for administering jam signals to an approaching missile. The DIRCM system consists of a missile-approach warning (MAW) system which identifies an approaching threat, the acquisition, pointing and tracking (APT) system which is a beam director, the jam source or laser and the controller [39]. The MAW system generally consists of an array of sensors which are typically electro-optical starring sensors which are used to obtain a 360° surveillance of the platform surroundings. The MAW system provides a warning to the controller with a bearing of the approaching threat direction. The controller then sends the bearing information to the APT which then acquires a higher precision direction of the approaching threat. The APT then points the laser beam in the appropriate direction and signals the controller to administer the jam signal.

A closed loop DIRCM system injects a constant laser beam to the missile seeker optics and concurrently reads the beam's reflection from the seeker (cat-eye effect). The reflected beam is used to determine the type of scanning that the missile seeker is using and this is then used to determine the appropriate jam signal to use against the seeker. The retro-reflected beam is continually monitored in order to determine if the jam signal is causing the seeker break lock, in order to determine if the jam signal being administered is effective or not.

An open loop system cannot identify the missile threat and therefore utilises either a single pre-selected jam signal or a sequence of jam signals in a specific order to defeat the missile. The pre-selected jam signal and the sequence of jam signals are chosen based on the expected missile types expected in the platform environment. The open-loop system also monitors the effect of the jam signal by observing if a direction change has occurred in the missile flight path.

A closed loop DIRCM system is more effective because the missile seeker scanning method, is detected before the jam signal is selected and this ensures the correct allocation of jam signals to the threat. However, note that the closed loop system is much more complex than the open loop system since the reflected beam from the seeker head has to be detected and accurately decoded to determine the seeker type. If the protected platform deployment environment is well known, the pre-selection of a jam signal also proves to be effective and the open loop system therefore performs just as effectively

in this case. There has been claims of implemented closed loop DIRCM systems, but there are no systems that have proven to be effective as closed loop systems in field trials [18, 39].

2.8.3 Studies conducted on IR jam signals

A number of studies have been conducted on the operation of the reticle based seeker [12–17, 19, 55, 56, 64–66], but there are few studies conducted on the effect of a jam signal on the reticle based seeker [13–17, 19]. One of the first significant studies on the effect of a jam signal on the con-scan seeker was performed by Tranchita *et al.* in 1993 [14]. The study was a theoretical analysis of the interaction of the jam signal with the target induced signal generated by the target nutation on the reticle. The modulated target signal and the jam signal are represented as a Fourier series and the analysis is conducted for a 50% duty cycle. The main findings of the study are that the jam signal will cause the nutation circle on the reticle to nutate by a difference frequency given by $f_\delta = f_j - f_t$ where f_δ is the difference frequency at which the nutation circle will oscillate, f_j is the jam signal frequency and f_t is the frequency of the target signal. This means the nutation circle will not be stationary on the reticle but will oscillate continually by the difference frequency. It is predicted that this will induce an oscillatory behaviour in the line of sight (LOS) rotation rate which results in an average tracking of the target over the difference frequency.

The first limitation with this analysis is that since the modulation action of the reticle is modelled at 50% duty cycle, it represents only the positions where the target is far off-center since the nutation action will basically produce AM and not FM in this region. The second limitation is that the jam signal is also limited to a duty cycle of 50%.

Chang [15] followed the same analysis and found that the phase delay of the jam signal relative to the target signal is the important parameter in inducing break-lock. This is for the case when the jam and target signal frequencies are equal. The study also found that the effect of the J/S ratio is a function of the target dwell time on the reticle. The study suggests that the radiation detected by the seeker is proportional to the time that the nutation path is present on the reticle. Since this analysis follows the same assumptions as the study by Tranchita *et al.* [14], the same limitations will therefore apply. Both studies suggest that a simulation of the seeker interaction with the target is required to truly understand the effect of a jam signal against the con-scan seeker [14, 15].

Bae *et al.* [13] developed a simulation to evaluate jam signal effectiveness against the con-scan seeker.

The study only tested J/S ratios of 1 and 2 and finds that an increase in the J/S ratio causes an increase in the jam signal effect. The tested jam frequency range is 50 Hz to 150 Hz. The study found that the average phase error oscillates at the difference frequency of the target and jam signals which is the same conclusion that Tranchita *et al.* [14] and Chang [15] found. The study also finds that the variance of the average phase error is highest when the jam signal frequency is close to the nutation frequency [13]. The jam signal is least effective at the nutation frequency. This means the jam signal is most effective when the jam frequency is close to the nutation frequency of the seeker but it is least effective when the jam frequency matches the nutation frequency.

Qian *et al.* [17] tested J/S ratios of 1 and 10 and $f_j = f_t$ and $f_j = 2f_t$ where f_j is the jam signal frequency and f_t is the target signal frequency. The study found that an increase in the J/S ratio from 1 to 10 produced an increase in the jam signal effectiveness. The study also found that the most effective jam signal frequency is $f_j = 2f_t$ which was different to what the previous studies had found.

Sahingil and Aslan [19] conducted a study with 3600 jam sequences and found only around 5% of those jam signals were effective against the missile seeker. This emphasized the difficulty in jamming the con-scan seeker. The study was conducted for a J/S ratio of 10, and swept the jam signal envelope or modulation frequency in the range 20 Hz to 140 Hz. The carrier frequency was swept from 50 Hz to 1 500 Hz and the duty cycle was also tested for the envelope and the carrier signal. The study concludes that the jam signal is most effective if it has parameters that are close to the target parameters and fails to be effective when the parameters deviate from the target parameters.

While these studies test the effect of the J/S ratio, the jam signal frequency and the duty cycle; the effect of these parameters is tested against a consistent pulse train. The effect of the jam signal parameters is not tested against different kinds of jam waveforms, and it cannot be assumed that the effect of these parameters is the same for different jam waveforms. The studies also only consider J/S ratios up to 10 while it is known that much higher ratios are required to induce break-lock [7].

2.9 CONCLUSION

The basic concepts related to the IR MANPADS and the evolution thereof were presented in this chapter. Due to the chemical composition of the atmosphere, there are atmospheric windows in which IR radiation can be optimally detected. These main bands are the SWIR, MWIR and the LWIR bands.

The first generation missile which utilized a spin-scan technology operated in the SWIR band and this restricted this MANPADS to tail on engagements. The second generation MANPADS makes use of the conical-scan seeker (also known as con-scan) which operates in the MWIR band. The second generation seeker therefore has the advantage of being able to track at different angles and not only at the tail of the aircraft.

Due to the destructive effects of MANPADS, a number of measures have been taken to reduce the proliferation of MANPADS. Such measures include the introduction of laws that govern the use, storage and exchange of MANPADS, such as the Wassenaar agreement. While such agreements prove useful when enforced, there is currently little or no monitoring of the enforcement of the agreement. It is also known that the acquisition of MANPADS by rebel groups is mainly by theft or corruption, these actions are not easily monitored when a state is weakened. Since a number of countries such as Syria, still experience civil war, the probability of further proliferation of MANPADS is still high. This means countermeasures have to be well developed to ensure the safety of military and civil aircraft.

The introduction of the MANPADS prompted the much required development of countermeasures in the 1960s. Flares advanced from the simple MTV flare to the more complex spectral flare which is more effective against two colour missiles. Jammers advanced from using a hot element with a mechanical modulator to the more advanced laser jammer which produces much higher J/S ratios. The DIRCM system encompasses the use of a laser for jamming and this system has been shown to be effective against the con-scan seeker. The basic subsystems that describe a DIRCM system were described. While a number of studies have been conducted on the interaction of the jam signal with the target signal, the studies are restricted to the low frequency type of jam signal. This leaves a gap in understanding the effects of the jam signal parameters in different jam signal waveforms.

CHAPTER 3 MODELLING AND SIMULATION

3.1 CHAPTER OBJECTIVES

This chapter describes the seeker design that was used to simulate the conical-scan seeker and the processor used to track the target. The effect of jamming the conical-scan seeker is only as accurate as the model used to represent the seeker to be jammed. The designed seeker was therefore thoroughly tested to ensure acceptable performance. The chapter describes the design choices that were made and the motivation behind them. The model validation process is also given to show that the model is a reasonable representation of the missile behaviour. Some of the results found by other authors are also used as validation of the expected behaviour of the conical-scan seeker.

3.2 SEEKER OPTICS

The radiation from the scene is collected by the primary mirror and reflected onto the secondary mirror as described in the previous chapter. This portion of the seeker was not modelled since it only provides the means by which the target radiation is projected onto the reticle. The reticle was simulated in a wagon wheel pattern with transparent and opaque sections as shown in Figure 3.1. The wagon wheel reticle was chosen since it is the typical choice for a number of similar studies [13, 15–17]. The nutation circle is shown in the dotted line and was designed to be 60% of the reticle radius. When the target is in the center of the FOV, the nutation circle is centred on the reticle center as shown in Figure 3.1(a). When the target moves off center the nutation circle moves from the center of the reticle and is centred at the position of the target. The nutation radius was chosen to be 0.6° whereas the reticle radius was chosen to be 1°. The area outside of the reticle is considered opaque and the detector can therefore not detect the target beyond the boundary of the reticle. The point at which the outside of the nutation path touches the outer edge of the reticle is the edge of the total FOV. In this case, the edge of the FOV is 1.6°. The total FOV can also be given as a diameter, which is 3.2° in this case. As seen in Figure 3.1(b), the nutation circle can move up to 1.6° as this is the maximum point at which the nutation circle still

touches the reticle and is therefore the last point of the total FOV. The point seen at the zero angle on

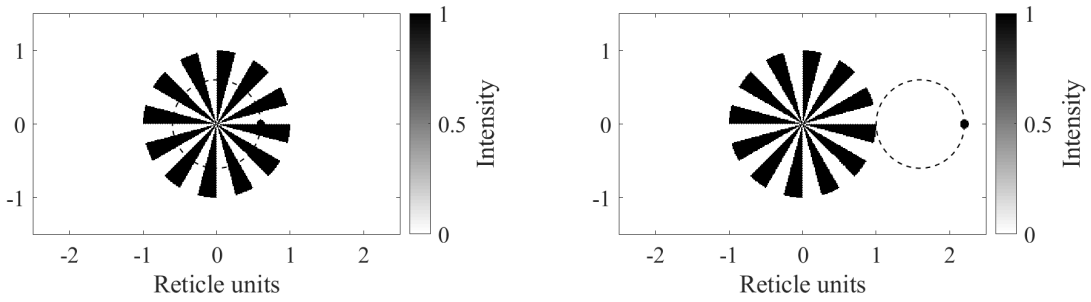

(a) Target error = 0 **(b)** Target error = 1.6°

Figure 3.1. (a) Simulated wagon wheel reticle with no error and (b) simulated wagon wheel reticle with error of 1.6°.

the nutation radius in Figure 3.1 is the point source that represents the target. The scene is scanned by moving the target in 1° increments up till the 360° of the nutation circle is covered. This represents the nutation action that is achieved in a practical circuit using spinning mirrors. The reticle is kept stationary and the target is nutated about the reticle on the nutation circle and each time the target is moved, the reticle image and the target image are multiplied to determine the detector signal at that point in time. The scan cycle of the scene is 10 ms which means the target point source must move through the 360° circle in 10 ms. This means the step size in the temporal space or the sampling rate is 27.8 µs. The target intensity is multiplied by 1 in the regions where the reticle is transparent and the by 0 when the reticle is opaque. The resultant signal is the detector signal.

The present analysis did not consider background clutter, flare countermeasures, or other objects in the image: only the target as a small and the sole object in the field of view. These assumptions are believed to be reasonable as the FOV is realistic, and the effects of the target and jammer can be analysed without interference from other sources.

The reticle consists of 12 spokes which means 12 opaque parts and 12 transparent parts. This results in 24 sections in the reticle. The nutation frequency was chosen to be 100 Hz as this is the nutation frequency used in a number of similar studies. [13–17, 19, 55, 56] The resulting carrier frequency is

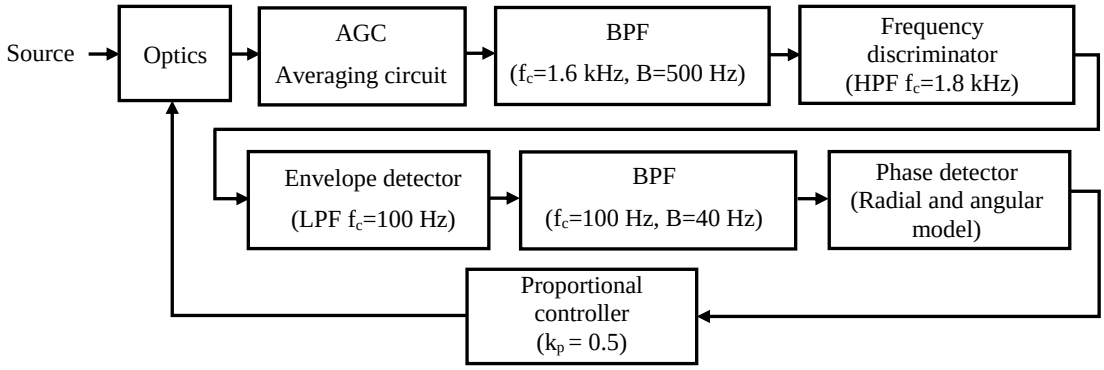

Figure 3.2. Signal processing block diagram [23]. Used with permission..

therefore $12 \times 100 = 1.2$ kHz. The reticle image generated for the simulator was developed by W. du Plessis [67].

3.3 SEEKER PROCESSING

The signal processing used to demodulate and track the target is shown in Figure 3.2. The detector signal passes through an AGC system which adjusts the amplitude of the signal to a fixed magnitude for further processing (the information is contained in the frequency of the signal and not the signal's amplitude). The AGC circuit is implemented using an averaging circuit. The mean value over the previous scan cycle is used to determine the gain of the current detector amplitude. Depending on the missile type, the AGC may or may not be followed by a hard limiter. In this study it was chosen to not use a hard limiter in common with the majority of authors [13–17, 19, 55, 56]. Note that because the effect of the saturation or hard limiting in electronic components was not modelled, the results obtained here assumed linearity and therefore represent the highest possible effect achievable with the specific jam codes. Initial experiments indicated that hard limiting changes the effectiveness of the various jam codes. Jam codes for seekers with hard limiting requires more research.

The signal is then passed through a BPF which is centred at 1.6 kHz to remove any low- and high-frequency background signals and noise. The carrier filter is centred at 1.6 kHz in the simulation, and not at the carrier frequency in order to extend the linear region of the static gain curve of the seeker, allowing a wider range of radial positions to be demodulated accurately [22, 55]. This is explained further in Section 3.5.3. The signal is then passed through a frequency discriminator which converts the FM signal to an AM signal. The frequency discriminator is implemented using a HPF with a cut-off frequency of 1.8 kHz. The signal is then passed through an envelope detector which gives the envelope of the signal. The envelope detector is implemented using a full-wave rectifier and a LPF with a cut-off

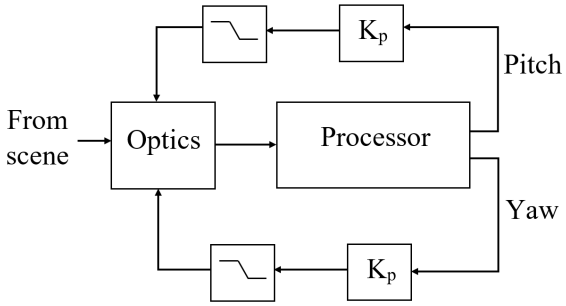

Figure 3.3. Model track loop.

frequency of 100 Hz. The high-frequency components that are generated by rectification are filtered out by the BPF centred on the nutation frequency, and a phase detector is then used to determine the phase of the signal. The BPF is centred at the nutation frequency of 100 Hz with a bandwidth of 40 Hz to provide a reasonable quality estimate of the envelope. The phase detector is implemented using a second order polynomial fit to the data as a reference for the radial and angular position of the target. The phase detector produces the target angular error (target displacement from the optical axis) and the the BPF at the spin frequency produces the radial error. The target displacement from the optical axis is therefore given in polar form and is converted to rectangular representation which results in the pitch and yaw errors.

3.4 SEEKER TRACKING

The signal processing circuitry produces a radial and angular position of the target and this information is converted into a pitch and yaw error which is used for steering the seeker. The model track loop is shown in Figure 3.3. The yaw and pitch errors computed by the processor are multiplied by the proportional gain. A limiter is then applied to the control signal to limit the amount by which the gimbal can be steered. These two error signals are used to steer the seeker gimbal optical axis towards the target. The Ziegler-Nichols Method was used for tuning the controller, and the gain of 0.5 was found to be the optimal gain to use [68]. This gain was therefore chosen for the proportional controller. The gain is applied to the error signals, steering the gimbal with proportional control. A proportional controller is used because of its simplicity and this is the controller of choice in a number of simulations [13, 16]. The gimbal rate is limited to 0.18° per nutation cycle in order to model the effect of the inertia of the gimbal assembly. A value of 0.18° was chosen since it is estimated that the gimbal rate of the second generation MANPADS is 18°/s and this translates to a maximum of 0.18°/10 ms [55].

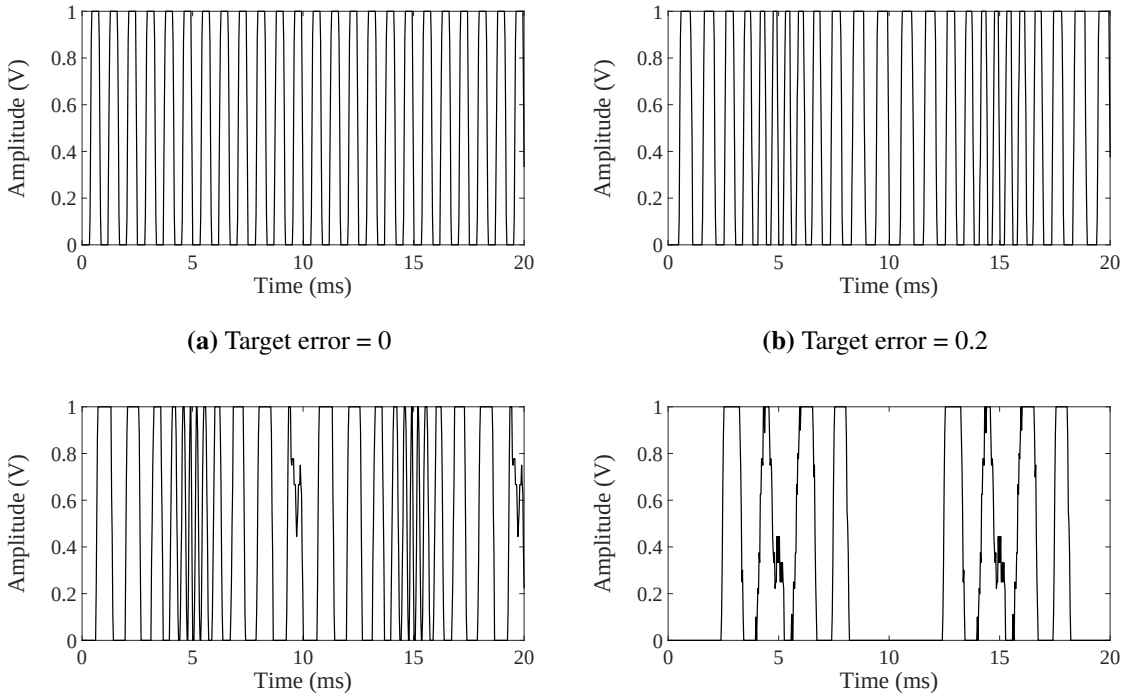

(a) Target error = 0

(b) Target error = 0.2

(c) Target error = 0.4

(d) Target error = 0.6

Figure 3.4. The validation of the detector signal at (a) 0, (b) 0.2, (c) 0.4 and (d) 0.6 target error.

3.5 MODEL TESTING AND VALIDATION

The model was validated by testing each subsystem to confirm expected performance and the results are given in this section.

3.5.1 Detector signal

The detector signal is obtained by multiplying the reticle image with the target image at each sample time. The scene image is restricted by the reticle geometry and the detector will only be exposed to the scene that falls onto the reticle geometry. The detector output at each point in time is computed by multiplying the scene image at that time instant and the reticle image at the same time instant. If the target point source falls in the opaque part of the reticle, the detector signal produces a low output. When the target point source falls on the transparent portion at that time instant, the detector will produce a high output. This results in an array of pulses which vary in pattern depending on the target position on the reticle space. The detector signal was tested to see the validity of the output by varying the target position and observing the resultant detector signal.

As seen in Figure 3.4, the detector output varies for different target positions. Figure 3.4(a) shows the

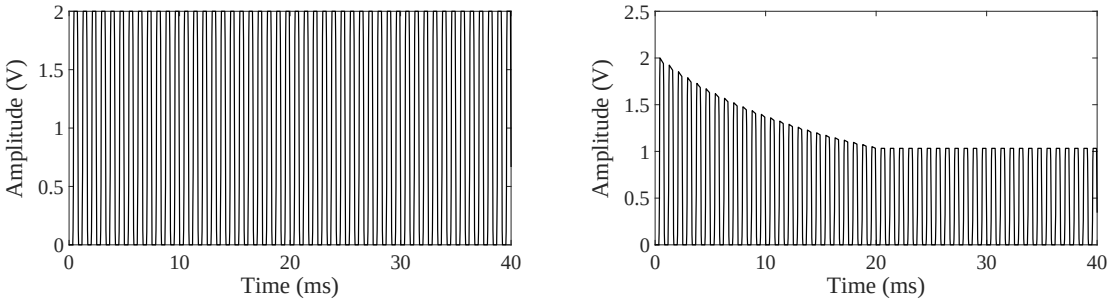

(a) AGC input **(b)** AGC output

Figure 3.5. The validation of the AGC at the (a) input and (b) output

detector signal for a target with zero error, meaning the target is in the center of the FOV. As seen in the figure, the detector output is not frequency modulated and the signal is at a constant carrier frequency. The output shown in Figure 3.4(b) is the output for a target at an error of 0.2° off center. The detector signal is slightly frequency modulated. As seen in Figure 3.4(c) the detector signal modulation index increases and the signal varies from low frequency to high. The signal in Figure 3.4(d) is for a target error of 0.6° off center. As seen in the figure, the detector signal has periods where there is no signal at all and this is the portion where the nutation circle falls off the reticle. This is expected for target positions greater than 0.4° because the nutation circle radius is 0.6 and the reticle radius is 1° and therefore the nutation circle can only move by 0.4° before the circle falls off the reticle. The detector signal is therefore considered validated.

3.5.2 AGC circuit

The AGC circuit receives the detector signal as input and adjusts the signal amplitude to ensure that the signal is processed at the correct amplitude. The AGC is used to either amplify or attenuate the detector signal to normalize it to some predefined amplitude. As seen in Figure 3.5, the AGC receives the detector signal at an amplitude of 2 V and adjusts the amplitude to 1 V. The AGC was implemented using an averaging circuit. The current detector input is multiplied by the mean of the two previous cycles. As seen in Figure 3.5(b) the AGC takes two cycles or 20 ms to adjust the detector signal from 2 V to 1 V.

The AGC was tested by applying a low frequency jam signal at a frequency of 10 Hz as seen in Figure 3.6. The AGC initially shoots up to the limit of the circuitry because it uses the mean of the previous two cycles which will initially be zero when the circuitry starts operating. These are transient

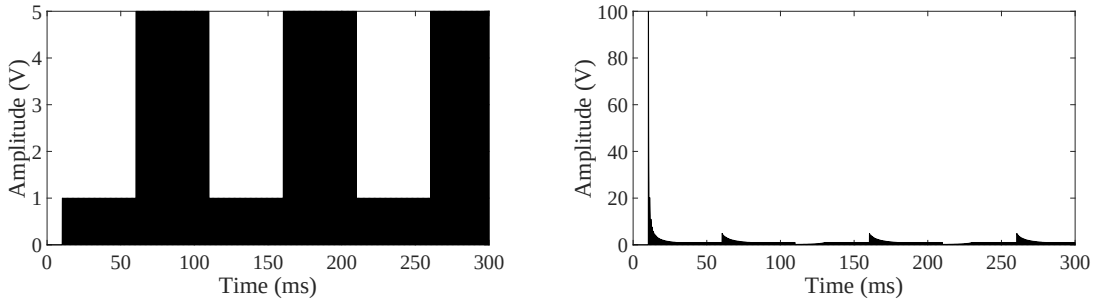

(a) AGC input **(b)** AGC output

Figure 3.6. The validation of the AGC at the (a) input and (b) output

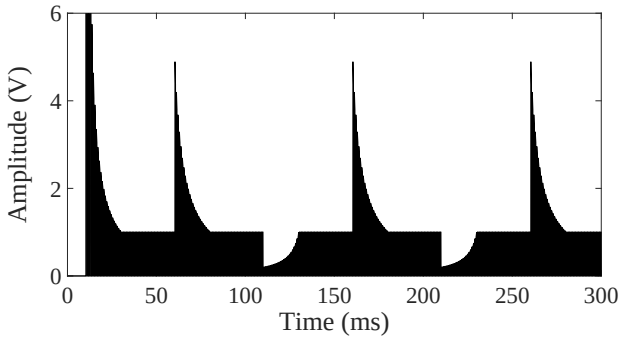

Figure 3.7. AGC response to 10 Hz jam signal.

effects and are not used for steering the seeker. The AGC output shown in Figure 3.6(b) is zoomed in and shown in Figure 3.7. It should be noted that since the response in Figure 3.6 and in Figure 3.7, is shown for a long period (300 ms), the modulation of the reticle is not visible. It should therefore be noted that the black regions in Figure 3.6 and in Figure 3.7, contains similar modulation as in Figure 3.5.

As seen in Figure 3.6(a), the detector signal increases from 1 V to 5 V when the jam signal is switched on at 60 ms and drops to 1 V again when the jam signal switches off at 110 ms. This response is counteracted by the AGC as seen in Figure 3.7. The amplitude rises to 5 V as the jam signal switches on at 60 ms and the AGC attenuates the signal and achieves the desired signal amplitude of 1 V at 80 ms. The signal stays at the required level of 1 V until the jam signal switches off at 110 ms. Since the AGC will be operating at a lower gain, the output decreases when the jam signal is switched off. The AGC responds by amplifying the signal and achieves the required level of 1 V at 130 ms. The response is repeated as the jam signal is switched on and off. This response is as expected and therefore

serves as validation for the AGC circuit.

The choice of the AGC time constant is an important one since it is desirable for the AGC to respond speedily to changes in the input amplitude, but it is also undesirable for the AGC to distort the input signal as it responds to changes in the signal. The choice of the time constant is application dependant and should be specific to the expected conditions of operation [69]. It is expected that the target intensity will increase as the missile approaches the target and this will result in an increase in the detector signal amplitude. The change in target intensity is dependant on the speed of the missile and it is known that the early generation missiles were flying at a typical speed of 600 $\mathrm{m\,s^{-1}}$. This means the missile can cover a distance of 12 m in 20 ms and this is not expected to significantly alter the signal intensity [55]. Since the seeker scans the scene in 10 ms intervals, it is best to have the time constant greater than 10 ms so that the actual target information is not distorted during a scan. The time constant of the AGC was therefore chosen to be 20 ms in order to distribute the effect of amplification or attenuation over two scan cycles rather than one cycle. The effect of different time constants is shown in Figure 3.8. Figure 3.8(a) shows the input signal operating at 10 V. The AGC output shown in Figure 3.8(b) operates at a time constant of 10 ms and as seen in the figure, the amplitude reaches 1 V at 10 ms. The response in Figure 3.8(c) is for a time constant of 20 ms. As seen in the figure, the response settles at 20 ms. The response in Figure 3.8(d) is for a time constant of 30 ms and the response is as expected. This further validates the AGC circuit in terms of the response time.

3.5.3 Carrier filter circuit

The output of the AGC is processed by the carrier filter which attenuates background noise signals. The carrier bandpass filter was designed with a center frequency of 1.6 kHz and a bandwidth of 500 Hz. It might be expected that since the carrier frequency of the seeker is 1.2 kHz, then the center frequency should also be 1.2 kHz. The choice to use a center frequency of 1.6 kHz was motivated by two factors. The first being that, the higher the center frequency is, the higher the range of frequencies will be passed through the filter. This will allow a wider range of target positions to be demodulated correctly or this will increase the linear region of the seeker. The second reason is that a number of studies made a similar design choice and therefore choosing the same filter cutoff will make allowance for the comparison of results [2, 13]. The frequency response of the carrier filter is shown in Figure 3.9, with Figure 3.9(a) showing the magnitude response and Figure 3.9(b) showing the phase response. As seen in Figure 3.9(a), the center frequency of the filter is 1.6 kHz and the -3 dB points are at 1.127 kHz and 2.07 kHz respectively. These points are marked in red in Figure 3.9(a). The chosen filter is a FIR

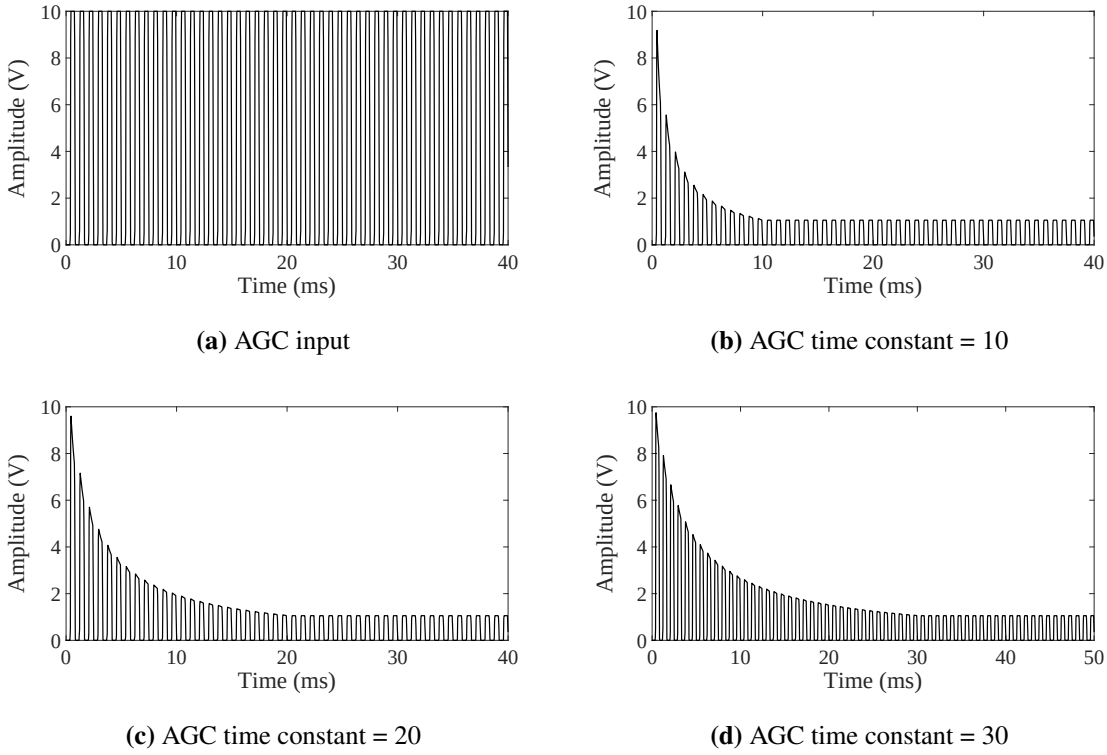

(a) AGC input

(b) AGC time constant = 10

(c) AGC time constant = 20

(d) AGC time constant = 30

Figure 3.8. The validation of the AGC with different time constants. (a) Input signal, (b) $\tau = 10$, (c) $\tau = 20$ and (d) $\tau = 30$.

digital filter with an order of 50. Due to the filter order chosen, the bandwidth is greater than 500 Hz, but this allows a wider range of values to be demodulated accurately and was therefore the chosen filter.

The filter was tested in the time domain and the results are shown in Figure 3.10. The input signal is the detector signal for a target at an offset error of 0.1° and the output signal is the carrier filter output. As seen in the figure, the filter does modulate the signal because there are frequency variations in the signal. If the filter receives a detector signal operating at the target carrier frequency of 1.2 kHz it produces the result shown in Figure 3.11. As seen in the figure, the filter attenuates the signal by the same amount and this is as expected because of the constant frequency in the signal.

3.5.4 Frequency discriminator circuit

The frequency discriminator is implemented using a slope detector which converts the frequency modulated signal into an amplitude modulated signal. The slope detector is a filter that has a wide slope that allows a wide range of frequencies to be attenuated linearly. The lower frequencies are subject to

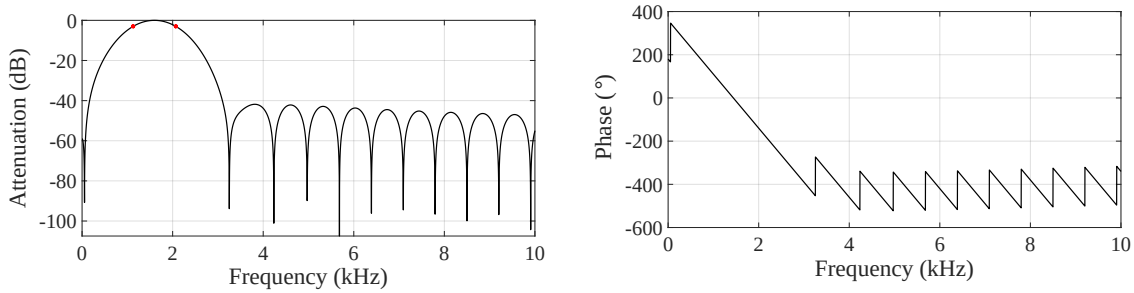

(a) Magnitude response **(b)** Phase response

Figure 3.9. The frequency response of the carrier BPF. (a) Magnitude and (b) Phase response.

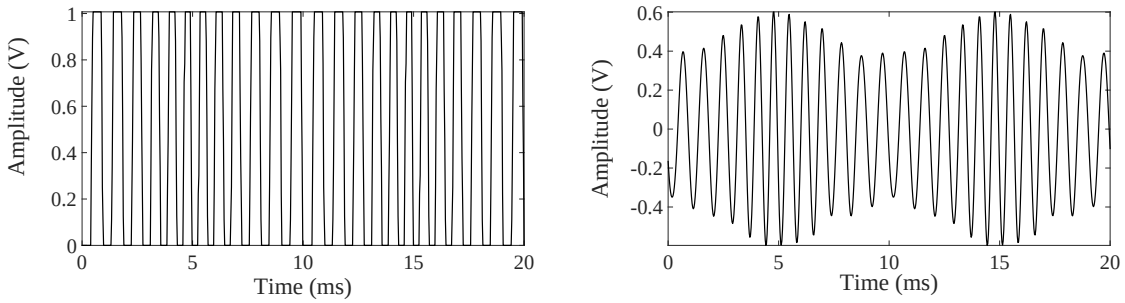

(a) BPF input **(b)** BPF output

Figure 3.10. The response of the carrier filter with 0.1° target error. (a) Input and (b) Output.

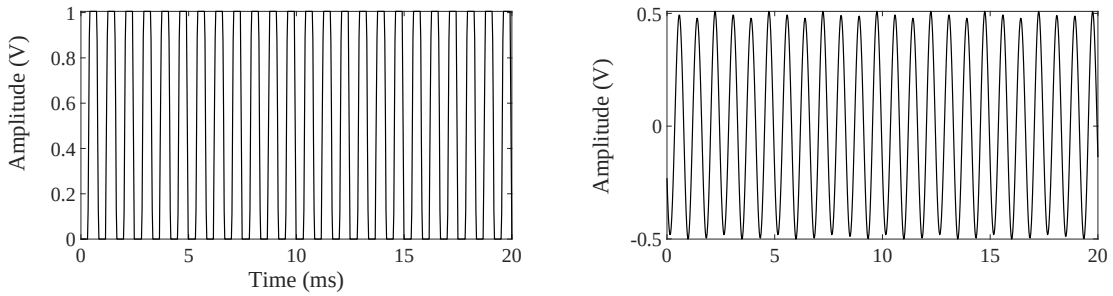

(a) BPF input **(b)** BPF output

Figure 3.11. The response of the carrier filter with 0° target error. (a) Input and (b) Output.

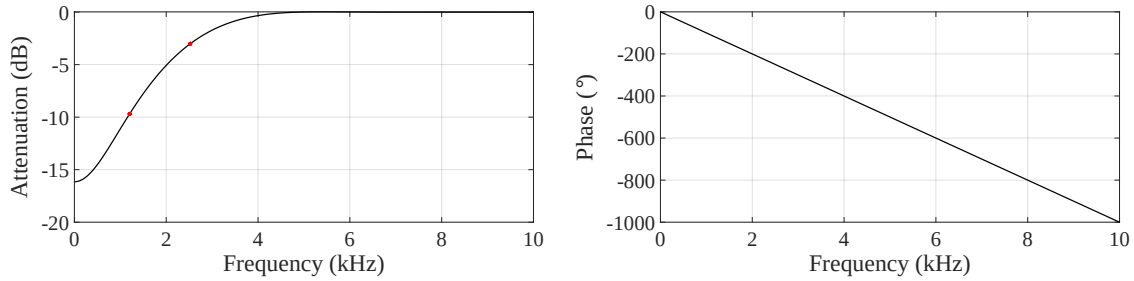

(a) Magnitude response **(b)** Phase response

Figure 3.12. The frequency response of the slope detector. (a) Magnitude and (b) Phase response.

a higher attenuation factor while the higher frequencies are subject to a lower attenuation. The slope detector can be implemented using either a LPF or a HPF, because both can achieve the same objective. The difference between the two is that the LPF will attenuate the higher frequencies more, while the HPF will attenuate the low frequencies more. A high pass filter was chosen as the slope detector since this will allow the demodulation of more target positions due to the high frequencies in the signal. The frequency response of the frequency discriminator is shown in Figure 3.12. Figure 3.12(a) shows the magnitude response and Figure 3.12(b) shows the phase response of the circuit. As seen in the figure, the 3 dB point is at 2.5 kHz and the carrier frequency is at -9 dB attenuation. The HPF implementation uses a FIR digital filter with a filter order of 20.

The filter was tested in the time domain and the results are shown in Figure 3.13. The input signal is the output of the carrier BPF described in Section 3.5.3 with the target at an offset of 0.1° error and the output signal is the frequency discriminator output. As seen in Figure 3.13, the filter attenuates low frequencies more than it does high frequencies. This is because a HPF was used for the slope detector.

The slope detector was tested against a signal with no frequency modulation which is representative of a target at 0° error and as seen in Figure 3.14, the slope detector applies equal attenuation to the signal.

3.5.5 Envelope detector circuit

The envelope detector is used to detect the low frequency modulation signal or envelope signal. The envelope detector consists of a rectifier and a LPF. The rectifier was implemented using a square function and the LPF was implemented using a FIR digital filter with a filter order of 100. The LPF has

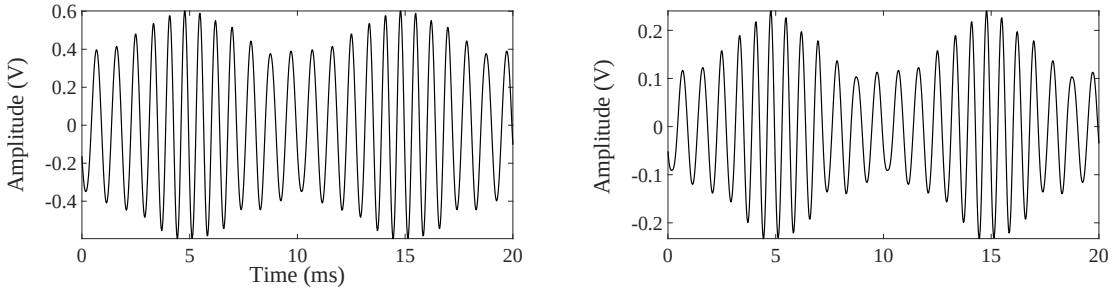

(a) HPF input **(b)** HPF output

Figure 3.13. The response of the frequency discriminator with 0.1° target error. (a) Input and (b) Output.

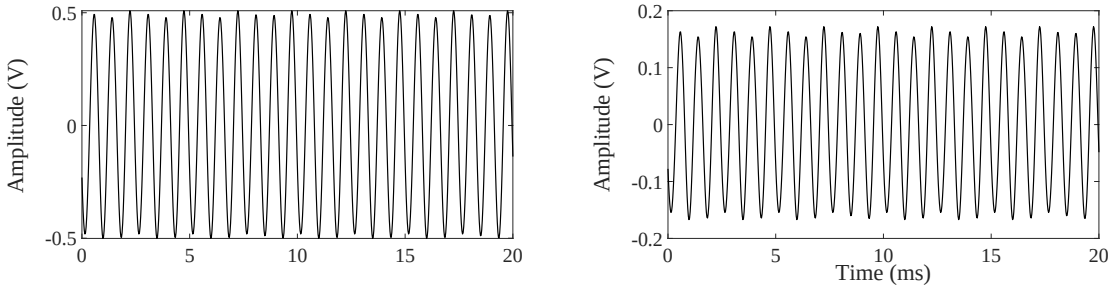

(a) HPF input **(b)** HPF output

Figure 3.14. The response of the frequency discriminator with 0° target error. (a) Input and (b) Output.

the 3 dB point at 238 Hz as seen in Figure 3.15(a). This is close to the nutation frequency of 100 Hz which is the expected envelope frequency. The envelope detector was tested in the time domain and the results are shown in Figure 3.16. The input signal is the output of the slope detector HPF described in Section 3.5.4 with the target at an offset of 0.1° error. As mentioned previously, the envelope detector consists of a rectifier and a LPF. The output of the rectifier and the LPF are shown in Figure 3.16. As seen in the figure, the rectifier is effectively the absolute value of the signal and the LPF detects the envelope of the signal. The envelope detector was tested against a signal with no frequency modulation which is representative of a target at 0° error and as seen in Figure 3.17, the envelope detector produces a constant amplitude to indicate that there is not error in the input signal.

3.5.6 Nutation filter circuit

The nutation filter circuit removes the remaining high frequency components in the signal that are produced by rectification. The filter is centred at the nutation frequency of 100 Hz and was implemented

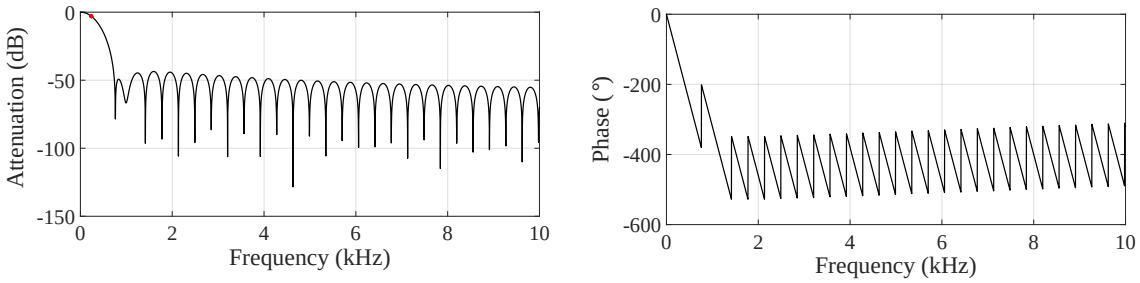

(a) Magnitude response **(b)** Phase response

Figure 3.15. The frequency response of the envelope detector. (a) Magnitude and (b) Phase response.

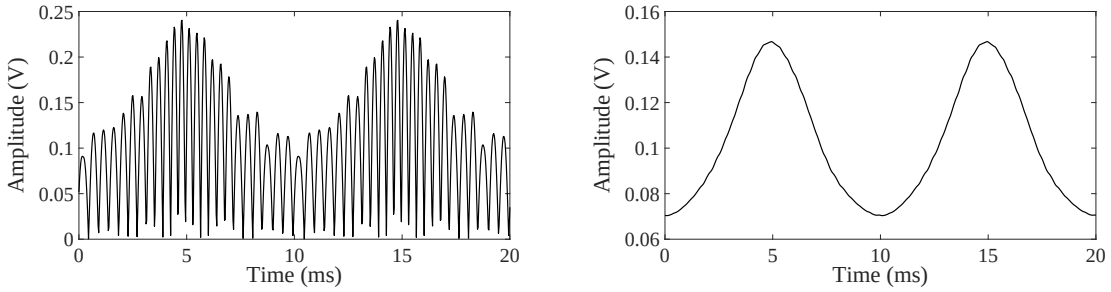

(a) Envelope detector input **(b)** Envelope detector output

Figure 3.16. The response of the envelope detector with 0.1° target error. The output of the (a) Rectifier and (b) envelope LPF.

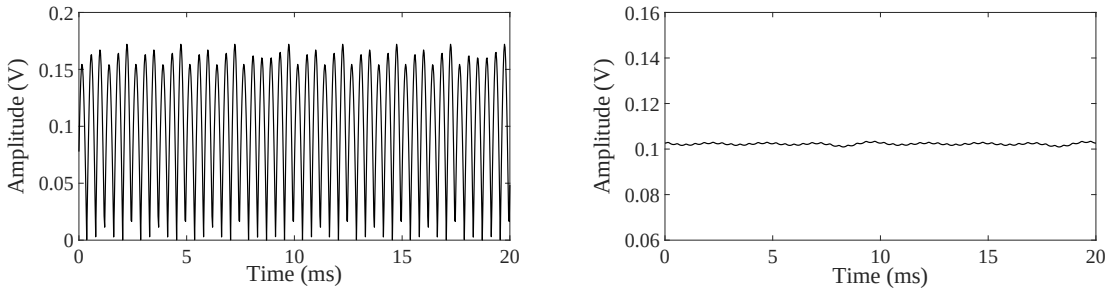

(a) Envelope detector input **(b)** Envelope detector output

Figure 3.17. The response of the envelope detector with 0° target error. The output of the (a) Rectifier and (b) envelope LPF.

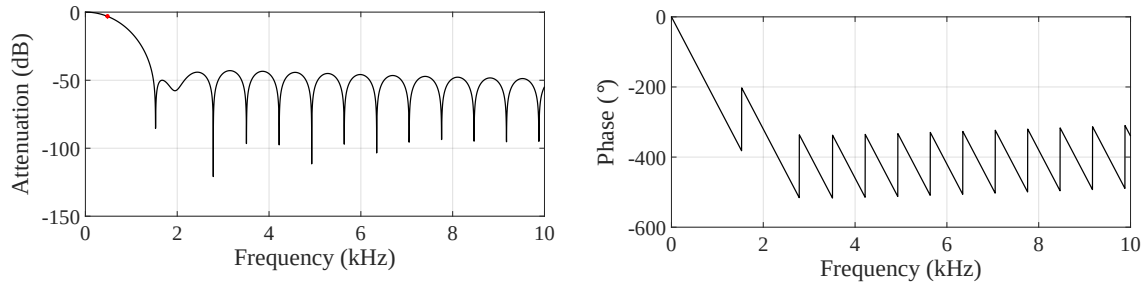

(a) Magnitude response **(b)** Phase response

Figure 3.18. The frequency response of the nutation filter. (a) Magnitude and (b) Phase response.

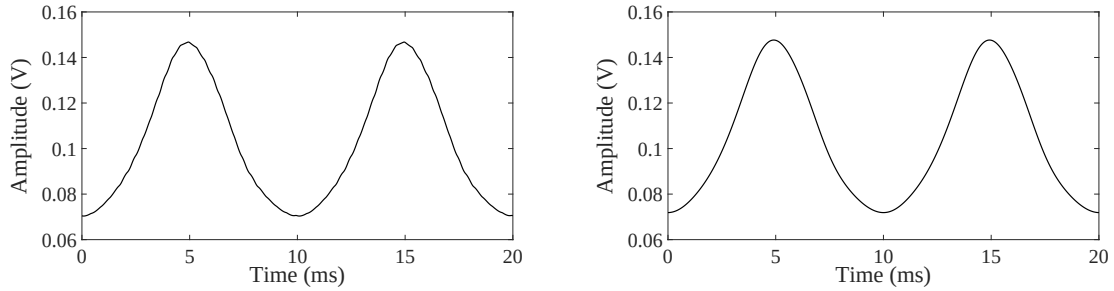

(a) Nutation filter input **(b)** Nutation filter output

Figure 3.19. The response of the nutation filter with 0.1° target error. (a) Input and (b) Output.

using a FIR digital filter with a filter order of 50. The frequency response of the filter is shown in Figure 3.18. As seen in the figure, the filter is effectively a LPF because the filter order is too low to produce a BPF at a 100 Hz. The response of the nutation BPF in the time domain is shown in Figure 3.19. The input signal is the output of the envelope detector described in Section 3.5.5 with the target at an offset of 0.1° error. As seen in Figure 3.19(a), the sinusoid consists of high frequency components that make the signal to be noisy. The nutation filter removes the high frequency components and the resultant output is much smoother as seen in Figure 3.19(b). The nutation filter performs as expected. The filter was tested against a target at 0° error and the resultant output is shown in Figure 3.20. The output of the nutation filter is a direct current (DC) signal which indicates zero error and the target is at the center of the FOV.

In order to test the demodulation capability, the output of the nutation filter (which has been slightly amplified for visibility purposes) was plotted against the detector signal and the results are shown in

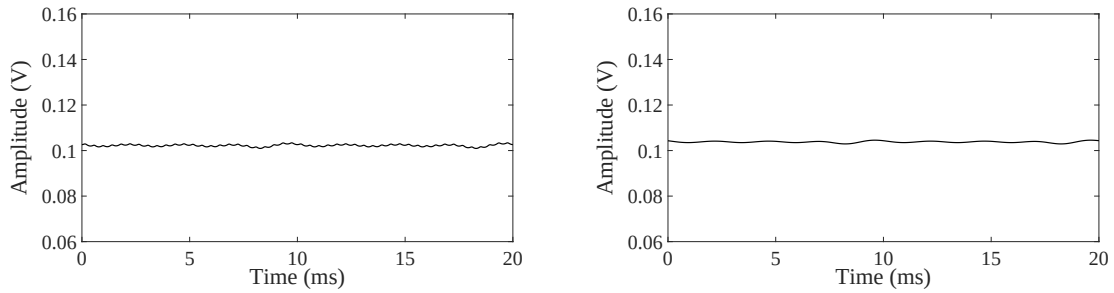

(a) Nutation filter input

(b) Nutation filter output

Figure 3.20. The response of the nutation filter with 0° target error. (a) Input and (b) Output.

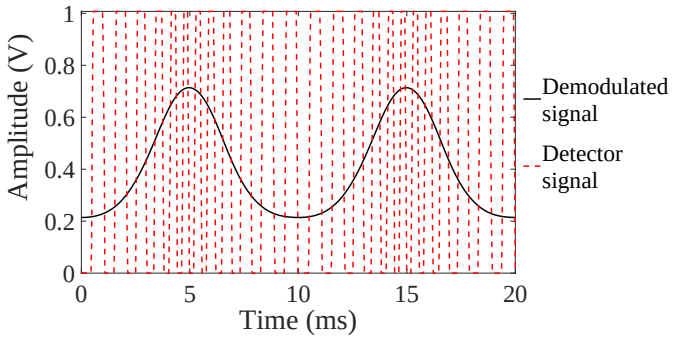

Figure 3.21. Validation of demodulation.

Figure 3.21. As seen in the figure, the FM signal is successfully converted to an AM signal with the peaks of the AM signal corresponding to the high frequency portion of the FM signal and the troughs corresponding to the low frequency portion of the FM signal.

3.5.7 Target position modelling

Once the detector signal is FM demodulated, the output signal is used to determine the angular and radial position of the target. The amplitude of the signal is used to determine the radial position and the phase is used to determine the angular position of the target. The higher the amplitude modulation of the signal, the further the radial position is from the center. The phase of the signal relative to some reference, is used to determine the angular position of the target. With the radial and angular position of the target decoded, the seeker can be steered to keep track of the target.

3.5.7.1 Radial position modelling

The envelope signal amplitude modulation was measured for target radial positions ranging from 0° to 1° and the response is shown in Figure 3.22. The figure illustrates how the envelope signal amplitude

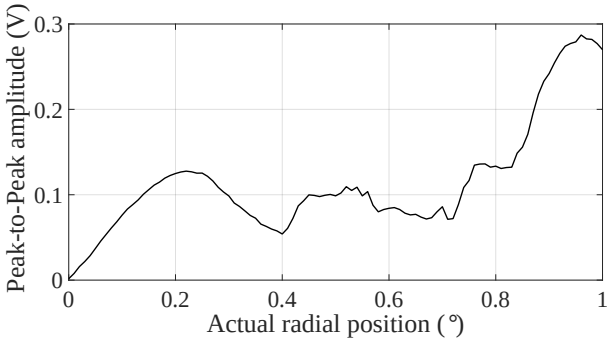

Figure 3.22. Radial position modelling.

varies with a variation in the actual target position. As seen in the figure, the signal amplitude increases with an increase in the target position in an almost linear fashion until the the target position exceeds 0.2°. The region 0° to 0.2° is the linear region of the seeker. The signal amplitude decreases for radial displacement from 0.2° to 0.4°. This is the point at which the nutation circle starts to fall off the reticle, and as a result the detector signal is not pure FM. This is the reason why the signal amplitude does not have a consistent pattern beyond 0.4°. But the fact that the amplitude tends to increase can be used to still guide the missile even though this will not be as accurate. This is the reason why the conical-scan seeker is said to be most ideal for target tracking when on target but is not the best choice for target acquisition [59].

The model for the radial position of the target was generated using the peak to peak amplitude of the envelope signal. The amplitude of the envelope signal is used as the input and the actual target radial position as the corresponding output of the model. The resultant curve is shown in Figure3.23. As seen in Figure 3.23, the fitted curve was modelled using a linear fit to the data since this a practical model that can be implemented in the seeker. The R^2 value is a statistical measure of how far the data is from the fitted regression curve [70]. An R^2 value of 1 represents a 100% fit to the data and a value of 0 represents 0% fit. As seen in Figure 3.23, the linear fit produces an R^2 value of 0.9877. This shows that the linear fit is a good fit to the measured data. Note that this fitting was done for the radial position 0° to 0.2° since this is the linear region. The peak to peak value of the envelope signal is therefore amplified by the factor 1.52 and the value 0.0075 subtracted in order to obtain the actual radial position of the target. The model is shown against the response for the radial positions 0° to 1° which is the reticle region, in Figure 3.23(b). As seen in the figure, the model cannot accurately represent the behaviour beyond 0.2°, and that the model tends to produce values that are less than the actual target position value. This means the seeker will be steered much less than required when the

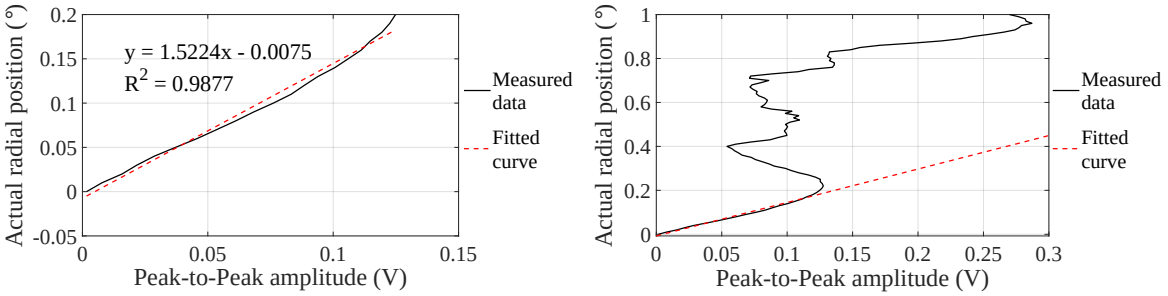

(a) Measured and fitted target position in range 0° to 0.2°.

(b) Measured and fitted target position in range 0° to 1°.

Figure 3.23. Radial position modelling with fitted curve. The response in the (a) linear region and (b) IFOV.

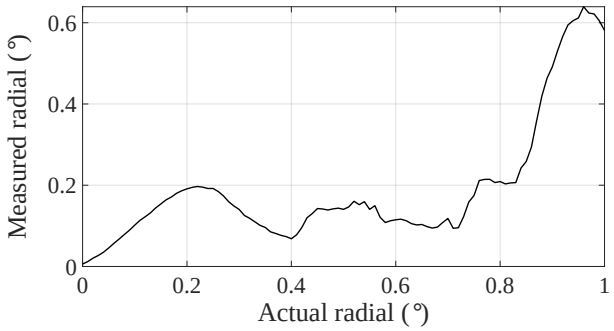

Figure 3.24. Actual radial position versus Measured radial position.

target is at positions greater than 0.2°.

3.5.7.2 Static gain curve

The radial model was used to measure the range of radial positions in the FOV with the results shown in Figure 3.24. As seen in the figure, the model is able to accurately measure the positions in the range 0° to 0.2°, but is not able to accurately measure the other radial positions. The response shown in Figure 3.24 is the static gain curve for the designed seeker and can be compared with the typical gain curve for a conical-scan seeker (repeated here for convenience) as shown in Figure 3.25 [19]. As mentioned previously, the linear region of the seeker is 0° to 0.2°, and the FM region is the range 0° to 0.4°. The static gain curve illustrates that the conical-scan seeker can accurately measure radial positions in the linear region and this is due to the limited bandwidth caused by the filtering process in the seeker. When the target signal error is greater than 0.2°, the detector signal creates high frequency components that are not in the limited bandwidth of the seeker. The filtering process then distorts the

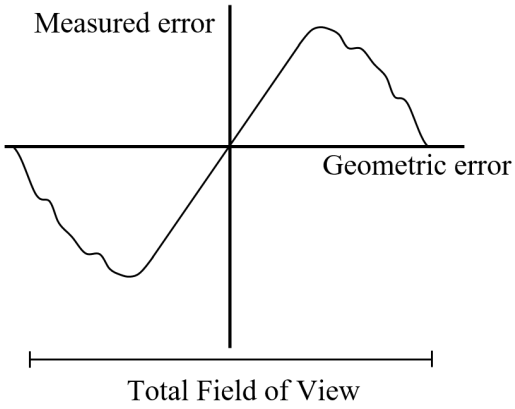

Figure 3.25. Typical static gain curve. Adapted from [19]. Used with permission.

signal and therefore causes inaccurate measurements in the region beyond 0.2°. The static gain curve is generally shown in the FM region as shown in Figure 3.25, and this typical static gain curve can be compared to the FM region of the modelled seeker in Figure 3.24. It should also be noted that the static gain curve is symmetrical at the center point and was not illustrated for the opposite direction since the response would be symmetrical.

Most authors do not indicate the achieved static gain response, but one study was found with a linear region cutoff at 0.1° [19] and another with a cutoff of 0.2° [65]. The response found by Han *et al.* [65] is shown in Figure 3.26 and this response is quite similar to the response obtained in Figure 3.24. The linear region of the seeker shown in Figure 3.26 is 0.2° which is the same as the linear region found in the seeker under study. The FM region in the study by Han *et al.* is 0° to 0.5° as seen in Figure 3.26. This is also close to the FM region of the seeker under study. It should be noted that the static gain curve is influenced by the size of the nutation circle used since this will determine the linear region and the FM region of the seeker. In the present study, the nutation circle has a radius of 0.6° and therefore the nutation circle exits the seeker FOV at a target position of 0.4°. If the nutation circle was 0.5° for instance, then the FM region would be 0.5° since that is the point at which the nutation circle would begin to exit the reticle which has a radius of 1°. Therefore the static gain response is a function of the design parameters used to model the seeker.

3.5.7.3 Angular position modelling

The phase of the envelope detector signal was used to determine the angular position of the target. The phase detector was implemented using a Schmitt trigger to identify the index at which the peak of the signal occurs. A Schmitt trigger is a comparator circuit with hysteresis which generates pulses based

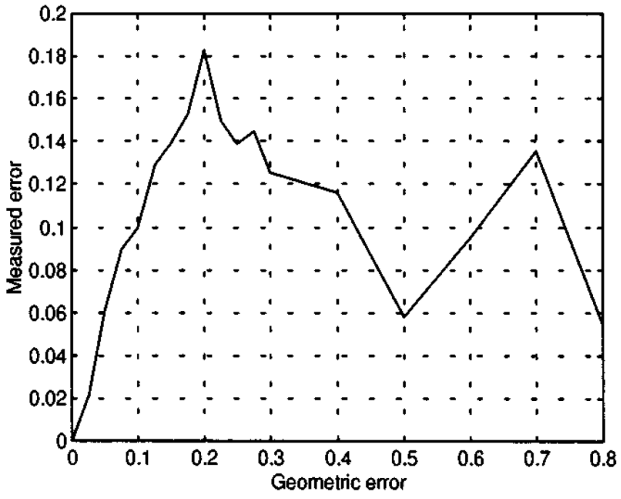

Figure 3.26. Static gain curve found by Han *et al.* [65]. Used with permission.

on pre-set thresholds which determine when the trigger is switched on and off as shown in Figure 3.27. The blue line in the figure, is the reference signal which is a simple sinusoid. The phase of the sinusoid was set such that the peak would occur at the expected peak position for zero angular error. The black signal is the demodulated signal. The red line is the Schmitt-trigger output signal. The threshold of the Schmitt-trigger is 95% of the maximum of the demodulated signal. The trigger is used to estimate the peak even though the trigger does not occur at the peak. When the Schmitt-trigger is set to high, the model uses the delay between the peak value of the reference signal with the position at which the Schmit-trigger was enabled. This is used to estimate the angular position of the target. The delay of the signal relative to the reference was measured and plotted as shown in Figure 3.28. In order for the signal index to produce the desired angular position, the response is offset by a value of 170 as seen in Figure 3.28(b). As seen in the figure, the phase detector has a dead zone where an increase in the target angle does not produce an increase in the measured angle. This is due to the pulse width of the Schmitt-trigger which makes it difficult to detect the phase difference when the phase is 180° as seen in Figure 3.29. This spans 20° in the range 175° to 195°.

3.5.8 Tracking performance

Once the target radial and angular errors are computed by the seeker, a proportional controller is used to reduce the error to zero. The tracking performance of the seeker was tested by setting a target radial error and observing the movement of the seeker head to reduce the error to zero. The response of the seeker to different target errors, is shown in Figure 3.30. As seen in the figure, the seeker reduces the smaller errors easier than the larger errors. The time taken for the large errors to be reduced to zero is

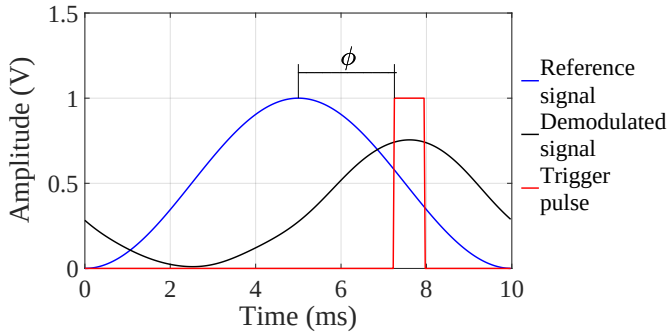

Figure 3.27. Schmitt trigger illustration.

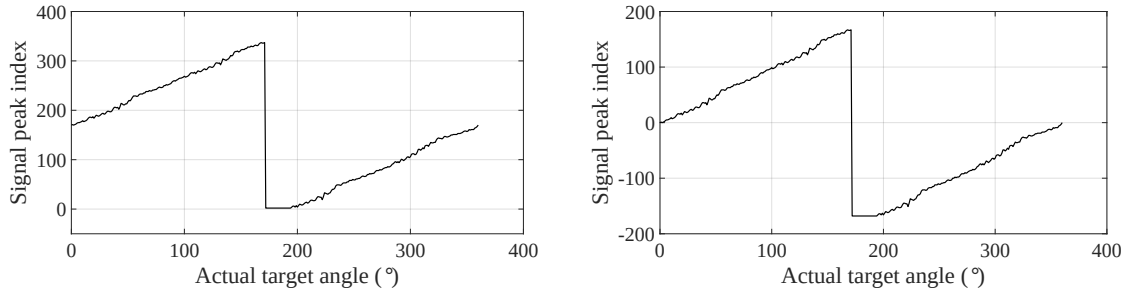

(a) Signal peak index

(b) Adjusted signal peak index

Figure 3.28. Signal index. (a) Before and (b) after applying offset.

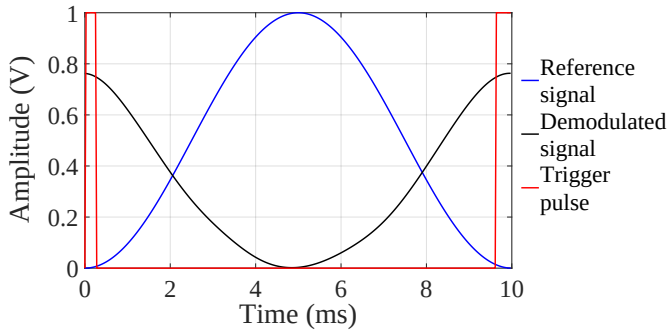

Figure 3.29. Schmitt trigger dead zone illustration.

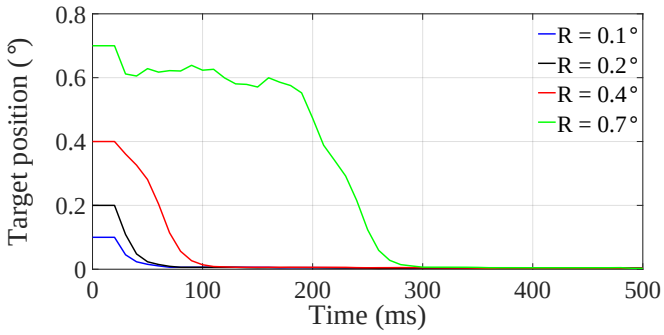

Figure 3.30. Tracking performance for different target positions.

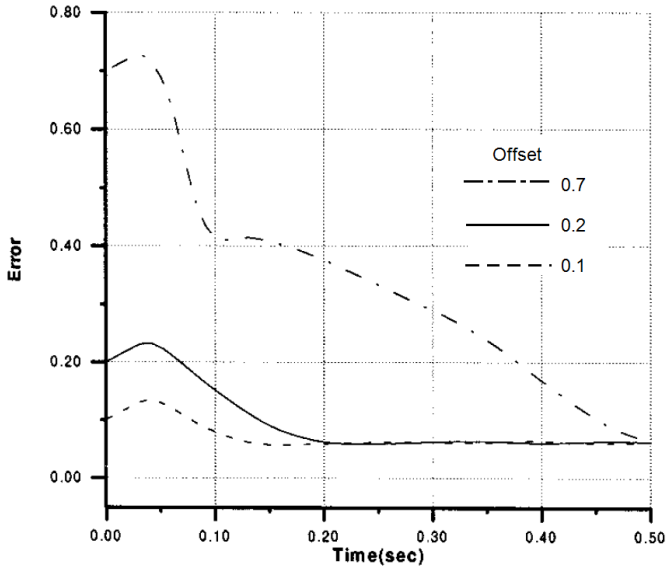

Figure 3.31. Tracking performance for different target positions [65]. Used with permission.

longer than the time taken for the smaller errors, and this is expected due to the steering range required for larger errors and also due to the reduced measurement accuracy at large errors. It can be seen that the slope of the seeker response is consistent for low errors and is variable for large errors. This is due to the measurement inaccuracies that occur at the larger errors. The response of the conical-scan seeker designed by Han *et al.* [65] is shown in Figure 3.31. As seen in the response by Han *et al.* [65], the slope of the error signal also tends to vary for large errors. The slope is more constant for smaller errors.

In order to test the tracking ability in both the radial and angular errors, the target position was offset in the yaw and pitch directions and these are represented as the x and y directions respectively. The target was offset by (x = 0.2, y = -0.3) which is equal to the radial error of 0.36° and an angular error

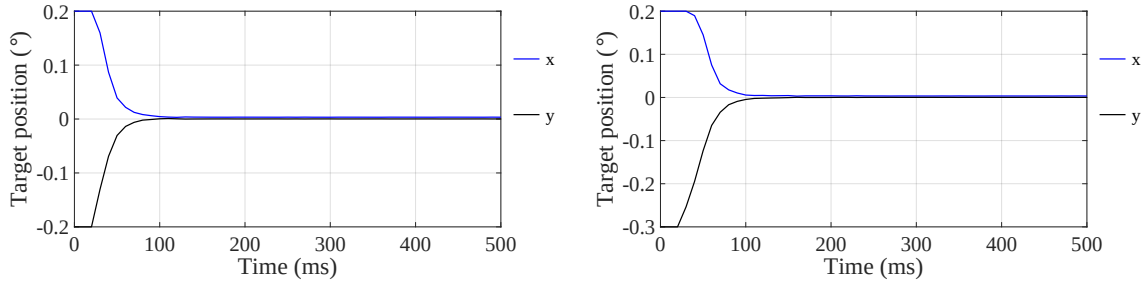

(a) Target position x = 0.2, y = -0.3

(b) Target position x = 0.2, y = -0.2

Figure 3.32. Tracking performance for different x and y offset. Target offset of (a) x = 0.2, y = -0.3 and (b) x = 0.2, y = -0.2.

of 303.7°. The target was also offset by (x = 0.2, y = -0.2) which is equal to a radial error of $\frac{\sqrt{2}}{5}$ and an angular error of 315°. The response of the seeker to these errors is shown in Figure 3.32. As seen in the figure, the error successfully converges to zero which shows successful tracking. This therefore validates the tracking ability of the seeker under study.

3.6 TRACKING PERFORMANCE UNDER JAMMING

The studies that evaluated the effect of a jam signal on the con-scan seeker found that the average phase error of the seeker oscillates at the difference frequency [14]. The difference frequency is the frequency of the nutation minus the jam frequency. This was tested and the results are shown in Figure 3.33. The low frequency jam signal was used for this test, at 110 Hz and 150 Hz. Since the nutation frequency is 100 Hz, the difference frequency in the first case is 10 Hz and as seen in Figure 3.33(a), the angular error produces 5 oscillations in 0.5 s. The angular position therefore oscillates at 10 Hz as expected. The jam frequency of 150 Hz is expected to produce oscillations at 50 Hz. As seen in Figure 3.33(b), the angle oscillates at 44 Hz. This is less than the expected 50 Hz but it could be attributed to the gimbal limits in the seeker which restrict rapid motion. The oscillatory behaviour of the phase error confirms the correct operation of the seeker.

3.7 CONCLUSION

This chapter explained the development of the conical-scan seeker used in this investigation. The seeker optics were modelled using a wagon wheel reticle which is typical in a number of similar studies [13, 15–17]. The wagon wheel reticle is typically used because it is similar to the reticle used in the SA-14 missile seeker and therefore has significance [55]. Images of the rotating reticle and the scene were multiplied on a pixel basis and integrated over all pixels in the image to generate the

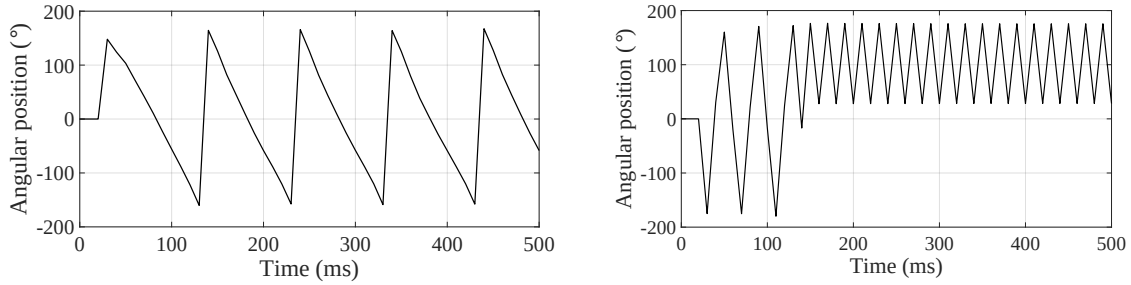

(a) Angular error with a jam frequency of 110 Hz **(b)** Angular error with a jam frequency of 150 Hz

Figure 3.33. Response of angular position to a jam frequency of (a) 110 Hz and (b) 150 Hz.

detector signal. The detector signal was tested by varying the target position in the seeker FOV and the resultant detector signal observed. The zero offset target position produces a constant frequency pulse train and an offset produces a FM signal and this was as expected. The carrier filter, slope detector filter, envelope detector filter and the nutation frequency filter were all tested in the time and frequency domains. The frequency response of the filters was found to be satisfactory and the time response was found to be as expected. Each processing block was tested using a target off center with an error of 0.1° and also with a target that is on center at an error of 0°. The results were found to be satisfactory. The demodulated signal peak to peak amplitude was used to model the radial error to be used for steering the seeker. The model for the target radial position produces an R^2 value of 0.9877. The demodulated signal phase was used to model the angular position of the target. The tracking ability of the seeker was tested and it was found that the seeker successfully reduces the target error to 0° for both small and large target positions. The response of the seeker was found to correspond to results found by other authors who conducted similar studies [65].

CHAPTER 4 JAM SIGNAL EFFECTIVENESS

4.1 CHAPTER OBJECTIVES

The aim of this chapter is to describe the tests that were conducted to evaluate the effectiveness of the selected jam signal waveforms and the results thereof. The chapter begins with a description of how jam signal effectiveness is measured. This is useful for quantifying how much more effective one waveform is from another and will assist in the comparison of waveforms. The chapter then gives an introduction to the general experimental configuration for the tests that were conducted. This is useful to understand the conditions under which the tests took place.

The waveforms used for jamming the conical scan seeker are then presented with an overview of each waveform. The results of the conducted tests for the fixed carrier, low frequency, AM, FM and the AM-FM hybrid jam signals are then presented. For each jam waveform the tests conducted to evaluate the effect of increasing the J/S ratio are presented. The chapter then evaluates the carrier frequencies at which each waveform is most effective. The effect of varying the duty cycle is then tested. The combination of parameters that produce the greatest seeker error are then used against the seeker and the time taken to achieve the greatest error is determined. The combination of the best performing parameters is used to determine the greatest error achievable for each waveform.

The aim of these tests is to identify the strengths and weaknesses of each jam waveform so that the best waveform can be identified. This will allow the primary research question to be answered which is:

- Which jam waveform is the most effective against the conical-scan seeker?

The effect of the J/S ratio, frequency and duty cycle will be tested for each waveform and this will allow the secondary research question to be answered which is:

- What is the best parameter combination of the most effective jam signal in terms of J/S ratio, jam frequency and duty cycle?

4.2 JAM SIGNAL EFFECTIVENESS EVALUATION

In order to determine the effectiveness of each jam signal, the parameters that are used to quantify effectiveness have to be defined. This section gives a brief overview of the chosen parameters used to measure effectiveness and the reason these specific parameters were selected. The parameters used to measure jamming effectiveness are:

- the maximum achievable radial seeker error obtained with the specific waveform,
- the minimum J/S ratio required to achieve a significant error,
- the range of effective carrier frequencies when applicable,
- the range of effective modulation frequencies when applicable, and
- the minimum required duty cycle when applicable.

As discussed in the review chapter (Chapter 2) and in the modelling and simulation chapter (Chapter 3), it is expected that the angular error will oscillate as a result of a jam signal. It is therefore not appropriate to use the raw angular error signal to evaluate the effect that is induced in the seeker. It is more desirable to know how far off center these oscillations took place. The radial error can be used to deduce the position on the reticle that these oscillations occurred. This is useful because the further off center the oscillations take place, the easier it is for the target to be lost by the seeker. The maximum radial error induced by the jam signal was therefore used as a measure of jam signal effectiveness. Since the radial error is primarily considered for evaluating jam signal effectiveness, the term seeker error may be used to refer to the radial error. The angular error is explicitly termed as such. The reason for selecting the specified criteria for evaluating or measuring jam signal effectiveness is explained in the following subsections.

4.2.1 Minimum J/S ratio

It is desirable to achieve the greatest seeker error while using the lowest J/S ratio. This is because more electrical power is required to achieve high J/S ratios, and given that the operational space is airborne, the available power is restricted. Power efficiency is therefore a critical parameter to consider

in choosing a viable jam signal. The jam signal that achieves a high seeker error while utilizing a low J/S ratio will therefore be considered superior to one that requires a high J/S ratio.

4.2.2 Range of effective frequencies

Preference will be given to jam signals that are effective across a wide range of carrier and modulation frequencies (as applicable). Due to the ageing, mechanical wear, storage and tolerances of a missile, the nutation frequency could be different to the expected frequency. The nutation frequency affects the carrier frequency and this could result in the seeker operating at a frequency that is different to the design frequency. This is significant since the effectiveness of a jam signal is dependant on the frequency of operation of the missile seeker. Having a jam signal that is effective across a wide range of carrier and modulation frequencies makes the jam signal robust, versatile and possibly effective against a wider range of conical-scan seekers. This is the reason for considering the range of carrier and modulation frequencies as a measure of jam signal effectiveness. The standard deviation of the response to changes in the frequency or modulation index will be measured to assess the sensitivity of the jam signal to changes in the frequency used. Given that the frequency of the threat missile might not always be known before administering the jam signal, it is desirable to have a jam signal that can be effective even when there is a mismatch in the expected frequency. The standard deviation will give an indication of how much the jam effect can be increased or reduced due to a frequency mismatch. The standard deviation is a measure of how the error will on average deviate from the mean error. A standard deviation of 0.2° with a mean error of 0.5° for instance, says that the error will on average deviate from the mean by 0.2° to a maximum of 0.7° and a minimum of 0.3°. For the purpose of this study, the standard deviation will be considered large if it exceeds 0.1°. A value of 0.1° was chosen because it has significance in the seeker FOV. Given that on average the linear region of the con-scan seeker is in the range 0° to 0.2°, an error of 0.1° is a 50% movement in the linear region. Thus a jam signal that was expected to produce a significant effect at some frequency could produce a significantly less effect because of a frequency mismatch if the standard deviation is high. This requirement of a low standard deviation ensures that there is a certain level of confidence in a jam waveform. Some waveforms consist of a carrier signal and a modulation signal while others consist of only the carrier or the modulation signal. The tests were therefore conducted as applicable.

4.2.3 Minimum duty cycle

The minimum duty cycle is one of the considered parameters because a lower duty cycle is less power intensive than a high duty cycle. It is also not always the case that the jam signal is most effective at the conventional 50% duty cycle and therefore testing a range of duty cycles could potentially allow

some jam signals to achieve greater seeker errors.

4.2.4 POE

A point called, the POE is defined as 90% of the maximum error achieved by the respective jam signal waveform. The POE is therefore equivalent to the 90'th percentile where only the top 10% of the jam codes are considered effective. This point is used to separate the effective and non-effective jam codes (combinations of frequencies, duty cycles and J/S ratios). Frequencies, duty cycles and J/S ratios that produce an error of 90% or more of the maximum will be considered to be effective while those that do not reach this error will be considered non-effective. This approach is taken so that an objective comparison can be made between the waveforms. It is possible for instance to have a jam signal that produces its maximum error at a J/S ratio of 100 but also achieve 90% of that error at a much lower J/S ratio with a different parameter combination. The POE ensures that sufficiently good jamming (at 90% of the maximum effect) can be obtained at the lower J/S ratio, thereby preventing that the J/S ratio might be maximized unnecessarily. A high J/S ratio is obviously undesirable since it is more power intensive and should therefore be avoided. The duty cycle and the J/S ratio are both power considerations, and a low value is desired in both cases. It is possible to have an instance where operating at a lower duty cycle requires a higher J/S ratio or vice versa and a compromise must be reached in such cases. It is assumed that a reduction in the J/S ratio achieves greater electrical power savings than the reduction in the duty cycle. Therefore a reduction in the J/S ratio is preferred over a reduction in the duty cycle in cases where the two conflict. In such cases, the best performing signal parameters will be those that require the lower J/S ratio to reach the point of effect.

4.3 EXPERIMENTAL CONFIGURATION

The procedure that was followed to test the effect of a specific jam signal waveform operating at a chosen J/S ratio and specific carrier or modulation frequency is outlined below.

1. The target is temporally stationary in inertial space.
2. The distance between the seeker and the target is fixed in space and the seeker is stationary in this sense.
3. The seeker head can move in the pitch and yaw directions to track the target. This movement is not limited.
4. The relative phase of the target signal and the jam signal was kept constant throughout each experiment.

5. The target is placed on the optical axis of the seeker (the target's nutation circle center falls on the centre of the reticle, this is considered zero error).
6. The seeker is exposed to the target signal only for 30 ms, during which the transient effects are expected to die out.
7. The jammer signal is switched on after the initial 30 ms and the tracking error induced in the seeker is measured for a period of 500 ms.
8. The tracking behaviour in the first 100 ms is ignored (to avoid transient perturbations).
9. The maximum error observed in the 100 ms to 500 ms time window is used as a measure of seeker error.

The experimental parameters and the applied limitations are given below.

- The J/S ratios used are 2, 5, 10, 20, 50 and 100. These were chosen as they were considered to be a good spread between low and high ratios. The maximum J/S ratio is 100 because this is the maximum available J/S ratio on developing DIRCM systems [7].
- All tests, other than the test to evaluate the J/S ratio, were conducted with the J/S ratio fixed at 100.
- All tests, other than the test to evaluate the duty cycle, were conducted with the duty cycle fixed at 50%.
- All tests for waveforms containing a carrier signal were conducted at the carrier frequency range 600 Hz to 2 kHz with a 100 Hz step size.
- All tests for waveforms containing a modulation signal (or envelope signal) were conducted at the modulation frequency range 0 Hz to 200 Hz with a 10 Hz step size.
- All tests for waveforms containing a frequency modulated signal were conducted at the modulation index range of 1 to 6 with a step size of 0.1 in the index. A modulation index of 1 means the carrier frequency of the signal varies by the modulation frequency which is 100 Hz. A modulation index of 1 will result in the frequency varying from 1.1 kHz to 1.3 kHz. The minimum modulation index was chosen to be 1 since it is known that a laser used for DIRCM application can operate from a modulation of 1 upwards [11]. The upper limit was chosen due to the filter limits in the seeker processing circuitry.
- The range of effective frequencies is the range of frequencies that achieve 90% or more of the maximum error achieved.

- The duty cycle test was performed in the range 10% to 100% in 10% increments.
- The sensitivity of the jam signal waveform to changes in the carrier or modulation frequency was measured using the standard deviation of the induced error. The standard deviation is measured across the carrier, modulation frequencies and modulation indices.
- The mean and standard deviation are measured with the J/S ratio fixed at 100 so that the effect of changes in frequency or modulation index can be assessed.

Optical break lock (OBL) occurs at 1.6° in the seeker under study since the seeker total FOV is 3.2°. OBL occurs when the seeker looses lock of the target and the target is no longer in the seeker FOV. When applying countermeasures to the missile, the aim is to achieve OBL. It is therefore desirable to achieve an error of 1.6° or more in the tests conducted in this study.

4.4 JAM SIGNAL MODELLING

The general consensus in the literature is that the jam signal waveform should be similar to the target signal in order to have an effect on the con-scan seeker [13–16, 18, 19]. Simple logic however seems to indicate that a jam signal that exactly matches the target signal will amplify the target signal, therefore making the target easier to track, This is called illuminating the target with a jammer [18] and is obviously undesirable. The combination of the carrier frequency and the envelope amplitude was used to characterise the jam signals that were tested.

The range of applicable signals to the present study is shown in Figure 4.1 and the corresponding characteristics shown in the associated table in Figure 4.1. The target signal as a source consists of a constant amplitude and no carrier. The fixed carrier jam signal consists of a constant amplitude and a constant frequency (with the frequency range close to the seeker carrier frequency). The FM jam signal consists of a constant amplitude with a varying carrier frequency. The FM jam signal is assumed to have a repetition rate or modulation frequency that is equal to the nutation period or frequency respectively. The low frequency jam signal consists of a variable amplitude and no carrier signal. The low frequency jam signal oscillates at a frequency close to the seeker nutation frequency. The AM jam signal consists of a variable envelope amplitude with a fixed carrier frequency. The hybrid AM-FM jam signal, varies in the envelope amplitude and consists of a variable carrier frequency.

4.5 FIXED CARRIER JAM SIGNAL

The fixed carrier jam waveform consists of a carrier signal at a constant amplitude. This signal does not contain a modulation signal, and therefore modulation related tests were not conducted for this

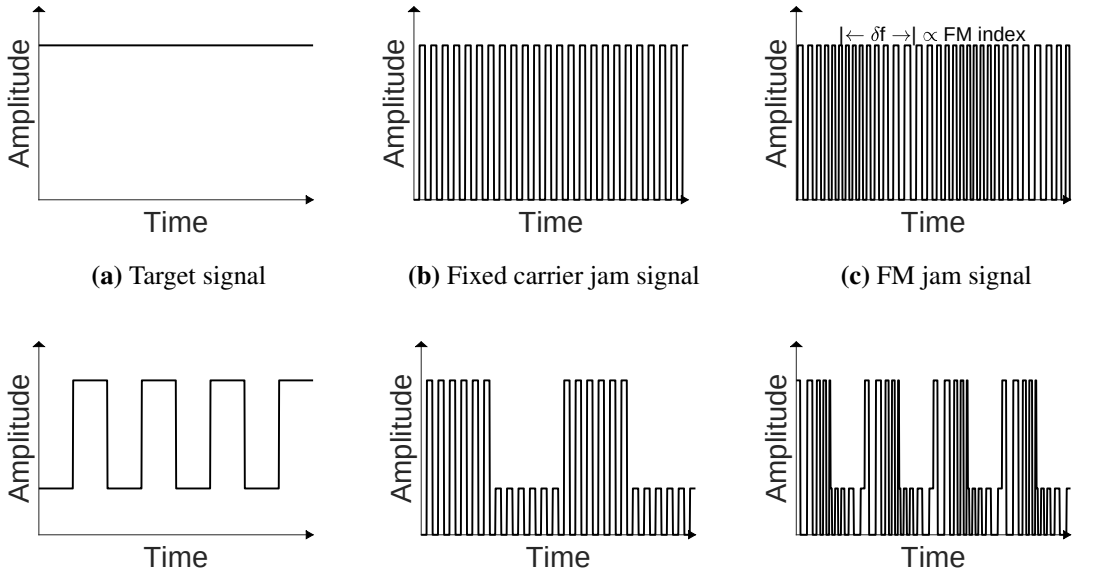

(a) Target signal **(b)** Fixed carrier jam signal **(c)** FM jam signal

(d) Low frequency jam signal **(e)** AM jam signal **(f)** AM-FM hybrid jam signal

Envelope	Carrier		
	Baseband (No carrier)	Constant frequency	Variable frequency
Constant amplitude	Target	Fixed carrier	FM
Variable amplitude	Low frequency	AM	AM-FM hybrid

Figure 4.1. Catalogue of target and jamming signals. (a) Target, (b) Fixed carrier, (c) FM, (d) Low frequency, (e) AM and (f) AM-FM hybrid jam signals.

waveform.

4.5.1 Effect of J/S ratio

This section describes the effect of the J/S ratio by testing the jam signal effectiveness across a wide range of frequencies at different J/S ratios. The literature suggests that an increase in the J/S ratio causes an increase in the jammer effect [13–19]. The aim of this experiment was to test this claim by increasing the J/S ratio and observing the point at which the jam signal produces the greatest error.

The effect of varying the J/S ratio of the fixed carrier waveform is shown in Figure 4.2. An annotated heat map was also used to show the error values induced in this test. As seen in the figure, the jam

signal is most effective at the highest J/S ratio of 100. The maximum seeker error achieved at a J/S ratio of 2 is 0.13° and the maximum achieved at a J/S ratio of 100 is 0.49°. This shows that the significant increase in the J/S ratio produces some increase in the seeker error, but the increase is not significant. Since the range of effective J/S ratios are those that achieve at least 90% of the maximum error, these would have to achieve a seeker error of at least 0.44°. The effective J/S ratio is only at 100 in this case.

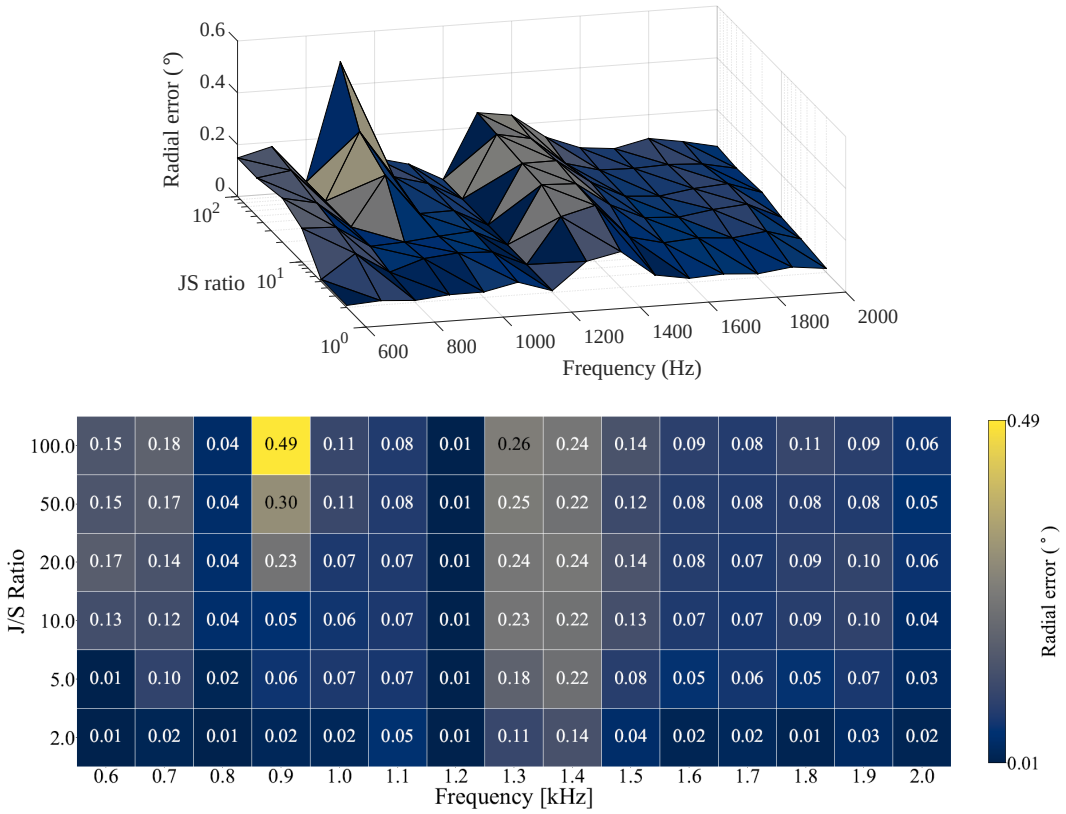

Figure 4.2. Effect of the J/S ratio in the fixed carrier jam signal.

4.5.2 Effect of carrier frequency

The effect of varying the carrier frequency and the associated heat map is shown in Figure 4.2. As seen in the figure, the jam signal effect significantly dies out at the 1.2 kHz carrier frequency. This is because the carrier frequency of 1.2 kHz is the target carrier frequency generated by the chopping action of the reticle for an on-axis target (i.e., the design point for normal operation). This means when the fixed carrier jam signal operates at a frequency of 1.2 kHz then the target is easier to track and the jam signal actually amplifies the target signal. Operating the fixed carrier jam signal at the carrier frequency of 1.2 kHz should therefore be avoided. At low to high J/S ratios the jam effect tends to produce a greater effect for frequencies between 1.3 kHz to 1.4 kHz.

The effect of the jammer seems to be low at 900 Hz for low J/S ratios, but at higher J/S ratios the effect significantly increases. The maximum error of 0.49° was achieved at 900 Hz. It is interesting to note that the frequencies surrounding 900 Hz are not effective even at high J/S ratio.

In the case of the fixed carrier jam signal, no frequencies achieve an error that is 90% of 0.49° (0.44°). The effective frequency is therefore only at 900 Hz, but only at high J/S. The mean error induced by the jam signal with J/S ratio of 100, across the measured frequencies is 0.14° and the standard deviation is 0.12°. The mean shows that the fixed carrier jam signal produces a low effect on average as can be seen on the Figure

4.5.3 Effect of duty cycle

The effect of varying the duty cycle was investigated to determine if the jam signal waveform would be more effective at a duty cycle that is different from the conventional 50% duty cycle. A jam signal that performs better at a low duty cycle is more power efficient than the jam signal that operates at a higher duty cycle. The effect of the duty cycle is shown in Figure 4.3 with the associated heat map. The response shown in Figure 4.3(a) shows the error at each carrier frequency while the effect shown in Figure 4.3(b) shows the maximum effect across all the frequencies for each duty cycle. The heat map in Figure 4.3(c) shows the seeker error at the different test points. As seen in Figure 4.3(a), there is an increase in the jam signal effect with an increase in the duty cycle. The effect tends to decrease at around 100% duty cycle and this is the case for all the carrier frequencies. This is because the jam signal becomes a DC signal at a duty cycle of 100%, and therefore the seeker error is expected to be zero in this case. When considering the maximum error achieved for each duty cycle as shown in Figure 4.3(b), it can be seen that the fixed carrier signal achieves a greater seeker error when the duty cycle of the jam signal is in the range 70% to 90% duty cycle. While the fixed carrier signal only produces a 0.49° error at the conventional duty cycle of 50%, the effect rises to 0.74° at a duty cycle of 80%. This maximum error is achieved at a carrier frequency of 1.1 kHz which is different from the carrier frequency that produced the largest error at a 50% duty cycle. The range of effective duty cycles are those that achieve at least 90% of 0.74° (i.e. 0.67°) and these are 70% to 90% duty cycle. While operating the jam signal waveform at 80% duty cycle might be considered more power intensive than operating at the conventional 50% duty cycle, the increased jam signal effectiveness justifies the need to operate at the higher duty cycle when using the fixed carrier waveform. The fixed carrier jam signal achieves an error of 0.07° at a duty cycle of 10% which is the minimum error achieved in this test.

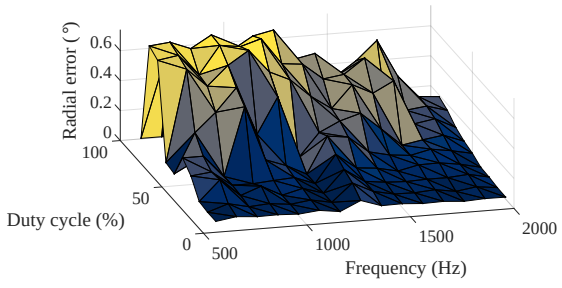

(a) Effect of duty cycle across all frequencies

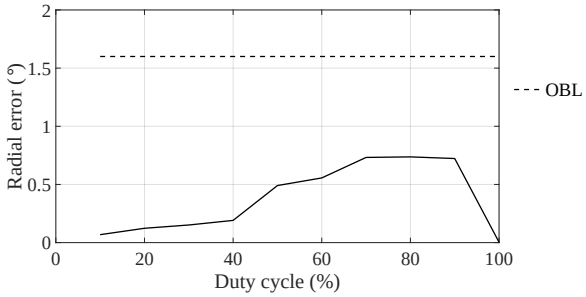

(b) Maximum effect of change in duty cycle

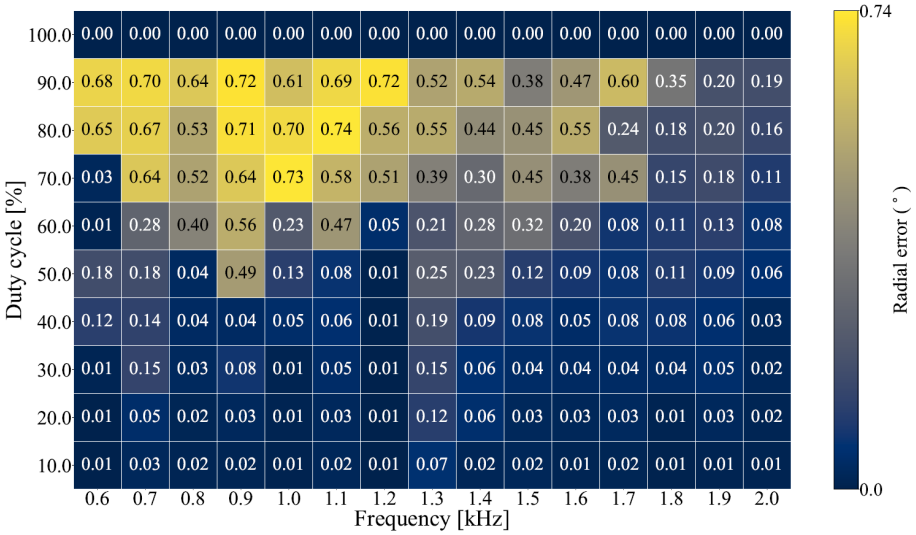

(c) Measured seeker error at various duty cycles

Figure 4.3. Effect of the duty cycle in the fixed carrier jam signal.

4.5.4 Best parameter combination for fixed carrier jam signal

As seen in the duty cycle plot shown in Figure 4.3(b) and 4.3(c) , the fixed carrier jam signal produces a maximum error of 0.74° at a duty cycle of 80%. Given that a duty cycle of 70% is also considered effective producing an error of 0.73°, this is chosen as the best performing jam signal in the fixed carrier type of waveform. This signal operates at a J/S ratio of 100, a carrier frequency of 1 kHz and at a duty cycle of 70%. This signal achieves 98.6% of the maximum error of 0.74° and it uses a lower duty cycle. That makes this signal the best performer.

4.5.5 Temporal response

The temporal response of the fixed carrier jam signal was evaluated using the best performing parameter combination. The parameters used for evaluation were a J/S ratio of 100, a carrier frequency of 1 kHz

and at a duty cycle of 70%. As seen in Figure 4.4, the jammer is switched on at 30 ms and therefore there is no effect on the seeker in the first 30 ms. While all the other tests were evaluated in 500 ms, the time response of the best performing jam signal was observed for 1 s. This is to observe if the jam signal performs any better with an increase in time. The temporal response is shown in Figure 4.4 and as seen in the figure, the maximum error of 0.73° is achieved at 460 ms and the error does not increase over time. The radial response oscillates at the mean error of 0.44° and the angular response oscillates about a mean of 12°. The angular error moves from a minimum of 44° to a maximum angle of -95° (which is 265°). The first quadrant of the reticle is the region with an angle of 0° to 90°, the second quadrant is 90° to 180°, the third 180° to 270° and the fourth 270° to 360°. The angular response shown in Figure 4.4(b) shows that the target position oscillates in the first, second and third quadrants of the reticle with this jam signal.

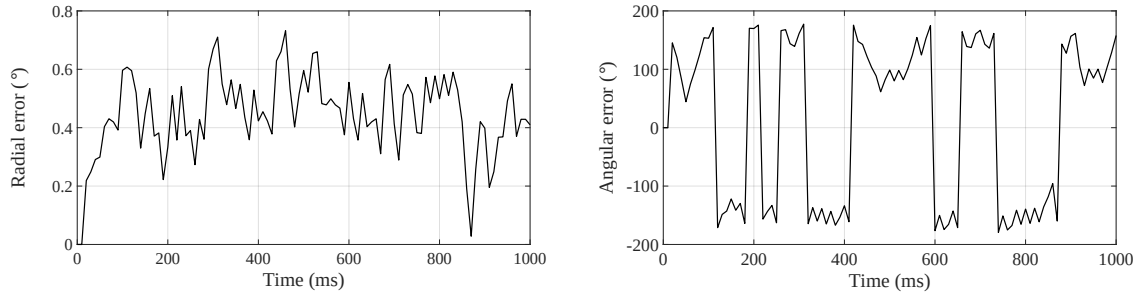

(a) Radial error **(b)** Angular error

Figure 4.4. Temporal response with fixed carrier jam signal. (a) Radial and (b) angular errors.

4.5.6 Overall performance of fixed carrier jam signal

The fixed carrier jam signal achieved an overall maximum of 0.74° radial error. The lowest effective J/S ratio is 100 which achieves an error of 0.74°. The effective carrier frequency is only at 900 Hz. The fixed carrier jam signal is sensitive to changes in the carrier frequency with a standard deviation of 0.12°. The range of effective duty cycles was found to be 70% - 80% with the lowest duty cycle achieving an error of 0.73°.

4.6 LOW FREQUENCY JAM SIGNAL

The low frequency jam signal consists of a constant envelope or modulation frequency and no carrier signal. Since the low frequency waveform does not contain a carrier signal, the effect of the carrier frequency was not tested with this waveform.

4.6.1 Effect of J/S ratio

The effect of varying the J/S ratio of the low frequency waveform is shown in Figure 4.5 with the associated heat map. As seen in the figure, the seeker error is minimal at a J/S ratio of 2, but increases significantly at a J/S ratio of 5. The error then increases slightly with an increase in the J/S ratio up to a J/S of 20 and then the effect saturates at this point. The maximum error achieved in this experiment was 0.958° at a J/S ratio of 20. It is interesting that the maximum error is achieved at a J/S ratio of 20 rather than the maximum tested ratio of 100. The range of effective J/S ratios for this experiment are those that achieve a seeker error of 90% of 0.958° which is 0.86°. The range of effective J/S ratios are 20 to 100. The maximum seeker error achieved at a J/S ratio of 2 is 0.13° and the maximum achieved at a J/S ratio of 100 is 0.943°.

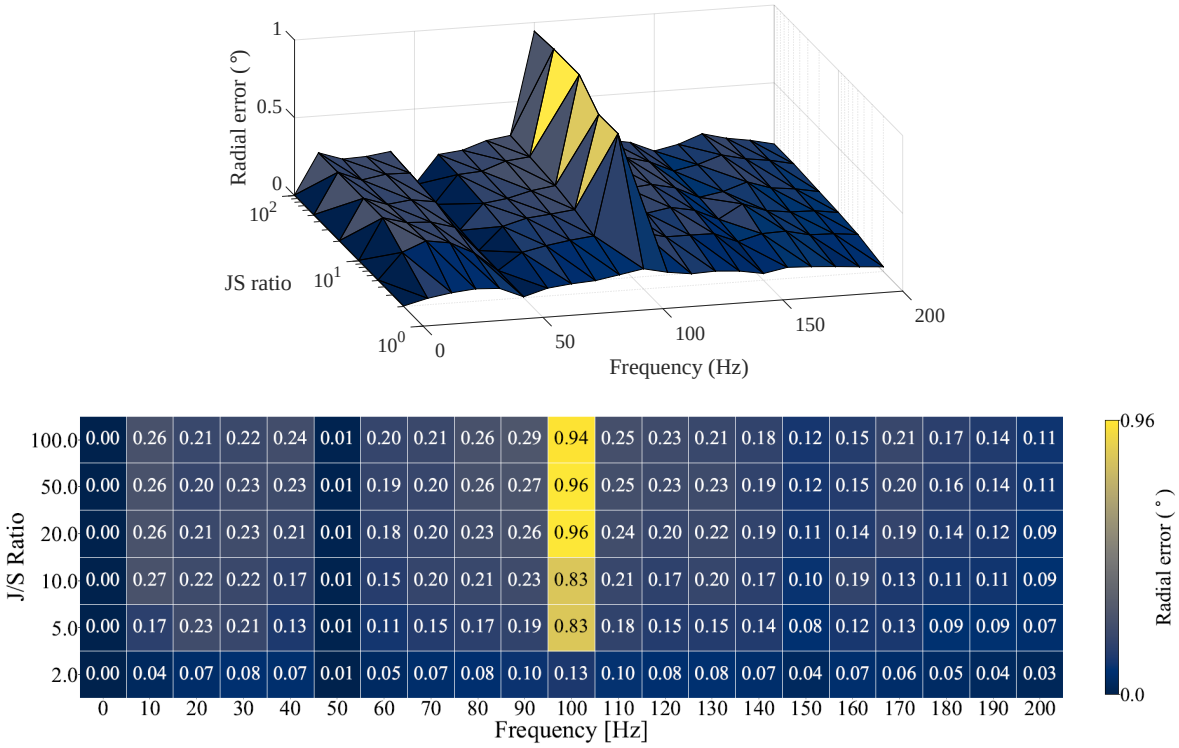

Figure 4.5. Effect of the J/S ratio for the low frequency jam signal.

4.6.2 Effect of modulation frequency

The effect of varying the modulation frequency is shown in Figure 4.5. The seeker error induced by this jam signal is interesting in that the effect is localized to a single frequency. The seeker responds when the jam frequency is 100 Hz but the jam signal has an insignificant effect elsewhere. It is also interesting to note that the seeker error completely dies out at a jam frequency of 50 Hz. A jam signal

operating at 50 Hz has a cycle of 20 ms and this means it will be completely on for one scan cycle (which is 10 ms) and then completely off for the next scan cycle. This means it will just increase the target signal in one scan cycle and decrease the target signature in the next. This is not effective as the target is still quite visible in both scan cycles. A jam signal operating at 100Hz switches on during half of the scan cycle and switches off during the other half of the scan. This makes it difficult for the processor to accurately demodulate the target position, making this frequency more effective. The effective frequencies are those that can achieve 90% of 0.958° which is 0.86°. The effective frequency is therefore only at 100 Hz. The mean error is 0.22° and the standard deviation is 0.18°. This shows that the jam signal does not perform close to the maximum on average since the maximum error is 0.958°.

4.6.3 Effect of duty cycle

The effect of varying the duty cycle in the low frequency jam signal, is shown in Figure 4.6 with the associated heat map. The seeker response shown in Figure 4.6(a) shows the error at each modulation frequency and the effect shown in Figure 4.6(b) shows the maximum effect across all the frequencies for each duty cycle. The heat map in Figure 4.6(c) shows the seeker error at the different test points It can be seen from Figure 4.6(a) and Figure 4.6(c) that the jam signal effect at 100 Hz is most significant at a duty cycle of 50% and not as significant at other duty cycles for this frequency. The frequencies 20 Hz and 30 Hz are more effective at the other duty cycles. As seen in Figure 4.6(b), there is an increase in the jam signal effect with an increase in the duty cycle and the effect tends to saturate with an increase in the duty cycle from 40% and then drops from 80% duty cycle upwards. The drop at 100% duty cycle is expected since the jam signal becomes a DC signal at 100% duty cycle. While the jam signal effect tends to saturate between 40% and 90% duty cycle, the actual maximum seeker error is achieved at a duty cycle of 70%. The duty cycle of 70% produces a seeker error of 0.97° and this occurs at a modulation frequency of 30 Hz. The range of effective duty cycles must achieve an error of at least 90% of 0.97° which is 0.87°. The range of effective duty cycles are therefore 40% to 80%. The jam signal only achieves a seeker error of 0.1° at a duty cycle of 10% and the effect increases up to 0.97° at a duty cycle of 70%.

4.6.4 Best parameter combination for low frequency jam signal

The maximum error with the low frequency jam signal is achieved in the duty cycle test with a maximum error of 0.97°. This error is achieved at a duty cycle of 70%, at a modulation frequency of 30 Hz and a J/S ratio of 100. The jam signal operating at a duty cycle of 50% achieves a maximum error of 0.958° in the J/S ratio test (see Figure 4.5). This is 98.7% of the maximum error achieved in

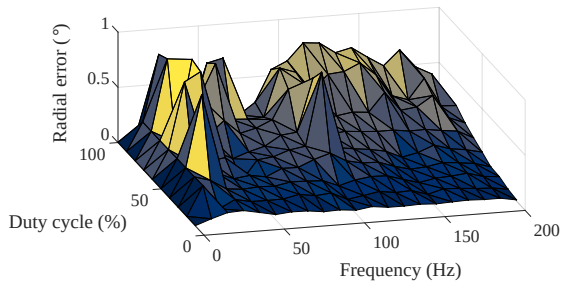

(a) Effect of duty cycle across all frequencies

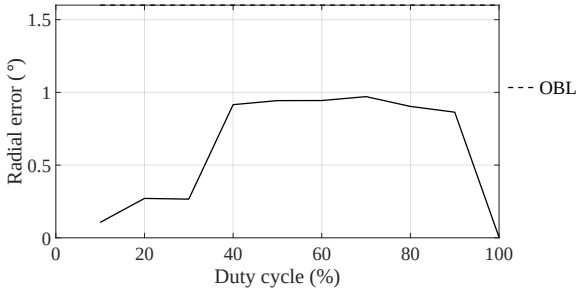

(b) Maximum effect of change in duty cycle

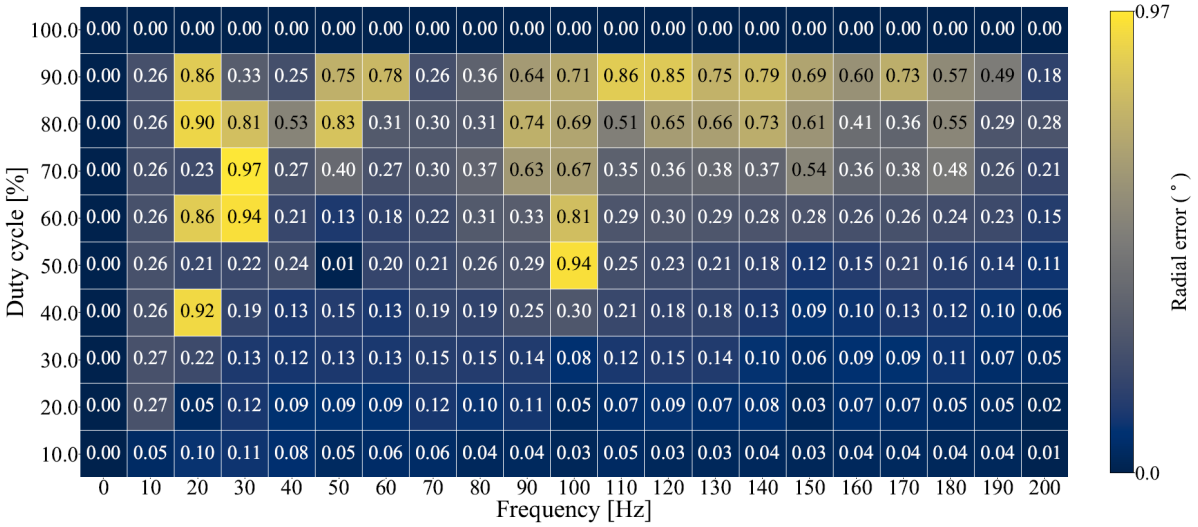

(c) Measured seeker error at various duty cycles

Figure 4.6. Effect of the duty cycle in the low frequency jam signal.

the duty cycle test (0.97°) and this error is achieved while operating at a J/S ratio of 20. The jam signal operating at a duty cycle of 40% achieves 94% of the maximum error while operating at a J/S ratio of 100. Since the jam signal operating at 40% duty cycle requires a much higher J/S ratio to be effective, the jam signal operating at 50% duty cycle is considered more power efficient. The signal that operates at 50% duty cycle is therefore selected as the better performing jam signal and is therefore the signal that will be used for further evaluation. The best performance with the low frequency jam signal is therefore achieved at a J/S ratio of 20, a modulation frequency of 100 and at a duty cycle of 50%. And the maximum error achieved with these parameters is 0.958°.

4.6.5 Temporal response

The response of the seeker in the time domain to the best performing jam signal in the low frequency type, was evaluated at a J/S ratio of 20, a modulation frequency of 100 Hz and at a duty cycle of 50%.

As seen in Figure 4.7, the jammer is switched on at 30 ms and therefore there is no effect on the seeker in the first 30 ms. The maximum error is achieved at 440 ms, but the error is at 99.5% of the maximum at 240 ms. The seeker error increases to 0.953° (99.5% of the maximum) at 240 ms and oscillates about 0.83° till the 1 s mark. While the low frequency jam signal achieves its maximum error at a later time, the jam signal does sustain a larger error at which oscillations take place when compared with the fixed carrier jam signal. The angular error oscillates about -93° with very small oscillations in the third and fourth quadrant of the reticle.

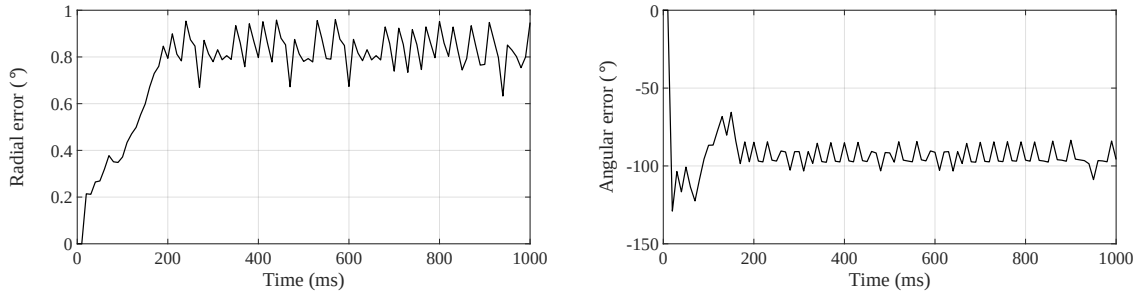

(a) Radial error **(b)** Angular error

Figure 4.7. Temporal response with low frequency jam signal. (a) Radial and (b) angular errors.

4.6.6 Overall performance of low frequency jam signal

The low frequency jam signal achieved an overall maximum of 0.97° radial error. The lowest effective J/S ratio is 20 which achieves an error of 0.96°. The effective modulation frequency is only at 100 Hz with a duty cycle of 50%. If the duty cycle is between 40% and 80% excluding 50%, the effective modulation frequency is either 20 Hz or 30 Hz. The low frequency jam signal is sensitive to changes in the modulation frequency with a standard deviation of 0.18°. The range of effective duty cycles was found to be 40% - 80% with the lowest duty cycle achieving an error of 0.92°.

4.7 AM JAM SIGNAL

The AM jam signal consists of a carrier signal with a fixed frequency and a modulation signal at a lower frequency.

4.7.1 Effect of J/S ratio

The effect of varying the J/S ratio of the AM jam signal waveform is shown in Figure 4.8 with the associated heat map. As seen in the figure, the AM jam signal produces an insignificant effect at a J/S ratio of 2 but the effect significantly increases when the J/S ratio is 5. The jam effect increases steadily with an increase in the J/S ratio from 5 to 100. The highest seeker error achieved in Figure 4.8 is 1.1°

at a J/S ratio of 100. The range of effective J/S ratios are those that achieve 90% of 1.1° which is 0.99°. The effective J/S ratios are 50 and 100. The maximum error at a J/S of 5 is 0.81° which is 73.6% of the maximum error.

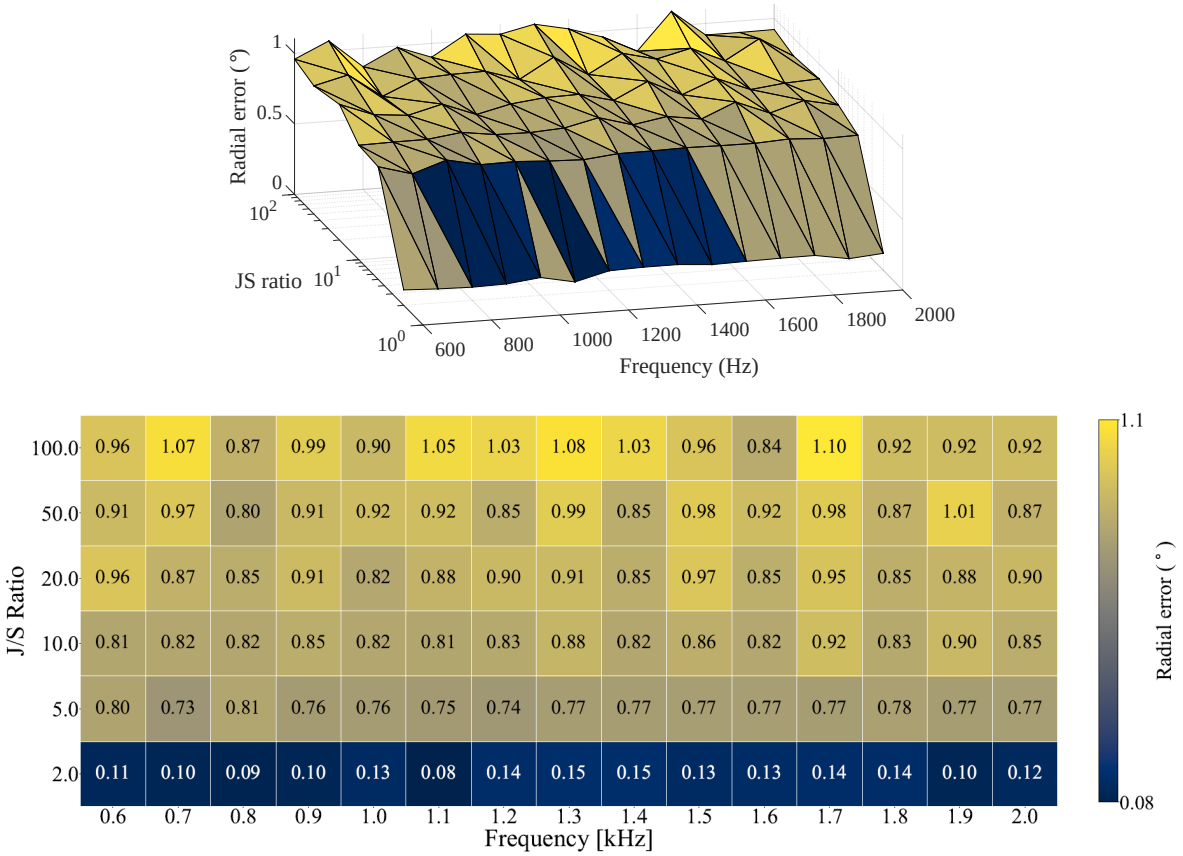

Figure 4.8. Effect of the J/S ratio for the AM jam signal.

4.7.2 Effect of carrier frequency

The effect of varying the carrier frequency is shown in Figure 4.8. The frequency is varied from 600 Hz to 2 kHz and as seen in the figure, the error produced by this jam signal is quite consistent across the tested carrier frequencies. The greatest seeker error was achieved at a carrier frequency of 1.7 kHz at a J/S ratio of 100. The mean error is 0.98° and the standard deviation is 0.08°. This is the lowest standard deviation found so far. The mean error is 89% of the maximum which shows that on average the jam signal produces an error close to its maximum. The low standard deviation shows that this jam signal is consistent in its effect and is effective against a wide range of carrier frequencies. Since 90% of the maximum error (which is 0.99° in this case) is the mark that is used to measure the range of effective frequencies, the range of effective frequencies in this case are [0.7, 0.9, 1.1 - 1.4, 1.7,

1.9] kHz. This is a wide range of frequencies that successfully achieve at least 90% of the maximum error. This makes this jam waveform more robust than the other considered waveforms so far.

4.7.3 Effect of modulation frequency

The effect of changes in the modulation frequency of the AM jam signal is shown in Figure 4.9. The error shown in Figure 4.9(a) is the effect of varying the modulation frequency from 50 Hz to 150 Hz across all the carrier frequencies. The effect shown in Figure 4.9(b) is the maximum seeker error obtained across all the carrier frequencies at each modulation frequency. The heat map in Figure 4.9(c) shows the seeker error at the different test points. As seen in Figure 4.9(b), the seeker error is at a maximum at 100 Hz modulation frequency reaching a maximum of 1.1°. The seeker error does not vary much in the range 60 Hz to 90 Hz and 110 Hz to 140 Hz, but the effect drops at a modulation frequency of 50 Hz. The effective modulation frequencies must achieve an error of 0.99° or more and as seen in Figure 4.9(c), the effective modulation frequency is only 100 Hz. The mean error achieved for the various modulation frequencies is 0.74° and the standard deviation is 0.17°. The mean error is 67% of the maximum error achieved. Since the mean error was 89% of the maximum when the carrier frequency was varied, it can be concluded that varying the modulation frequency has a greater effect than varying the carrier frequency in the AM jam signal.

4.7.4 Effect of duty cycle

The effect of varying the duty cycle of the modulation signal for the AM jam signal is shown in Figure 4.10. Only the duty cycle of the modulation signal was varied in this experiment. The seeker response shown in Figure 4.10(a) shows the effect of varying the duty cycle for all the considered carrier frequencies and the effect shown in Figure 4.10(b) shows the maximum effect achieved for each duty cycle across all the carrier frequencies. The annotated heat map is shown in Figure 4.10(c). As seen in the Figure 4.10(b), the seeker error increases with an increase in the duty cycle from 20% to 50% duty cycle. The error decreases with a further increase in the duty cycle. It can be seen that the AM signal achieves a greater seeker error when the duty cycle of the jam signal is at the 50% mark. The seeker error does not improve with an increase in the duty cycle beyond 50%. The range of effective duty cycles, are those that achieve at least 0.99° error or more. These duty cycles are in the range 30% - 50%. This is similar to the effect observed with the low frequency jam signal. It should be noted though that the AM jam signal produces a significantly higher seeker error at a duty cycle of 10% when compared to the fixed carrier and the low frequency jam signals. The seeker error at 10% duty cycle is 0.936° and the maximum error achieved in the duty cycle test is 1.1°. The seeker error at 10% duty cycle is therefore 85% of the maximum error achieved in this test. The fixed carrier produces

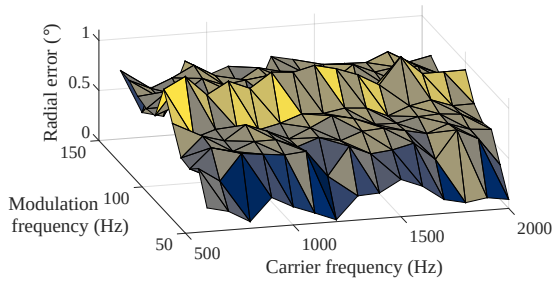

(a) Effect of envelope frequency across all carrier frequencies

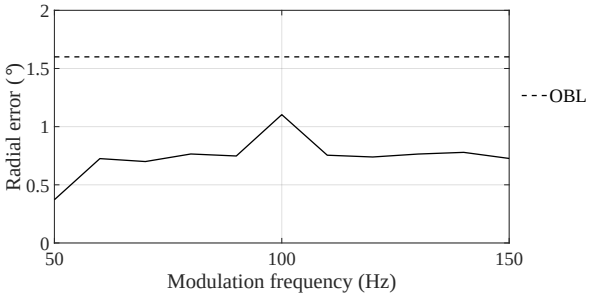

(b) Maximum effect of change in modulation frequency

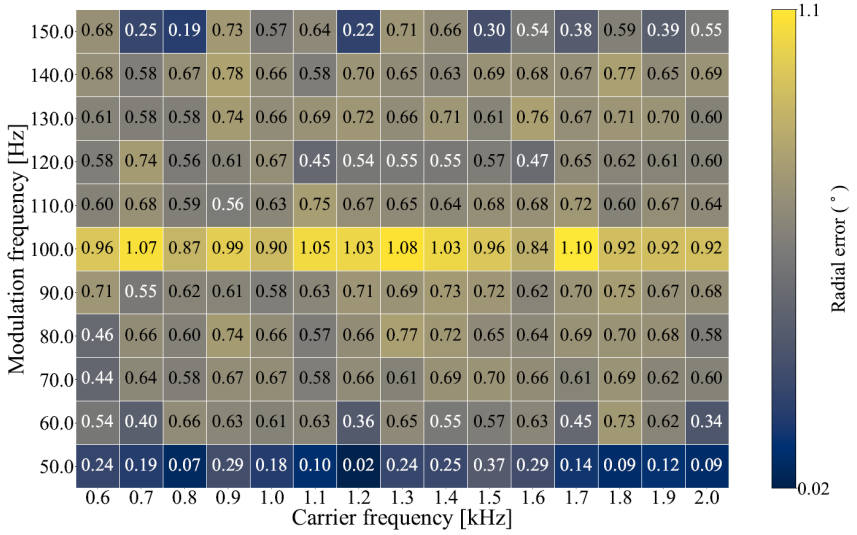

(c) Measured seeker error at various envelope frequencies

Figure 4.9. Effect of the modulation frequency in the AM jam signal.

9.2% of the maximum seeker error and the low frequency produces 10.9% of its maximum error at a duty cycle of 10%. This gives the AM jam signal an advantage over the fixed carrier and the low frequency jam signals as it produces a significant seeker error even at a 10% duty cycle.

4.7.5 Best parameter combination for AM jam signal

The maximum error achieved with the AM jam signal is 1.1° at a J/S ratio of 100, carrier frequency of 1.7 kHz, modulation frequency of 100 Hz and a duty cycle of 50%, as seen in Figure 4.8. Varying the modulation frequency and the duty cycle did not improve this error. The minimum duty cycle to achieve effective jamming was at 30% duty cycle, at a J/S of 100, it is a better performer than the jam signal that achieves 1.1° error at 50% duty cycle. The J/S ratio test showed that 90% of the maximum error can be achieved at a J/S ratio of 50. A J/S ratio of 50 produces a maximum error of 1°

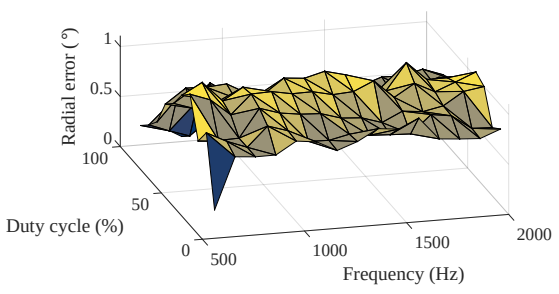

(a) Effect of duty cycle across all frequencies

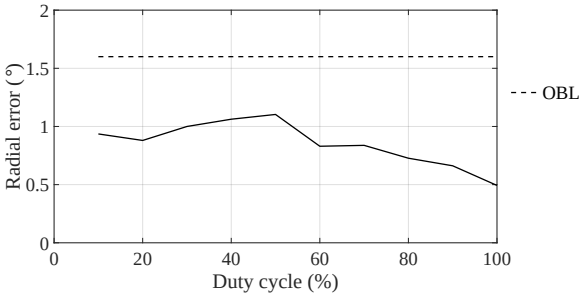

(b) Maximum effect of change in duty cycle

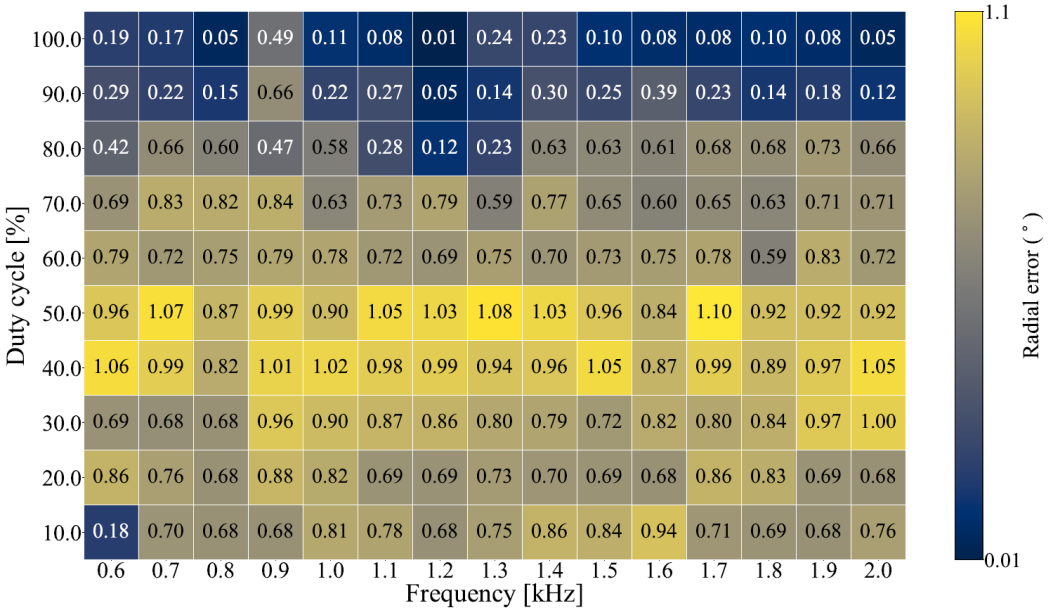

(c) Measured seeker error at various duty cycles

Figure 4.10. Effect of the duty cycle in the AM jam signal.

which is the same as the error attained in the duty cycle test with a duty cycle of 30%. Since the J/S parameter is more significant than the duty cycle parameter in terms of power consumption, it can be concluded that the jam signal operating at the lower J/S is the better signal. The best performing AM signal therefore achieves a maximum error of 1° with a J/S ratio of 50, carrier frequency of 1.9 kHz, modulation frequency of 100 Hz and a duty cycle of 50%.

4.7.6 Temporal response

The temporal response of the best performing signal, was evaluated at a J/S ratio of 50, a carrier frequency of 1.9 kHz, a modulation frequency of 100 Hz and at a duty cycle of 50%. The results are shown in Figure 4.11. As seen in Figure 4.11, the maximum error is achieved at 260 ms. The error

oscillates about a mean of 0.8°. This mean oscillation point is lower than the oscillation position of 0.83° obtained with the low frequency jam signal. The angular error oscillates about a mean of 85° and the error ranges from 70° to 94°. The target position therefore oscillates towards the edge of the first quadrant of the reticle.

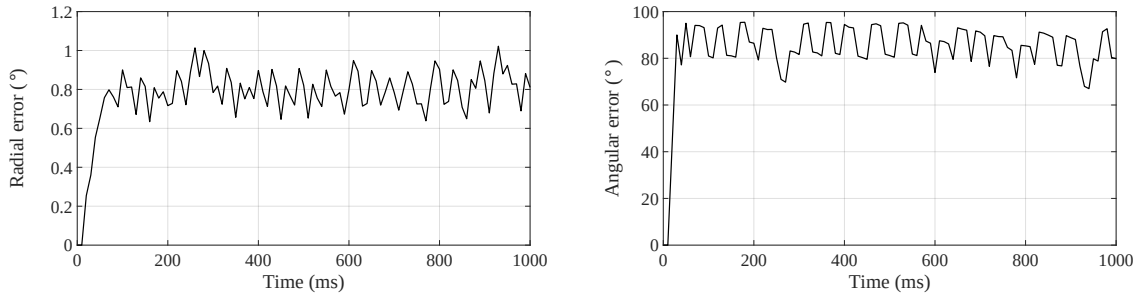

(a) Radial error **(b)** Angular error

Figure 4.11. Temporal response with the AM jam signal. (a) Radial and (b) angular errors.

4.7.7 Overall performance of AM jam signal

The AM jam signal achieved an overall maximum of 1.1° radial error. The lowest effective J/S ratio is 50 which achieves an error of 1°. The range of effective carrier frequencies is [0.7, 0.9, 1.1 - 1.4, 1.7, 1.9] kHz. The AM jam signal is insensitive to changes in the carrier frequency with a standard deviation of 0.08°. The effective modulation frequency is only at 100 Hz. The standard deviation of varying the modulation frequency is 0.17°. The AM jam signal is sensitive to changes in the modulation frequency. The range of effective duty cycles was found to be 30% - 50%.

4.8 FM JAM SIGNAL

The FM jam signal consists of a carrier signal with a variable frequency and a modulation signal with a constant frequency. The carrier frequency is varied according to the modulation index. Since the carrier signal is inherently varied in the FM jam signal, the effect of duty cycle was not tested for this jam signal.

4.8.1 Effect of J/S ratio

The effect of varying the J/S ratio of the FM waveform is shown in Figure 4.12. Due to the wide range of tested modulation indices, the heat map shown in Figure 4.12, only shows the odd indices for readability purposes. The odd indices were chosen due to the maximum value occurring at an odd index. The odd indices will be used for the other FM tests as well. The maximum error achieved is 0.715° and is achieved at a J/S ratio of 100 at a modulation index of 5.5. It can be seen in Figure 4.12

that the J/S ratio of 2 - 10 are not effective in all the modulation indices. The seeker error increases at a J/S ratio of 20 and increases gradually up to the maximum J/S. 90% of 0.715° is 0.64°, and this is the point of effect. The range of effective J/S ratios are therefore 50 and 100.

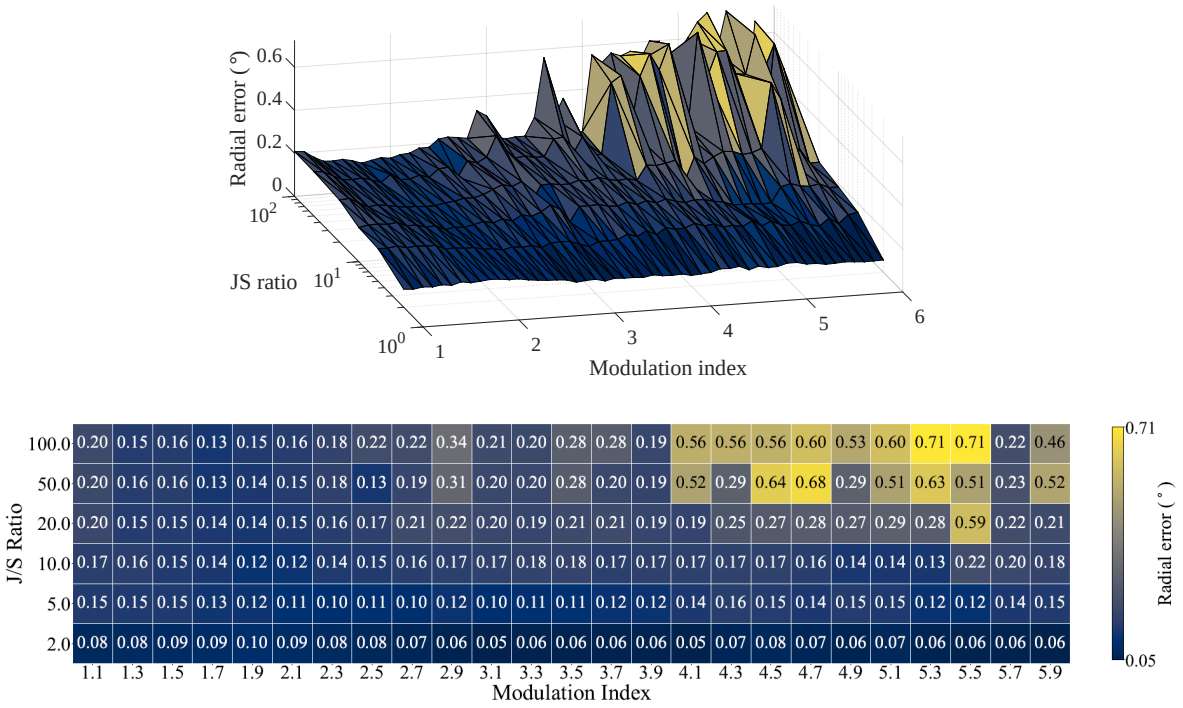

Figure 4.12. Effect of the J/S ratio for the FM jam signal.

4.8.2 Effect of modulation index

The effect of varying the modulation index is shown in Figure 4.12. The modulation index is varied from 1 to 6 in increments of 0.1. For the purpose of readability, the heat map only shows odd indices in the range 1 to 6. As seen in Figure 4.12, the seeker effect is consistently higher at modulation indices between 4 and 6. The seeker error is generally low at modulation indices less than 4. The seeker effect tends to increase with an increase in the modulation index beyond an index of 4. The point of effect in this case is 0.64°, and the modulation indices that attain this error are specific indices between 4.5 and 6. It should be emphasized that it is only specific indices in the range 4.5 to 6 which are effective since it can be observed from Figure 4.12 that the FM jam signal is rather sensitive to slight changes in the modulation index. While the jam signal might be effective at a modulation index of 4.5, the effect might completely die out at a modulation index of 4.6. The mean error with changes in the modulation index is 0.35° and the standard deviation is 0.19°. The standard deviation shows that the error is highly variable with changes in the modulation index. This can also be observed in that the seeker error is small in the lower modulation indices and higher at higher modulation indices.

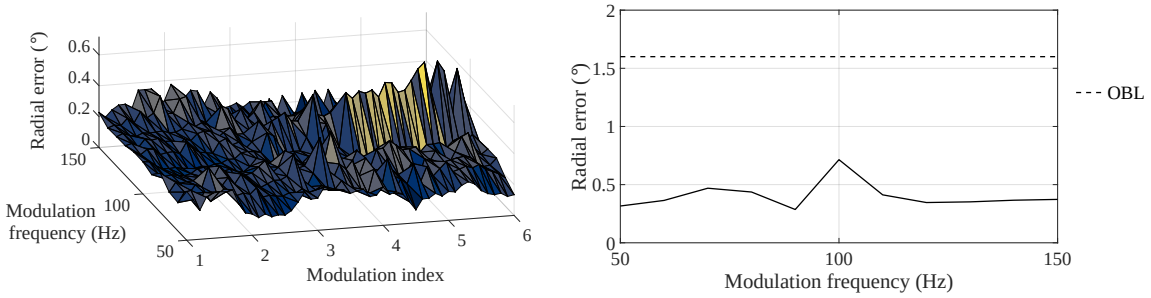

(a) Effect of envelope frequency across all carrier frequencies

(b) Maximum effect of change in modulation frequency

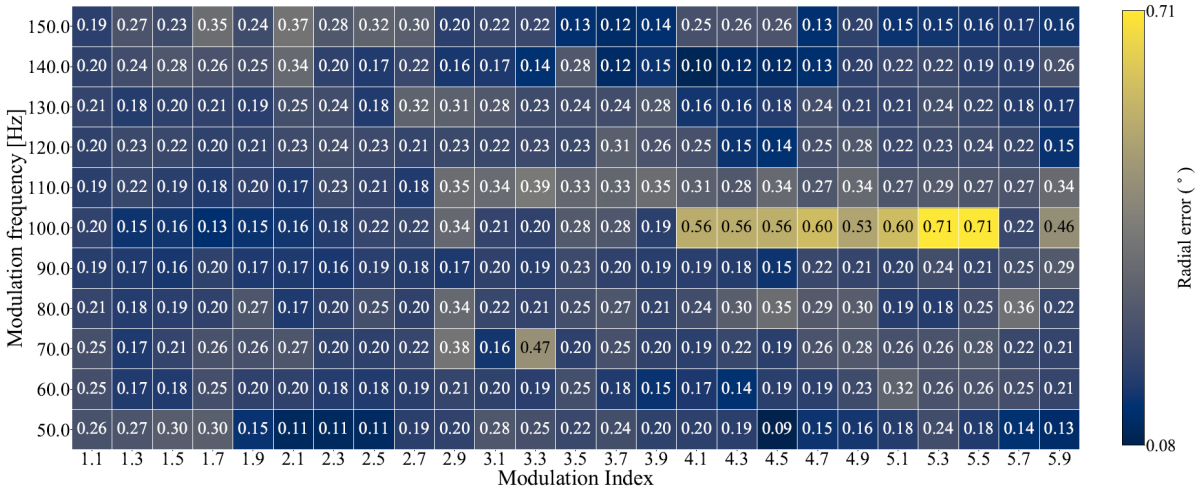

(c) Measured seeker error at various envelope frequencies

Figure 4.13. Effect of the modulation frequency in the FM jam signal.

4.8.3 Effect of modulation frequency

The effect of changes in the modulation frequency of the FM jam signal is shown in Figure 4.13. The associated heat map is shown in Figure 4.13(c). The error shown in Figure 4.13(a) is the effect of varying the modulation frequency from 50 Hz to 150 Hz across all the modulation indices. The effect shown in Figure 4.13(b) is the maximum seeker error obtained across all the modulation indices at each modulation frequency. As seen in Figure 4.13(b), the seeker error is at a maximum at a modulation frequency of 100 Hz. The range of effective modulation frequencies are those that achieve at least an error of 0.64°. The effective modulation frequency is only at 100 Hz. The mean error for changes in the modulation frequency is 0.4° and the standard deviation is 0.12°.

4.8.4 Best parameter combination for FM jam signal

The maximum error achieved with the FM jam signal is 0.715° at a J/S ratio of 100 and a modulation index of 5.5 as seen in Figure 4.12. It can be noted from Figure 4.12 that the effective modulation indices are in the range 4 to 6. Changes in the modulation frequency did not improve the maximum error achieved by the jam signal.

4.8.5 Temporal response

The temporal response of the best performing signal, was evaluated at a J/S ratio of 100, a modulation frequency of 100 Hz and at a modulation index of 5.5. As seen in Figure 4.14, the maximum error is achieved at 390 ms and the radial error oscillates about a mean of 0.63°. The overall mean error achieved is 0.55°. As seen in Figure 4.14(a), the radial oscillations are small when compared with the oscillations produced by other jam waveforms. The angular error oscillates from 170° to -141° (which is 219°) and the nutation circle therefore oscillates in the second and third quadrant of the reticle.

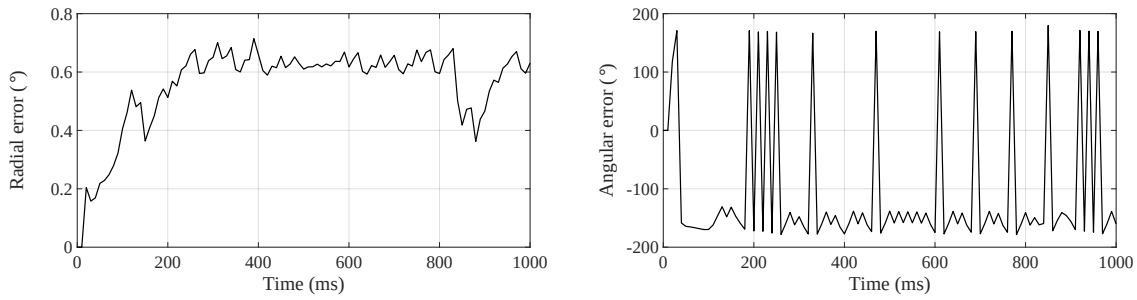

(a) Radial error **(b)** Angular error

Figure 4.14. Temporal response with the FM jam signal. (a) Radial and (b) angular errors.

4.8.6 Overall performance of FM jam signal

The FM jam signal achieved an overall maximum of 0.72° radial error. The lowest effective J/S ratio is 100 which achieves an error of 0.72°. The range of effective modulation indices is 4.5 - 6. The FM jam signal is sensitive to changes in the modulation index with a standard deviation of 0.19°. The effective modulation frequency is only at 100 Hz. The standard deviation of varying the modulation frequency is 0.12°. The FM jam signal is therefore sensitive to changes in the modulation frequency.

4.9 AM-FM HYBRID JAM SIGNAL

The AM-FM hybrid jam signal consists of a carrier signal with a variable frequency and a modulation signal with a constant frequency but variable amplitude. The carrier frequency is varied according to

the modulation index.

4.9.1 Effect of J/S ratio

The effect of varying the J/S ratio of the AM-FM hybrid waveform is shown in Figure 4.15. Due to the wide range of tested modulation indices, the heat map shown in Figure 4.15, shows odd indices because the maximum error is achieved at an odd index. As seen in the figure, the response is similar to that produced by the AM jam signal but with the variations that are seen with changes in the modulation index as with the FM signal. As seen in the figure, the jam effect is minimal at a J/S ratio of 2 but significantly increases at a J/S of 5. The effect then slightly but gradually increases with an increase in J/S ratio from 5 to 100. The maximum error 1° which is achieved at a J/S ratio of 100 and a modulation index of 1.5. The range of effective J/S ratios are those that achieve an error of 0.9° or more. The range of effective J/S ratios are 20, 50 and 100.

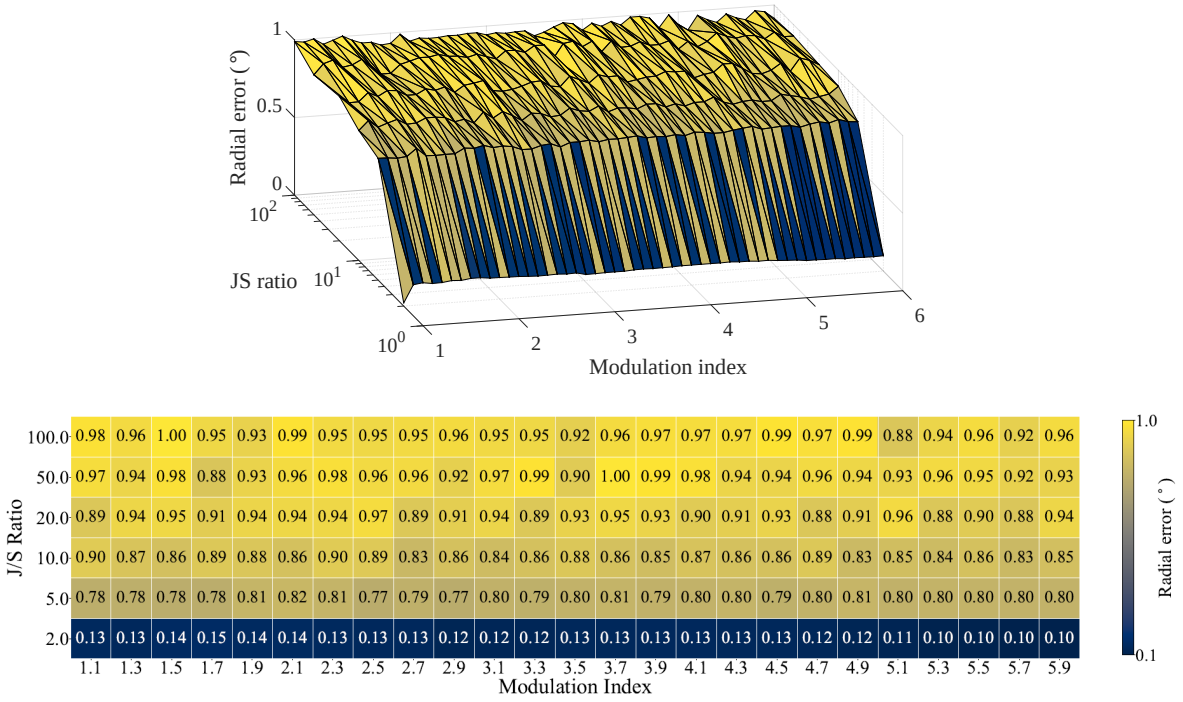

Figure 4.15. Effect of the J/S ratio for the AM-FM jam signal.

4.9.2 Effect of modulation index

The effect of varying the modulation index is shown in Figure 4.15. As seen in Figure 4.15, the seeker effect is quite consistent for all the tested modulation indices. Unlike the FM jam signal, the hybrid signal produces a similar effect for all the modulation indices tested. This effect is quite comparable to the effect seen with the AM jam signal. The range of effective modulation indices are those that

achieve an error of 0.9° or more. All the tested modulation indices are effective as they attain an error of at least 0.9°. This is the widest range of effective modulation indices found amongst the tested waveforms. The mean error for changes in the modulation index is 0.95° and the standard deviation is 0.03°. The AM-FM hybrid signal produces the lowest standard deviation when compared to the other jam signals. This means this jam signal produces on average a consistent error in the seeker with the least sensitivity to changes in the modulation index.

4.9.3 Effect of modulation frequency

The effect of changes in the modulation frequency of the AM-FM hybrid jam signal is shown in Figure 4.16. The error shown in Figure 4.16(a) is the effect of varying the modulation frequency from 50 Hz to 150 Hz across all the modulation indices. The effect shown in Figure 4.16(b) is the maximum seeker error obtained across all the modulation indices at each modulation frequency. The annotated heat map is shown in Figure 4.16(c). As seen in Figure 4.16(b), the seeker error is at a maximum at a modulation frequency of 100 Hz. The effective modulation frequency must achieve an error of 0.9° or more. This is only achieved at a modulation frequency of 100 Hz. This can be clearly seen in the heat map. The mean error for changes in the modulation frequency is 0.78° and the standard deviation is 0.09°.

4.9.4 Effect of duty cycle

The effect of varying the duty cycle of the modulation signal for the AM-FM hybrid jam signal is shown in Figure 4.17. The seeker response shown in Figure 4.17(a) shows the effect of varying the duty cycle for all the considered carrier frequencies and the effect shown in Figure 4.17(b) shows the maximum effect achieved for each duty cycle across all the carrier frequencies. The annotated heat map is shown in Figure 4.17(c). As seen in the figure, the seeker error increases with an increase in the duty cycle from 10% to 50% duty cycle. The error decreases with a further increase in the duty cycle. As shown in Figure 4.17(b), it can be seen that the AM-FM jam signal achieves the greatest seeker error when the duty cycle of the jam signal is at the 50% mark. The seeker error does not improve with an increase in the duty cycle beyond 50%. The range of effective duty cycles, are those that achieve 90% of the maximum error of 1°. This is the range of duty cycles that achieve at least 0.9° error or more. These duty cycles are 40% and 50%. It should be noted that the AM-FM jam signal produces a significant seeker error at a duty cycle of 10% similar to the AM jam signal. The AM-FM jam signal achieves an error of 0.77° while the AM jam signal achieved an error of 0.936° at 10% duty cycle.

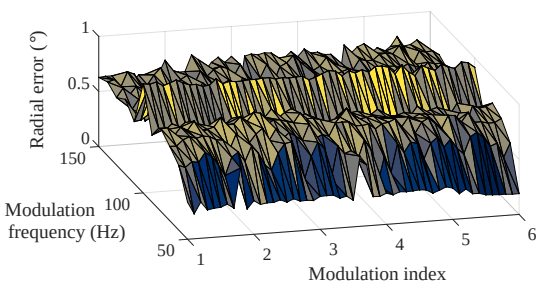

(a) Effect of envelope frequency across all carrier frequencies

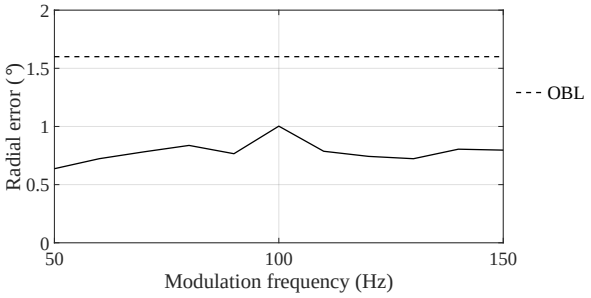

(b) Maximum effect of change in modulation frequency

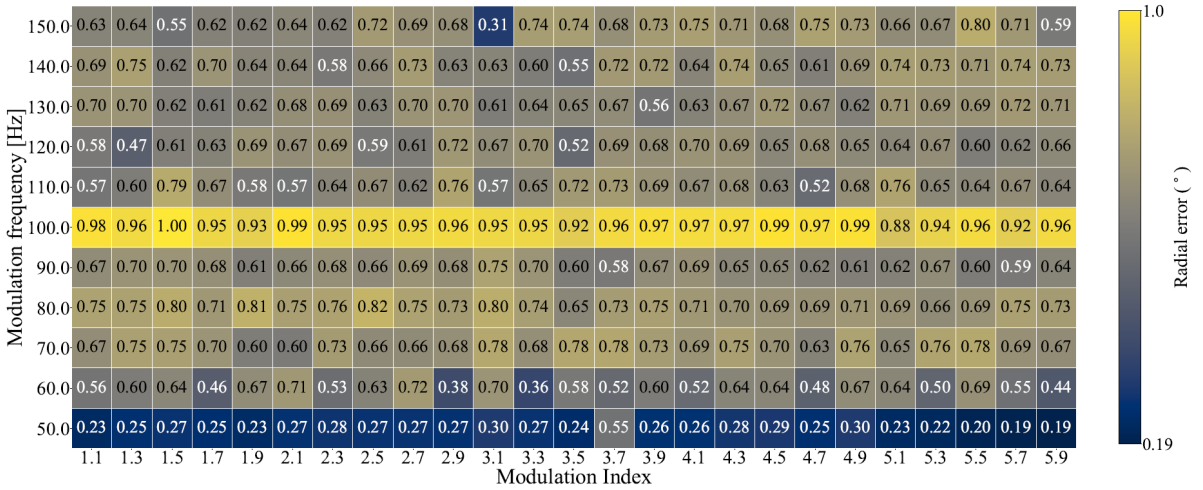

(c) Measured seeker error at various envelope frequencies

Figure 4.16. Effect of the duty cycle in the AM-FM jam signal.

4.9.5 Best parameter combination for AM-FM jam signal

The maximum error achieved with the AM-FM hybrid jam signal is 1° at a J/S ratio of 100, a modulation index of 1.5, an envelope frequency of 100 Hz and a duty cycle of 50%. The duty cycle test produced an error of 0.94° at a J/S ratio of 100 and a duty cycle of 40% which is a lower duty cycle than the duty cycle at which the maximum error is achieved. The J/S ratio test showed that the lowest effective J/S ratio was 20 which achieved a maximum error of 0.97°. Since the J/S ratio test produced the higher error when compared with duty cycle test and the J/S ratio is significantly less, the signal operating at a J/S of 20 was chosen as the best performer because it is less power intensive. The best performance is achieved at a J/S ratio of 20, a modulation index of 2.5 and an envelope or modulation frequency of 100 Hz.

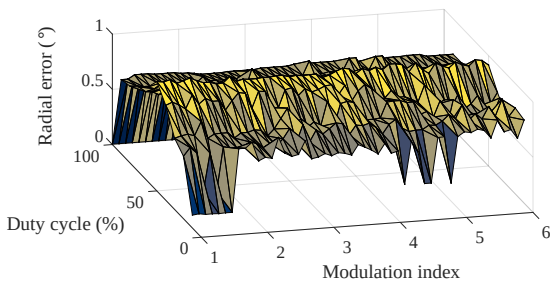

(a) Effect of duty cycle across all frequencies

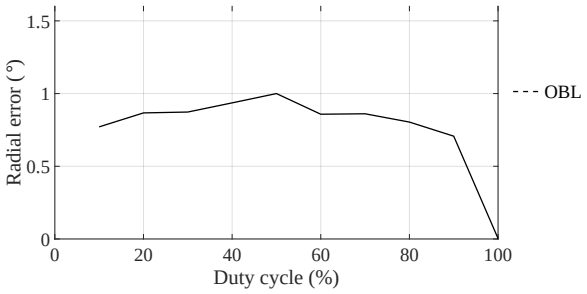

(b) Maximum effect of change in duty cycle

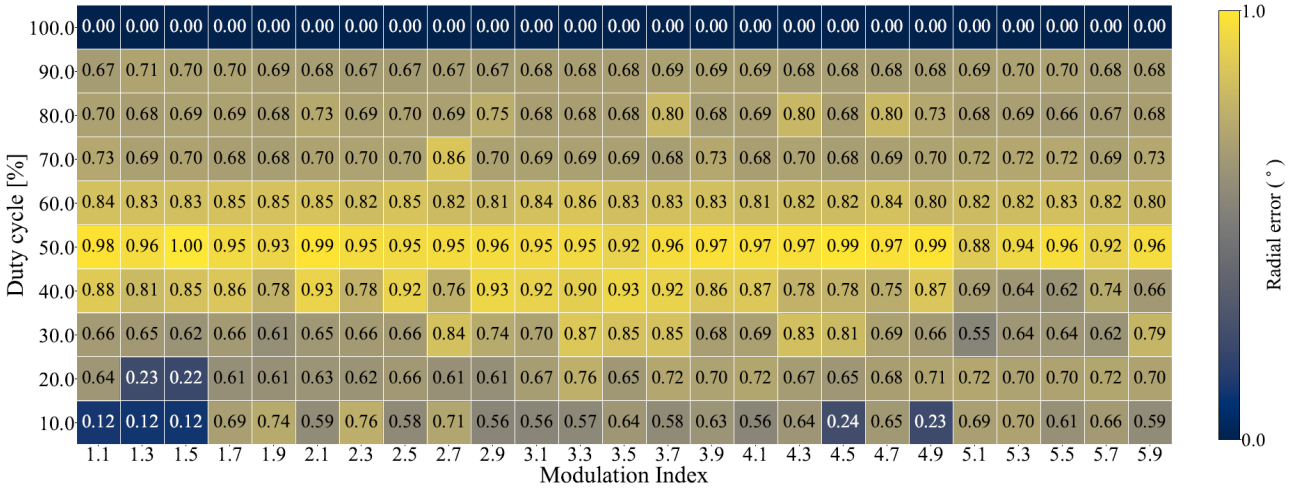

(c) Measured seeker error at various duty cycles

Figure 4.17. Effect of the duty cycle in the AM-FM jam signal.

4.9.6 Temporal response

The temporal response of the best performing signal, was evaluated at a J/S ratio of 20, a modulation index of 2.5 and a modulation frequency of 100 Hz. As seen in Figure 4.18, the maximum error is achieved at 390 ms and the error oscillates about a mean of 0.78°. The overall mean of the radial error is 0.76°. The angular error oscillates about -100° (which is 260°) in the third and fourth quadrant which is similar to the response induced by the low frequency jam signal.

4.9.7 Overall performance of AM-FM jam signal

The AM-FM jam signal achieved an overall maximum of 1° radial error. The lowest effective J/S ratio is 20 which achieves an error of 0.97°. The range of effective modulation indices is all the measured indices (i.e. 1 - 6). The AM-FM jam signal is insensitive to changes in the modulation index with a standard deviation of 0.03°. The effective modulation frequency is only at 100 Hz. The

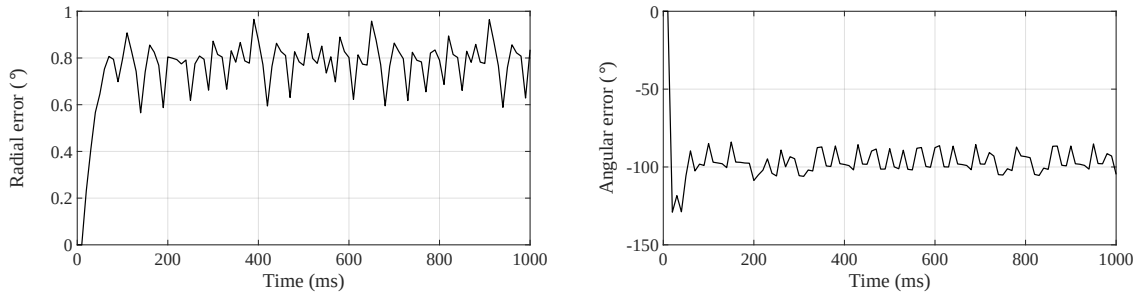

(a) Radial error **(b)** Angular error

Figure 4.18. Temporal response with the AM-FM jam signal. (a) Radial and (b) angular errors.

standard deviation of varying the modulation frequency is 0.09°. The AM-FM jam signal is insensitive to changes in the modulation frequency. The range of effective duty cycles was found to be 40% - 50%.

4.10 CONCLUSION

The jam signals that were used to test jam signal effectiveness were presented and the characteristics that define them were explained. The fixed carrier, low frequency, AM, FM and the AM-FM hybrid were evaluated and the results presented. The parameters that were evaluated are the

- minimum J/S ratio required to achieve the maximum error,
- range of carrier frequencies in which the jam signal is effective,
- range of modulation frequencies at which the jam signal is effective,
- minimum duty cycle required to achieve the maximum seeker error and
- the maximum error achieved.

The results show that in general an increase in the J/S ratio produces an increase in the jam signal effect. But it was also found that a number of jam signal designs achieve a maximum error at a lower J/S ratio, rather than the maximum J/S ratio. This means the effect of increasing the J/S ratio, saturates at some point in most cases. The fixed carrier and the FM jam signals require a high J/S ratio to be effective but the other jam waveforms are effective at lower J/S ratios.

It was found that the AM-FM jam signal is effective over the widest range of modulation indices since it produced a significant error in the seeker at all the tested modulation indices. It was found that all

the evaluated jam waveforms were effective at a modulation frequency of 100 Hz. The low frequency jam signal was found to produce a significant effect at other modulation frequencies given that the duty cycle is not 50%. At the duty cycle of 50% the low frequency jam signal is only effective at 100 Hz modulation frequency. The sensitivity of each jam waveform to changes in the frequency or modulation index as applicable was tested. The AM-FM jam waveform was found to be the least sensitive to changes in the modulation index and the modulation frequency. It was found that changes in the duty cycle do affect the performance of the jam signals. Some waveforms produce a significant effect at lower duty cycles but this is often at the expense of increasing the J/S ratio. The lowest effective duty cycle was found to be 30% in the AM jam signal.

CHAPTER 5 COMPARISON OF JAM SIGNAL WAVEFORMS

5.1 CHAPTER OBJECTIVES

This chapter aims to analyse the results that were obtained in Chapter 4 and to conduct a comparison of the tested jam signal waveforms. The effects of the J/S ratio are considered across the different waveforms and the effects are compared across the different waveforms. The effects of frequency and modulation index are then explored. This is to determine the effect of a frequency mismatch between the jam signal frequency and the threat missile induced target frequency. The analysis considers the sensitivity of each jam signal to changes in the frequency or modulation index as applicable and gives the implication of this sensitivity. The parameters for each jam signal that produced the best performance are then compared and a conclusion given on the best jam waveform to be used against the conical-scan seeker. The objective of this study was to answer the following questions:

- Which jam waveform is the most effective against the conical-scan seeker?
- What is the best parameter combination of the most effective jam signal in terms of J/S ratio, jam frequency and duty cycle?

These questions will be answered in this chapter.

5.2 SUMMARY OF RESULTS

A summary of the effectiveness of each jam waveform is presented in Table 5.1. The table summarises the results obtained in testing the critical jam signal parameters in each jam waveform. The first section of the table summarized the general performance of each jam waveform and the second section gives the best parameter combination based on the tests conducted. The first compared parameter is the maximum error each jam signal could achieve in the experiments. Since the main interest is in

finding the number of frequencies at which the jam signal is effective, the range of frequencies are not given but rather the number of frequencies or modulation indices at which the jam signal is considered effective. This facilitates comparison between waveforms that are measured in frequency and those that are measured using the modulation index. The sensitivity of the jam signal to changes in frequency is given as a percentage of the total FOV.

It can be seen that none of the jam waveforms achieve OBL. All the tests conducted in this study were conducted with a stationary seeker and a stationary target. This was to simplify the design of the missile under study. A system such as a heat seeking missile is complex and would require a large team of experts and a long period of time to accurately model the entire system that would be representative. This therefore justified the design of a simplified model that could be used to at least determine the effects of jamming on the seeker portion of the missile. Due to the seeker and the target being stationary, it is much easier for the seeker to track the target. And this is considered to be the main reason that OBL was not achieved in this study. Some studies suggest that a jam signal would not be effective against a conical-scan seeker if physical imperfections were not present [11, 18]. These physical imperfections are the vibrations in the seeker during flight and the optical scattering and reflection that occurs due to high J/S ratios. Since these imperfections are not modelled, the possibility of OBL significantly decreases.

5.3 MAXIMUM ERROR ACHIEVED

The maximum error achieved with each jam signal is shown as the first parameter in Table 5.1. The waveform that produces the highest error is the AM jam signal with a maximum error of 1.1°. The AM jam waveform is followed by the AM-FM jam signal which attains a maximum of 1°. The lowest seeker error is achieved with the FM jam signal with an error of 0.72°. The linear region of the designed seeker is 0.4°. It is clear that all the jam waveforms are able to produce an error that exceeds the linear region error which means the possibility of OBL could be achieved with any one of these waveforms when the missile is in flight. It is argued that OBL can be achieved with all of these waveforms based on the typical static gain curve of the conical-scan seeker (shown in Chapter 3). It was seen that the seeker struggles to accurately track targets that are outside the linear region. This is further degraded when the missile is in flight since the additional vibrations and changes in look angle caused by the high speed in flight, make the target harder to track. This suggests that the errors seen with the tested waveforms can be expected to be greater with a mobile missile in flight. But the possibility of OBL is expected to be greater for those waveforms that induce the highest errors in the

Table 5.1. Summary of jam signal effectiveness. Some combinations are not applicable (N/A).

Parameter	Fixed carrier	Low frequency	AM	FM	AM-FM
Jam effectiveness: OBL occurs at 1.6° induced track error					
Maximum error [°]	0.74	0.97	1.1	0.72	1
Lowest effective J/S ratio	100	20	50	100	20
Number of effective carrier frequencies	1	N/A	8	N/A	N/A
Number of effective modulation indices	N/A	N/A	N/A	10	50 (Full range)
Sensitivity to carrier frequency or index (σ) [%]	7.5	N/A	5	11.9	1.9
Number of effective modulation frequencies	N/A	1	1	1	1
Sensitivity to modulation frequency (σ) [%]	N/A	11.3	10.6	7.5	5.6
Range of effective duty cycles [%]	70 - 80	40 - 80	30 - 50	N/A	40 - 50
Best parameter combination for jam waveform					
J/S ratio	100	20	50	100	20
Carrier frequency or modulation index	1 kHz	N/A	1.9 kHz	5.5	2.5
Modulation frequency [Hz]	N/A	100	100	100	100
Duty cycle [%]	70	50	50	N/A	50
Induced error [°]	0.73	0.96	1	0.72	0.97

stationary seeker. The jam waveforms that produce greater seeker errors in the stationary seeker will therefore be preferred.

5.4 EFFECT OF J/S RATIO

The lowest J/S ratio is achieved with the low frequency and the AM-FM hybrid jam signals with a J/S ratio of 20. The two jam signals attain an error of at least 90% of the respective waveform maximum with a J/S ratio of 20. In the case of the low frequency jam signal, the achieved error reduces from 0.97° to 0.96° with a decrease in the J/S ratio from 100 to 20. This is a significant saving in power with an insignificant decrease in the jam effect. The AM-FM jam signal has a reduction of 0.03 in the maximum error with the reduction in J/S from 100 to 20. This is also a rather small decrease in effect for the power saving that is obtained. The fixed carrier and the FM jam signals require the maximum J/S ratio of 100 to be effective. In terms of J/S ratio, it can be concluded that both the low frequency and the AM-FM jam signals require the least J/S ratio to be effective.

5.5 EFFECTIVE CARRIER FREQUENCIES OR MODULATION INDICES

In order to compare the carrier frequencies and modulation indices effectively, the number of the respective frequencies and indices was used. The carrier frequency and modulation index are not applicable to the low frequency jam signal since it does not have a carrier signal. The low frequency is therefore not compared in this category. As seen in the table, the AM-FM jam signal is effective for the full range of modulation indices which is 50 indices. This range is much higher than the range in which the other jam waveforms are effective. This means if it is desired to have a jam signal that is effective across a wide range of con-scan seekers which operate at different frequencies, the AM-FM jam signal should be the jam signal of choice. The FM jam signal is the signal with the second widest range of effective modulation indices with ten effective indices. The AM jam signal is found to be effective at eight carrier frequencies and the fixed carrier is only effective at one frequency. It should be noted that the fixed carrier and the AM jam signals were tested in the range 600 - 2000 Hz with 100 Hz increments between the measurements, giving a total of 15 tested frequencies. This means the FM and the AM-FM hybrid waveforms were tested at more points when compared to the fixed carrier and the AM jam signals. This could be a contributing factor to the FM and AM-FM jam signals being superior to the other signals. But it can also be argued that the AM-FM jam signal is even more robust given that is was tested across a wider range of test points and was effective at every point. In terms of the sensitivity of each jam waveform to changes in the carrier frequency or modulation index, the AM-FM jam signal is the least sensitive with a standard deviation of 1.9%. The most sensitive to changes in the modulation index is the FM jam signal with a standard deviation of 11.9%. It can

therefore be concluded that the most robust jam signal in terms of sensitivity to changes in frequency with the widest range of effective indices is the AM-FM jam signal.

5.6 EFFECTIVE MODULATION FREQUENCY

The modulation frequency is not applicable to the fixed carrier jam signal since it does not contain a modulation signal. The comparison therefore does not apply to the fixed carrier jam signal in this category. It was found that all the jam waveforms are most effective at the nutation frequency of the seeker. The effect is significantly less when the jam signal operates at a different modulation frequency. It is interesting that the common consensus in the literature is that the jam signal is least effective when the jam signal frequency equals the target signal frequency. This is obviously only applicable to the carrier frequency and not to the modulation frequency since the modulation frequency as seen here, is most effective when it matches the seeker nutation frequency. The low frequency jam signal was able to achieve effect at other modulation frequencies but this was at other duty cycles. Since the jam signals are compared with all the tested parameters fixed at the same values, the effective modulation frequency was only considered at a duty cycle of 50%. In this case all the jam waveforms are only effective at 100 Hz. In terms of sensitivity to changes in the modulation frequency, the AM-FM jam signal is the least sensitive to changes in the modulation frequency with a standard deviation of 5.6% of the seeker FOV. The low frequency jam signal is the most sensitive to changes in the modulation frequency with a standard deviation of 11.3%.

5.7 EFFECTIVE DUTY CYCLES

The range of effective duty cycles for each jam waveform is shown in Table 5.1. The interest is in finding the minimum duty cycle that can achieve a significant error in the seeker, since this is more power efficient. The jam waveform with the lowest effective duty cycle is the AM jam signal with a duty cycle of 30%. The jam signal which requires the highest duty cycle to be effective is the fixed carrier jam signal with a duty cycle of 70%. While the AM jam signal can be effective at a duty cycle of 30%, this effect is achieved at a J/S ratio of 100. The power saving from the duty cycle is therefore overshadowed by the additional power required with the doubling of the J/S ratio.

5.8 PARAMETER COMBINATION DISCUSSION

The best parameter combination for each jam signal waveform is shown in the lower section of Table 5.1. As mentioned in Chapter 4, the effectiveness of each jam signal is not quantified solely on the maximum error achieved. The jam signal effect is quantified based on a range of other parameters which are important in a jamming engagement. In defining which jam signal is the most effective against the conical-scan seeker, the restrictions on the operating equipment is important. It can be seen

that the AM jam signal achieves the greatest seeker error when compared to the other jam waveforms but at best, it achieves this error with a J/S ratio of 50. The AM-FM jam signal achieves an error of 0.97° but at a J/S ratio of 20 which is less than half of the required J/S ratio in the AM jam signal. As mentioned previously the low duty cycle with the AM jam signal cannot be justified due to the much higher required J/S ratio. The AM-FM jam signal is effective at a duty cycle of 40% which is 10% more than the lowest duty cycle fond with the AM jam signal. The AM-FM jam signal is effective in the widest range of modulation indices and is therefore the most robust. This shows that the AM-FM jam signal would be the most flexible with mismatches between the set jam frequency and the actual missile seeker operating frequency. This is a desirable quality given that in a jamming engagement, the type of missile attacking the platform is not known, let alone the operating frequency of the threat. With the stated advantages of the AM-FM hybrid jam signal, it can be concluded that this jam signal is the most effective jam signal against the conical-scan seeker.

The general guide provided in the literature is that the most effective jam signal is one that is similar to the target induced signal [13–16, 18, 19]. The conducted study however found that of the tested waveforms, the AM-FM jam signal is the most effective; and this jam signal does not resemble the target signal at all. The target signal consists of a constant carrier signal operating at a constant frequency. The target can be matched to the fixed carrier jam signal. Since the AM-FM jam signal contains an FM carrier signal which has a variable frequency; the jam signal cannot be similar to the target induced signal. As seen in the results, the fixed carrier jam signal is not considered effective when operating at the 50% duty cycle which is the target duty cycle. Furthermore, it was found that the fixed carrier jam signal achieved no error when the jam frequency was matched to the target frequency. This is however expected since the matching of the target and jam frequency illuminates the target and makes the target easier to track. The fixed carrier jam signal becomes effective when the duty cycle is between 70% and 80%, but this effect is achieved at a J/S ratio of 100. It can therefore be argued that a jam signal does not necessarily have to be similar to the target signal to be effective against the conical-scan seeker.

The hypothesis given in Chapter 1, stated that an effective jam signal would contain a fixed carrier signal with the frequency close to the target frequency and a modulated envelope signal operating at a 50% duty cycle and at the nutation frequency. This hypothesis is therefore disproved since the most effective jam signal was found to be one that contains a variable carrier frequency due to the FM component of the signal. The hypothesis is further disproved by the fact that the fixed carrier jam

signal which contains a constant frequency is not most effective at a duty cycle of 50% but rather at a higher duty cycle of 70% and 80%. The hypothesis stated that the jam signal would be effective at a high J/S ratio since the higher the jam intensity is, the greater the jam effect is expected to be. In the case of the AM and AM-FM jam signals, the effect of the J/S ratio tends to saturate at some point and a further increase in the J/S ratio, yields no increase in the induced error. This completely disproves the hypothesis in that the expected correlation between the J/S ratio and the jam effect is not always positive and can therefore not be generalized for all the jam waveforms.

5.9 CONCLUSION

The tested jam waveforms were compared in this chapter. The jam waveforms were compared in terms of the maximum error achieved by each jam signal, the minimum J/S ratio required to achieve significant effect, the range of effective frequencies or modulation indices and the lowest duty cycle at which significant effect can be achieved. The AM jam signal produced the greatest seeker error against the conical-scan seeker with a maximum error of 1.1°. None of the jam waveforms achieved OBL against the seeker and this was attributed to the simple stationary design of the seeker which makes it easier to track the target. The AM-FM jam signal achieved 0.97° error while operating at less than half of the J/S ratio required by the AM jam signal. The AM-FM jam signal was found to be the most robust across a wide range of modulation indices making it the signal of choice when engaging with a threat of unknown operating frequency. The AM-FM jam signal was found to be the least sensitive to changes in the modulation index and in the modulation frequency. When comparing the strengths and weaknesses of each jam waveform, the AM-FM jam signal was chosen as the best performing jam signal against the conical-scan seeker. The hypothesis given in Chapter 1, required the jam signal to consist of a constant carrier and modulation frequency to be effective and this hypothesis was disproved given that the AM-FM jam signal consists of a variable frequency because of the nature of the FM signal. The hypothesis was also disproved in the requirement to operate at a duty cycle of 50%. The hypothesis also stated that the jam signal would be most effective at a J/S ratio of 100, which was disproved.

The conclusion of the study is that the jam signal does not necessarily have to be close to the target signal to be effective against the conical-scan seeker as shown by the results. The reason for the difference in findings between this study and the majority of studies found in the literature is attributed to the variety of waveforms that were tested in this study which produced further insight of the operation of the conical-scan seeker. It was also found that the most effective jam signals against the conical-scan

seeker tended to contain an AM element or a modulation signal as is the case of the low frequency, AM and AM-FM jam signals.

CHAPTER 6 CONCLUSION AND FUTURE WORK

6.1 CONCLUSION

This study investigated the effect of different jam waveforms against the conical-scan seeker with the intention to find the most effective jam waveform. The literature mainly tests the effects of the low frequency jam signal against the conical-scan seeker and other waveforms are not tested. This prompted the current study to investigate the effect of other types of waveforms against the conical-scan seeker.

Due to the inaccessibility of a physical missile, the study designed and simulated a missile seeker model which could be used as a representative for the conical-scan seeker. The model was extensively tested to ensure the expected performance from the seeker and the performance results were compared with results from other similar models. The tested jam waveforms are the fixed carrier, low frequency, AM, FM and the AM-FM hybrid jam signals. The parameters used for testing the jam signals are the J/S ratio, frequency and duty cycle with an intention to find the best parameter combination for effective jamming.

It can be concluded that the conical-scan jam signal is not easy to jam given that all the tested jam waveforms did not achieve OBL. This could be attributed to the target and the missile body of the model being stationary with only the seeker gimbal being dynamic. When comparing the tested jam signals against each other, it was found that the most effective jam signal against the conical-scan seeker is the AM-FM hybrid jam signal. The AM-FM hybrid jam signal was found to be the most robust in a wide range of modulation indices. This jam waveform was found to be the least sensitive against changes in the modulation index. The jam signal was found to be less power intensive when

compared with other waveforms since significant jam effect was achieved at low J/S ratios. The best parameter combination for this jam signal was a J/S ratio of 20, a modulation index of 2.5, a modulation frequency of 100 Hz and a duty cycle of 50%. The maximum seeker error induced by this jam signal is 1° which is 60.6% of the maximum error. The conclusion of this work was therefore that the most effective jam signal does not necessarily have to be similar to the target signal to be effective against the conical-scan seeker. It was found that contrary to the guide provided in the literature, the most effective jam signal does not contain parameters that are close to the target induced parameters since the AM-FM jam signal contains an FM carrier signal. The unique result found in this study is attributed to the wide range of jam signal waveforms that were tested. The results show that the effects of the critical parameters (J/S ratio, frequency and duty cycle) vary with the change in jam waveform.

6.2 LIMITATIONS AND FUTURE WORK

Given that the study was conducted with a stationary seeker that only has a moving gimbal, the results obtained in this study are not conclusive. The results provide a guide but should be validated using a mobile missile. The seeker gimbal was also not modelled in detail and the movement of the seeker was merely limited per rotation. This is an aspect that can be improved to ensure that the gimbal dynamics are representative of a real missile seeker. The use of a modified wagon wheel reticle should be tested since the modified reticle would improve the static gain curve of the seeker. The improvement in the static gain curve can advantage the seeker even further against jamming. The tested jam waveforms were restricted to the fixed carrier, low frequency, AM, FM and the AM-FM hybrid jam signals. Other waveforms that can be considered are the ramp jam signal that has a constant carrier frequency with a ramping amplitude, the ramping frequency jam signal, the sawtooth amplitude or frequency jam signal etc. Given that the details of the seeker design are not explicitly given in the literature, the effects of design tolerances on jam signal effectiveness will be studied in future. This includes the effect of various nutation circle sizes, the effect of different AGC duty cycles, the effect of having a limiter in the signal processor of the seeker and the effect of having different nutation frequencies. It is also envisaged that the optical scattering and reflection could be modelled to determine the effect of this scattering in aiding the effectiveness of jamming. This could also extend to the effect of scattering in the blinding type of jamming which aims to conceal the target from the seeker by saturating the sensitive seeker electronic components.

REFERENCES

[1] D. Richardson, "The modern manpads - an evolving threat," *Journal of Electronic Defence*, vol. 38, no. 7, pp. 26–32, Jul. 2015.

[2] J. R. Bartak, "Mitigating the MANPADS threat: international agency, US, and Russian efforts," M. Arts thesis, Naval Postgraduate School, Monterey, USA, Mar. 2005.

[3] M. A. Richardson, "The anatomy of the manpad," in *Proc. SPIE*, vol. 6738, Florence, Italy, Oct.23 2007, pp. 1–11.

[4] J. Bevan and M. Schroeder, *Man-portable Air Defence Systems (MANPADS)*. Geneva, Switzerland: Small arms survey, Jan. 2008, ch. 12, pp. 121–128.

[5] T. Jackson, "From under their noses: Rebel groups' arms acquisition and the importance of leakages from state stockpiles," *International Studies Perspectives*, vol. 11, no. 2, pp. 131–147, May 2010.

[6] A. R. Jha, *IR signature analysis and countermeasure techniques*, 1st ed. John Wiley and Sons, Sep. 2000, ch. 10, pp. 363–400.

[7] D. H. Titterton, *Development of Infrared Countermeasure Technology and Systems*, ser. Springer Series in Optical Sciences. London, UK: Springer, 2006, vol. 118, pp. 635–671.

[8] J. Jackman, M. Richardson, P. Yuen, D. James, B. Butters, R. Walmsley, and N. Millwood, "Effect of payload size on pre-emptive flare countermeasure against man-portable air-defence

(MANPAD) system," in *Proc. SPIE*, vol. 7836, Toulouse, France, Oct.12, 2010, pp. 1–8.

[9] E. C. Koch, "Review on pyrotechnic aerial infrared decoys," *Propellants, Explosives, Pyrotechnics*, vol. 26, no. 1, pp. 3–11, Jan. 2001.

[10] J. D. V. Ovost, *Global mobility : Anywhere, anytime, any threat? Countering the manpads challenge*, ser. Occasional papers series. Alabama, USA: Bibliogov, Dec. 2005.

[11] B. Molocher, "Countermeasure laser development," in *SPIE Technol. Opt. Countermeasures II; Femtosecond Phenomena II; and Passive Millimetre-Wave and Terahertz Imaging II*, vol. 5989, Bruges, Belgium, Nov.3 2005, pp. 16–25.

[12] C. J. Willers and M. S. Willers, "Simulating the dircm engagement: component and system level performance," in *Proc. SPIE*, D. H. Titterton and M. A. Richardson, Eds., vol. 8543, Edinburgh, UK, Nov.8 2012, pp. 1–16.

[13] T. W. Bae, B. I. Kim, Y. C. Kim, and S. H. Ahn, "Jamming effect analysis of infrared reticle seeker for directed infrared countermeasures," *Infrared Phys. Technol.*, vol. 55, no. 5, pp. 431–441, Sep. 2012.

[14] C. J. Tranchita, K. Jakstas, and R. G. Palazzo, "Countermeasure systems," in *The Infrared & Electro-Optical Systems Handbook*, D. H. Pollock, Ed. Raleigh, USA: ERIM and SPIE Press, Jan. 1993, vol. 7, ch. 3, pp. 235–285.

[15] T. L. Chang, "The IR missile (spin-scan and con-scan seekers) countermeasures," MSc. thesis, Naval Postgraduate School, Montery, USA, Sep. 1994.

[16] G. Y. Kim, B. I. Kim, T. W. Bae, Y. C. Kim, S. H. Ahn, and K. I. Sohng, "Implementation of a reticle seeker missile simulator for jamming effect analysis," in *Int. Conf. Image Process. Theory Tools Appl.*, Paris, France, Jul.7-10 2010, pp. 539–542.

[17] F. Qian, J. Guo, J.-F. Shao, and T.-F. Wang, "Study of jamming of the frequency modulation infrared seekers," in *SPIE Int. Symp. Photoelectronic Detection Imaging; Infrared Imaging Appl.*,

Beijing, China, Sep.11 2013, pp. 28–36.

[18] J. R. White, "Aircraft infrared principles, signatures, threats, and countermeasures handbook," Point Mugu, California, Sep. 2012.

[19] M. C. Sahingil and M. S. Aslan, "The effectiveness of the jammer signal characteristics on conical-scan systems," in *SPIE Conf. Modelling Simulation Defence Syst. Appl.*, vol. 9478, Baltimore, USA, May22 2015, pp. 86–101.

[20] J. Pascal, "Civil Aircraft Security Against MANPADS (CASAM) - WP110 Second Periodic Activity Report," Sagem, Report WP110SAG-100623-MB0, Jun. 2010.

[21] S. Ahn, Y. Kim, T. Bae, B. Kim, and K. Kim, "DIRCM Jamming Effect Analysis of Spin-Scan Reticle Seeker," in *Proceedings of the 2009 IEEE 9th Malaysia International Conference on Communications*. Kuala Lumpur, Malaysia: IEEE, Dec.15-17, 2009, pp. 183–186.

[22] T. M. Malatji and W. P. du Plessis, "Jammer signal effectiveness against a conical-scan missile seeker," in *2017 IEEE Africon*, Cape town, South Africa, Sep.18-20 2017, pp. 591–596.

[23] T. M. Malatji, W. P. du Plessis, and C. J. Willers, "Analysis of the jam signal effect against the conical-scan seeker," *Optical Engineering*, vol. 58, no. 2, pp. 1–10, Feb. 2019.

[24] C. J. Willers and M. S. Willers, "OSSIM: Optronics scene simulator white paper," Council for Scientific and Industrial Research (CSIR), Tech. Rep. 6700-PG-103400-01 Latest revision applies, 2011.

[25] T. M. Malatji, C. J. Willers, and M. S. Willers, "Propagation of a jam code signal in the conical-scan seeker processor," in *2018 International Conference on Intelligent and Innovative Computing Applications (ICONIC)*, Dec.6-7 2018, pp. 566–571.

[26] H. Fritzsche and M. Phillips. (2017, Oct.) Electromagnetic radiation. Online. Encyclopaedia Britannica. [Online]. Available: https://www.britannica.com/science/electromagnetic-radiation

[27] (2019, Mar.) Electromagnetic spectrum. Online. Encyclopaedia Britannica. [Online]. Available: https://www.britannica.com/science/electromagnetic-spectrum

[28] C. J. Willers, *Electro-Optical System Analysis and Design: A Radiometry Perspective*. Bellingham, WA: SPIE Press, 2013, vol. PM236.

[29] F. Neri, *Infrared sensors*, 2nd ed. Artech house, 2006, ch. 2.3, pp. 196–217.

[30] C. J. Willers, "Computational optical radiometry with pyradi," 2014. [Online]. Available: https://github.com/NelisW/ComputationalRadiometry

[31] D. Adamy, *Infrared and Electro-Optical Considerations in Electronic Warfare*, 1st ed. London, England: Artech House, 2004, ch. 4, pp. 77–105.

[32] Y. Zhou, Q. Wang, and T. Li, "A new model to simulate infrared radiation from an aircraft exhaust system," *Chinese Journal of Aeronautics*, vol. 30, no. 2, pp. 651–662, 2017.

[33] (2003) Aerodynamic heating. Online. The Great Soviet Encyclopedia. [Online]. Available: https://encyclopedia2.thefreedictionary.com/aerodynamic+heating

[34] S. P. Mahulikar, G. A. Rao, H. R. Sonawane, and H. S. S. Prasad, "Infrared signature studies of aircraft and helicopters," in *Progress In Electromagnetics Research Symposium Proceedings*, Moscow, Russia, Aug.18-21 2009, pp. 26–30.

[35] L. Jianwei and W. Qiang, "Aircraft-skin infrared radiation characteristics modeling and analysis," *Chinese Journal of Aeronautics*, vol. 22, no. 5, pp. 493–497, Oct. 2009.

[36] C. J. Willers, M. S. Willers, and F. D. Lapierre, "Signature modelling and radiometric rendering equations in infrared scene simulation systems," in *Proc. SPIE*, D. H. Titterton and M. A. Richardson, Eds., vol. 8187, no. 81870R, Prague, Czech Republic, Oct.6 2011.

[37] T. Kim, H. Lee, J. Bae, T. Kim, J. Cha, D. Jung, and H. H. Cho, "Susceptibility of combat aircraft modeled as an anisotropic source of infrared radiation," *IEEE Transactions on Aerospace and*

Electronic Systems, vol. 52, no. 5, pp. 2467–2476, Oct. 2016.

[38] D. H. Titterton, "A review of the development of optical countermeasures," in *Proc. SPIE*, vol. 5615, no. 1, London, UK, Dec.29 2004.

[39] ——, *Military Laser Technology and Systems*, 1st ed. Norwood, MA: Artech House, 2015.

[40] R. G. Driggers, C. E. Halford, and G. D. Boreman, "Parameters of spinning am reticles," *Appl. Opt.*, vol. 30, no. 19, pp. 2675–2684, Jul. 1991.

[41] Zeki Yildirim , "Self-defense of Large Aircraft," MSc. thesis, Naval Postgraduate School, Montery, California, Mar. 2008.

[42] D. Kumar, L. Smith, M. A. Richardson, R. Ayling, and N. Barlow, "Modelling a man-portable air-defence (MANPAD) system with a rosette scan two-colour infrared (IR) and ultraviolet (UV) seeker," in *Proc. SPIE*, vol. 9251, Oct.7 2014, pp. 1–14.

[43] C. R. Smith, R. Grasso, J. Pledger, and N. Murarka, "Trends in electro-optical electronic warfare," in *Technologies for Optical Countermeasures IX*, vol. 8543, Edinburgh, UK, Nov.14 2012, pp. 1–17.

[44] J. C. Whitmire, "Shoulder launched missiles (a.k.a. manpads): The ominous threat to commercial aviation," USAF Counterproliferation Center, Maxwell Air Force Base, Alabama, USA, Dec. 2006.

[45] (2017, Feb.) Wassenaar arrangement on export controls for conventional arms and dual-use goods and technologies. Online. Vienna, Austria. [Online]. Available: https://www.wassenaar.org/app/uploads/2019/consolidated/WA-DOC-17-PUB-001-Public-Docs-Vol-I-Founding-Documents.pdf

[46] M. Ashkenazi, P. M. Amuzu, J. Grebe, C. Kögler, and M. Kösling, "Manpads: A terrorist threat to civilian aviation?" in *BICC briefs*. Bonn International Center for Conversion (BICC), Feb. 2013, vol. 47.

[47] T. Keenan, "The libyan uprising and the right of revolution in international law," *International and Comparative Law Review*, vol. 11, no. 1, pp. 7–32, Jan. 2018.

[48] CNN. (2019, Apr.) Syrian civil war fast facts. Online. CNN. [Online]. Available: https://edition.cnn.com/2013/08/27/world/meast/syria-civil-war-fast-facts/index.html

[49] W. Knight. (2002, Nov.) 'Incompetence' saved rocket-attack airliner. Online. NewScientist. [Online]. Available: https://www.newscientist.com/article/dn3127-incompetence-saved-rocket-attack-airliner/

[50] W. L. Wolfe and G. Zissis, *The Infrared Handbook*. Infrared Information and Analysis Center, Environmental Research Institute of Michigan: Office of Naval Research, US Navy, 1978.

[51] R. D. Hudson, *Infrared System Engineering*. New York: Wiley-Interscience, 1969.

[52] J. M. Shima, "Fm demodulation using a digital radio and digital signal processing," MSc. thesis, University of Florida, Florida, USA, 1995.

[53] A. J. Noga, "Numerical FM Demodulation Enhancements," Rome Laboratory, US Air Force Materiel Command, Technical Report RL-TR-96-91, 1996.

[54] Z. W. Chao and J. L. Chu, "Digital simulation of frequency modulation reticles," *Optical Engineering*, vol. 29, no. 1, pp. 68–84, Jan. 1990.

[55] J. Jackman, "Pre-Emptive Infrared Countermeasures," PhD. thesis, Cranfield University, Cranfield, Bedford, UK, 2011.

[56] R. P. Birchenall, M. Richardson, B. Brian, and W. Roy, "Modelling an infrared man portable air defence system," *Infrared Phys. Technol.*, vol. 53, no. 5, pp. 372–380, Sep. 2010.

[57] B. van der Pol, "The fundamental principles of frequency modulation," *Journal of the Institution of Electrical Engineers - Part III: Radio and Communication Engineering*, vol. 93, no. 23, pp. 153–158, May 1946.

[58] S. G. Jahng, H. K. Hong, J. S. Choi, and S. H. Han, *Reticles - Nutating systems*, 2nd ed., ser. Encyclopedia of Optical and Photonic Engineering. Bosa Roca, USA: CRC Press, Sep. 2015, ch. Reticles - Nutating systems, pp. 2417–2430.

[59] A. R. Gèdance, "Comparison of infrared tracking systems," *J. Opt. Soc. America*, vol. 51, no. 10, pp. 1127–1130, Oct. 1961.

[60] M. D. Withey, "Infrared countermeasure flares," *The Imaging Science Journal*, vol. 58, no. 5, pp. 295–299, Oct. 2010.

[61] S. Y. AlchekhYasin, A. R. Erfanian, M. R. Mosavi, M. R. Mosavi, and A. Mohammadi, "The flare detection in the two color crossed array detectors infrared seeker," *International Journal of Computer Applications*, vol. 81, no. 4, pp. 34–42, Nov. 2013.

[62] J. S. Brusnahan, M. Fitzgerald, M. Morgan, and R. Pietrobon, "Bi-spectral ircm-flare formulations based on tetrazole-derivatives," *Propellants, Explosives, Pyrotechnics*, vol. 39, no. 1, pp. 133–137, Feb. 2014.

[63] D. H. Titterton, "Requirements for laser devices used in countermeasure applications," in *Proc. SPIE*, vol. 5989, Bruges, Belgium, Nov.3 2005.

[64] S. Craubner, "Digital simulation of reticle systems," *Optical Engineering*, vol. 20, no. 4, pp. 1–8, Aug. 1981.

[65] J. S. C. Sung-Hyun Han, HyunKi Hong, "Dynamic simulation of infrared reticle seekers and an efficient counter-countermeasure algorithm," *Optical Engineering*, vol. 36, no. 8, pp. 2341–2345, Aug. 1997.

[66] G. Olsson, "Simulation of reticle seekers by means of an image processing system," *Optical Engineering*, vol. 33, no. 3, pp. 730–736, 1994.

[67] W. du Plessis, "Reticle simulation," Private communication, Oct 2016.

[68] W. Altman and D. MacDonalds, *Tuning of PID controllers in both open and closed loop control systems*. Oxford, 2005, ch. 8, pp. 112–130.

[69] R. Keim. (2016, Nov.) Understanding automatic gain control. Online. All about circuits. [Online]. Available: https://www.allaboutcircuits.com/technical-articles/understanding-automatic-gain-control/

[70] A. Hayes. (2019, May) R-squared definition. Online. Investopedia. [Online]. Available: https://www.investopedia.com/terms/r/r-squared.asp

ADDENDUM A SCAN GEOMETRY PROBLEM

A.1 SCAN GEOMETRY PROBLEM

In order to understand how the detector signal behaves with changes in the target position, the scanning geometry will be explained fully in this addendum. The discussion given here is an extension of the discussion given in Chapter 2.

The geometry of the scan parameters with reference to the nutation circle and reticle can be described as shown in Figure. A.1. The radius of the nutation circle is r, the distance between the centre of the nutation circle and the centre of the reticle is given by R_0. The distance between the centre of the reticle and the target image is given by D, and the angle of the nutation vector is given by θ_n. The angle of the line extended between the reticle centre and the nutation centre is given by θ_c and the angle of the line extended between the reticle centre and the target instantaneous position is given by α. With the reticle centre as reference, the centre of the nutation circle can be expressed in rectangular coordinates as

$$x_n = R_0 \cos\theta_c \tag{A.1}$$

$$y_n = R_0 \sin\theta_c \tag{A.2}$$

The position of the target can then be expressed as

$$x_t = x_n + r\cos\theta_n \tag{A.3}$$

$$= R_0 \cos\theta_c + r\cos\theta_n \tag{A.4}$$

$$y_t = y_n + r\sin\theta_n \tag{A.5}$$

$$= R_0 \sin\theta_c + r\sin\theta_n. \tag{A.6}$$

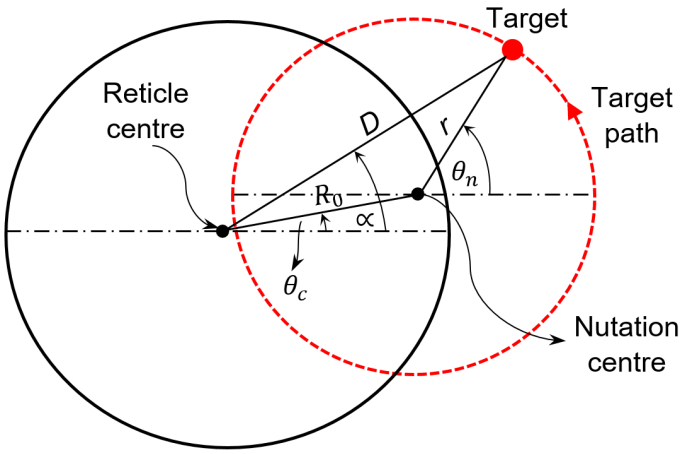

Figure A.1. Geometry of the scan process in the conical-scan seeker.

The angle from the reticle centre to the target is therefore given by

$$\alpha = \arctan\left(\frac{y_t}{x_t}\right) \tag{A.7}$$

$$= \arctan\left(\frac{R_0 \sin\theta_c + r\sin\theta_n}{R_0\cos\theta_c + r\cos\theta_n}\right) \tag{A.8}$$

It is known that the instantaneous frequency of an FM signal is given by [57]

$$f_i = \frac{1}{2\pi}\frac{d\phi}{dt}. \tag{A.9}$$

where ϕ is the phase of the signal. If the phase of the signal is given as $\phi = (\alpha + \psi)$, then the instantaneous frequency can be written as

$$f_i = \frac{1}{2\pi}\frac{d}{dt}\left(\arctan\left(\frac{y_t}{x_t}\right)\right). \tag{A.10}$$

After computing the derivative, the instantaneous frequency is given by

$$f_i = \frac{1}{2\pi}\frac{1}{1+\left(\frac{y_t}{x_t}\right)^2}\frac{d}{dt}\left(\frac{y_t}{x_t}\right). \tag{A.11}$$

Simplifying gives

$$f_i = \frac{1}{2\pi}\frac{x_t^2}{x_t^2+y_t^2}\left(x_t^{-1}\frac{d}{dt}y_t + y_t\frac{d}{dt}x_t^{-1}\right). \tag{A.12}$$

Deriving and simplifying gives

$$f_i = \frac{1}{2\pi}\frac{1}{x_t^2+y_t^2}\left(x_t\frac{d}{dt}y_t - y_t\frac{d}{dt}x_t\right). \tag{A.13}$$

Substituting Equation A.3 into x_t and y_t for derivation gives

$$f_i = \frac{1}{2\pi}\frac{1}{x_t^2+y_t^2}\left(x_t\frac{d}{dt}(R_0\sin\theta_c + r\sin\theta_n) - y_t\frac{d}{dt}(R_0\cos\theta_c + r\cos\theta_n)\right). \tag{A.14}$$

Noting that θ_c is not a function of time, it can simply be removed from the derivative. Substituting $\omega_n t$ into θ_n and deriving gives

$$f_i = \frac{1}{2\pi}\left(\frac{1}{x_t^2 + y_t^2}\right)\left(x_t \omega_n r \cos\omega_n t + y_t \omega_n r \sin\omega_n t\right). \tag{A.15}$$

Substituting Equation A.3 into x_t and y_t and replacing $\omega_n t$ with θ_n gives

$$f_i = \frac{\omega_n r}{2\pi}\frac{(R_0\cos\theta_c + r\cos\theta_n)\cos\theta_n + (R_0\sin\theta_c + r\sin\theta_n)\sin\theta_n}{(R_0\cos\theta_c + r\cos\theta_n)^2 + (R_0\sin\theta_c + r\sin\theta_n)^2}. \tag{A.16}$$

It is convenient to give the following trigonometric identities:

$$\sin^2\theta + \cos^2\theta = 1 \tag{A.17}$$

$$\cos\theta\cos\alpha + \sin\theta\sin\alpha = cos(\theta - \alpha) \tag{A.18}$$

Expanding Equation A.16 and using the above mentioned identities gives

$$f_i = \frac{r^2 f_n\left[1 + \frac{R_0}{r}\cos(\theta_c - \theta_n)\right]}{r^2\left[1 + \left(\frac{R_0}{r}\right)^2 + 2\left(\frac{R_0}{r}\right)\cos(\theta_c - \theta_n)\right]} \tag{A.19}$$

Substituting $\rho = \frac{R_0}{r}$ and simplifying gives the instantaneous frequency.

$$f_i = \frac{f_n\left[1 + \rho\cos(\theta_c - \theta_n)\right]}{\left[1 + \rho^2 + 2\rho\cos(\theta_c - \theta_n)\right]} \tag{A.20}$$